NANOENGINEERING OF TEMPERATURE SENSITIVE MAGNETIC FLUIDS FOR COOLING APPLICATIONS IN POWER TRANSFORMERS

A

THESIS

Submitted to

Thapar Institute of Engineering & Technology
Patiala

For the award of

DOCTOR OF PHILOSOPHY

Submitted by

Navjot Kaur
(901312010)

Under the Supervision of

Dr. B. N. Chudasama
(Associate Professor)

School of Physics & Materials Science
Thapar Institute of Engineering & Technology
(Deemed to be University)
Patiala
INDIA

July 2018

DEDICATION

This dissertation is dedicated to my parents for their love, patience, kindness, support and their belief in me.

CERTIFICATE OF ORIGINALITY

I certify that this thesis fully or partially has not been submitted for any other degree or diploma in any other university or other institute of higher learning.

I also certify that the thesis does not contain any material previously published in another name or written by another person except where due acknowledgement is made in the text.

I also certify that thesis has been written by me and that to my knowledge and belief any help. I have received in preparing the thesis and all sources used have been acknowledged in the thesis.

Navjot Kaur

Navjot Kaur
(Regd. No. 901312010)

School of Physics and Materials Science
Thapar Institute of Engineering & Technology
Patiala-147004 (INDIA)

26-07-2018
Dated:
Place: Patiala (India)

CERTIFICATE

This is to certify that the thesis entitled "**Nanoengineering of Temperature Sensitive Magnetic Fluids for Cooling Applications in Power Transformers**" which is being submitted by **Navjot Kaur (Roll No. 901312010)** for the partial fulfilment of the requirement for the Award of the Degree of Doctor of Philosophy in School of Physics and Materials Science, Thapar Institute of Engineering & Technology, Patiala (Punjab), India is an exclusive record of candidate's own research work under my supervision. This thesis in part or full has not been submitted in any other University or Institute for the award of any degree. This thesis is fit to be considered for the award of degree of Doctor of Philosophy.

(Dr. B. N. Chudasama)
Supervisor
Associate Professor
School of Physics and Materials Science
Thapar Institute of Engineering & Technology
Patiala-147004 (INDIA)

Dated: 26/07/2018
Place: Patiala (India)

ACKNOWLEDGEMENT

An acknowledgement in my thesis is just a small gesture. My thesis wouldn't been complete without acknowledging the important role that many people have had in my life. There has been a noteworthy contribution of many people in helping me to complete my doctoral work and my endeavour.

I would first and foremost like to express my heartfelt gratitude towards my guide, Dr. Bhupendra Chudasama, Associate Professor, School of Physics and Materials Science, Thapar Institute of Engineering & Technology (T.I.E.T), Patiala. The most influential person in my graduate career is my advisor, Dr. Bhupendra Chudasama. His passion, guidance and discipline have been indispensable to my growth as a scientist and as a person over these past four and a half years.

With great appreciation I would like to express my gratitude towards Dr. Rafat Siddique, Dean Research and Sponsored Projects and Dr. O. P. Pandey, Senior Professor and former Dean Research and Sponsored Projects, T.I.E.T, Patiala, for their invaluable support and cooperation. I am thankful to them for providing me the necessary research facilities to meet the goals of this assignment.

I would like to express my special appreciation and thanks to Dr. Kulvir Singh, Professor, School of Physics and Materials Science, T.I.E.T, Patiala, for encouraging my research and appreciating me to grow as a research scientist. Your advice on both research as well as on my career have been invaluable.

I am indebted to Dr. Manoj K. Sharma, Professor and former Head, School of Physics and Materials Science, T.I.E.T, Patiala, for his support and cooperation. I am especially thankful to my URB committee members, Dr. B. C. Mohanty, Dr. S. D. Tiwari and Dr. Amjad Ali, who have been simply unreal. My committee members have been very gracious and generous with their time and ideas. Thank you so much to all of them.

I would also like to thank all my lab mates. With great appreciation, I shall acknowledge my seniors, Dr. Chandni Khurana and Dr. Parveer Kaur for their love and support. Many thanks to Purnima Sharma and Yashpreet for their love and cheerful company. Thanks to my friend Amandeep Kaur with whom I started this journey. Special appreciation goes to my friends

Ravneet, Ramneet and Rimmy Singh for moral support and encouragement at every stage of this endeavour. I also acknowledge my pals, Dr. Samita, Dr. Satwinder, Santosh, Chhavi and Navjot Virk for their well wishes. I truly believe that this assignment would not have been complete without their help and co-operation. Words fail me to express my appreciation for them.

I am indebted to University Grants Commission, New Delhi, (Maulana Azad National Fellowship), for Junior and Senior Research Fellowship, SAI Laboratory, T.I.ET, Patiala for extending XRD facilities.

I would like to thank my parents who raised me with love and supported me in all my pursuits. I am grateful to my brother for his constant support. Last but not the least; I would like to pay my high regards to God for enlightening my soul with respect, love and concern for other humans and allowing me to enter a field, where I could practice this desire. Lastly, to all those who came and left me knowingly or unknowingly in these years of my life. Thank you.

Navjot Kaur

List of publications:

SCI Journals

1. Navjot Kaur and Bhupendra Chudasama, "*Structure Induced Tunable Magnetic Properties of MnZn ferrite nanoparticle*", Micro & Nano Letters, 2017, 12, 151 – 156. Impact factor: 0.84

2. Navjot Kaur and Bhupendra Chudasama "*Effect of thermal aging on stability of transformer oil based temperature sensitive magnetic fluids*", Journal of Magnetism and Magnetic Materials, 2018, 451, 647-653. Impact factor: 3.04

3. Navjot Kaur and Bhupendra Chudasama "*Tunable Curie Temperature of* $Mn_{0.6}Zn_{0.4}Fe_2O_4$ *Nanoparticles"*, Journal of Magnetism and Magnetic Materials, 2018, 465,164-168. Impact factor: 3.04

4. Navjot Kaur and Bhupendra Chudasama "*Synthesis of Magnetic Fluid Based Coolants for High Power Transformers*" Journal of Nanoscience and Nanotechnology, (communicated)

5. Navjot Kaur and Bhupendra Chudasama "*Effect of Aging on the Colloidal Stability of Magnetic Fluids*", Journal of Colloid and Interface Science, (communicated)

6. Navjot Kaur and Bhupendra Chudasama "*Magnetoviscosity of Mn-Zn ferrite based temperature sensitive magnetic fluids*", Journal of Colloid and Interface Science, (communicated)

Non-SCI Journals

1. Navjot Kaur and Bhupendra Chudasama, "*Synthesis of superparamagnetic silica-coated magnetite nanoparticles for biomedical applications*" AIP Conference Proceedings, American Institute of Physics, 2015, 1661, 070004.

Conference Presentations:

Oral Presentations

1. Navjot Kaur and Bhupendra Chudasama, "*Structural and Magnetic Properties of Mn -Zn Ferrite Nanoparticles*" National Conference on Advances in Engineering Materials (NAEM-2015) DIT University, Dehradun, Uttarakhand, India (2015).

Poster Presentations

1. Navjot Kaur and Bhupendra Chudasama, "Synthesis of Superparamagnetic Silica-Coated Magnetite Nanoparticles for Biomedical Applications" International Conferences on Condensed Matter Physics (ICCMP 2014), HP University, Shimla, India (2014).

2. Navjot Kaur and Bhupendra Chudasama, "*Synthesis of Transformer Oil based Temperature Sensitive Magnetic Fluids for Heat Exchange Devices"* International Conferences on Magnetic Materials and Applications (ICMAGMA-2015) VIT University, Vellore (2015)

3. Navjot Kaur and Bhupendra Chudasama, "*Effect of Thermal Aging on the Stability of Transformer Oil based Temperature Sensitive Magnetic Fluids"* International Conferences on Magnetic Materials and Applications (ICMAGMA-2017) Defence Metallurgical Research Laboratory (DMRL), Hyderabad (2017).

TABLE OF CONTENTS

PREFACE

Transformers generate heat through energy losses and get heated due to iron core and copper losses that results into elevated resistance within the windings, increased hysteresis loss and decreased saturation magnetization of the core and degradation of the transformer's insulation. Ultimately these will lead to significant and permanent efficiency reduction. Therefore, it is necessary to dissipate the heat generated by the core and windings so that the temperature of the transformer can be kept below a threshold at which the insulation begins to deteriorate. To inhibit temperature rise, transformers are cooled with mineral oils. The final, steady-state temperature of the transformer reflects equilibrium between power losses and heat dissipation properties of the coolant. As the oil is heats up, it experiences decrease in the density. Oil in contact with the transformer coils absorbs highest amount of heat and as a result it becomes least dense and starts rising relative to the surrounding oil. The rising oil makes contact with the walls of the housing, transfers heat to the walls and ultimately to the exterior environment. The cooled oil moves downward and replace the heated oil, which is rising from the windings. This natural convection caused by the interplay between the gravity and heat induced density variation represents the cooling mechanism most commonly utilized in commercial high power transformers.

Gravitational forces that circulate oil in transformers are relatively weak. Temperature gradients across the oil reservoirs are often observed to be quite large, which results into poor heat transfer. Transformer windings frequently develop "hot spots" that can cause insulation break-down. These factors can lead to significant and permanent efficiency reduction. Development of coolants with enhanced thermal conductivity and better dielectric properties is critical for uninterrupted operation of high power transformers.

Magnetic fluids can provide thermal and dielectric benefits over transformer oils. Magnetic fluids are colloidal suspensions of superparamagnetic nanoparticles coated with surfactant and dispersed in a carrier liquid. If used as a coolant, they can improve the cooling efficiency of transformers by enhancing the fluid circulation within windings because of the magnetically driven fluid flow. Magnetic field is present in the surroundings of windings and core of the transformer. This "leakage field" occurs because of electrical currents in the windings and reflects imperfect channeling of magnetic flux into the core. Its strength is highest in the immediate vicinity of the core and windings, and falls of rapidly with

increasing distance. This magnetic field gradient draws magnetic fluid towards the core. Since the core and windings generate heat, the temperature of the fluid rises as it approaches towards the core, resulting into the loss of magnetic properties and decrease in density. The magnetic fluid starts rising as the gravitational effect of density reduction begins to overcome the weakening of magnetic attraction. Movement of hot magnetic fluid is assisted by the attraction exerted by the core and windings on cooler more intense magnetic fluid, which displaces the hot rising fluid as it travels toward the core. Movement away from the heat source and contact with the walls of the housing causes the hot magnetic fluid to cool and reacquire magnetization. This convection cycle, driven by the magnetic and gravitational forces, involves much faster fluid flow and therefore greater cooling efficiency can be achieved with natural convection. In addition, magnetic fluids can increase the transformer capacity to withstand lightning impulses, while minimizing the effect of moisture in typical insulating fluids. Magnetic nanoparticles can also minimize dielectric breakdown in transformers.

Magnetization of magnetic fluid is temperature-dependent, decreasing steadily until the fluid reaches a characteristic "Curie temperature" at which, it loses all its magnetic strength. This property of temperature sensitive magnetic fluid can be exploit to design a smart coolant that can tune its cooling efficiency according to the operating temperature of the transformer by adjusting its magnetic field induced convective flow. These characteristics of magnetic fluid based coolant help in designing smaller, more efficient transformers, or to extend the life and loading capability of existing units. Despite of promising nature of this technology, very little efforts have been made to explore it. In our understanding the fundamental reason behind this is the inherent complexity involved in design and synthesis of stable, temperature sensitive magnetic fluids.

Ferrites are generally used to prepare magnetic fluids. Most substituted ferrites tend to have Curie temperatures too high for practical use in the proposed application. However, many mixed and rare earth doped ferrites exhibit Curie temperatures in the range of 100 °C – 300 °C. Among different temperature sensitive magnetic materials, Zn-containing spinel ferrites ($Me_{1-x}Zn_xFe_2O_4$) are most attractive because they allow large variation in their magnetic properties with small variation in the Zn content. For transformer cooling applications, temperature sensitive magnetic fluids also needs to be stable under extreme conditions of temperature and magnetic field.

This thesis provides an insight into the synthesis of stable temperature sensitive magnetic fluids with tunable Curie temperatures which are suitable for transformer cooling. Influence of particle size and size distribution on the colloidal stability of magnetic fluids and temperature induced aging of magnetic fluids is also the core focus of this thesis. The outcome of the doctoral research is organized in seven chapters.

This thesis begins with the Introduction of magnetic fluids, in **Chapter 1**. It summarizes various properties and applications of magnetic fluids. The concept of temperature sensitive magnetic fluids is introduced for cooling applications in power transformers. It also evaluates potential magnetic nanoparticles that are well suited for thermo-magnetic cooling, on the basis of moderate saturation magnetization and tunable Curie temperature and discusses the unique properties of MZ ferrite based magnetic fluids.

Chapter 2 summarizes existing literature on ferrite magnetic nanoparticles and their magnetic fluids. In the first section various methods developed for the synthesis of magnetic nanoparticles are reviewed. The focus of the literature review is to evolve correlation between synthesis conditions, particle size and their magnetic properties. In the second section, various techniques developed for the synthesis of magnetic fluids are reviewed. The focus here is on the correlation between tunable Curie temperature and saturation magnetization of fluids. In the third section of Chapter-2, literature on structural, magnetic and thermal properties of magnetic fluids are summarized. This chapter ends with discussion on stability and aging of magnetic fluids at elevated temperature.

Chapter 3 provides details of experimental protocols developed and followed for the synthesis of MZ ferrite magnetic nanoparticles. In the first part of this chapter, synthesis of uniform MZ ferrite nanoparticles is carried out by chemical co-precipitation method. A series of $Mn_{1-x}Zn_xFe_2O_4$ (x = 0 – 1) nanoparticles are synthesized by chemical co-precipitation method. Amongst them MZ nanoparticles with high saturation magnetization are used for further investigation. In the second part, a series of MZ nanoparticles are synthesized by co-precipitation method as a function of co-precipitation pH (10 – 13), reaction temperature (80 – 100 °C) and reaction time (1 – 4 h). The correlation between particle size and saturation magnetization have also been evaluated in this chapter.

In **Chapter 4**, protocols for the synthesis of magnetic fluids with tunable Curie temperature and saturation magnetization are described. In this chapter, synthesis of MZ

fluids having varying Zn content, an oleic acid as surfactant and commercial transformer oil as carrier liquid is explained. Magnetic properties of MZ fluids are analysed with modified Langevin theory. By fitting magnetization data with modified Langevin theory, magnetic particle diameter (D_m), saturation magnetization (M_s), polydispersity (σ), mean field constant (λ) and ferrimagnetic susceptibility (χ) are determined.

Evaluation of effect of aging on the colloidal stability of magnetic fluids is studied in **Chapter 5.** This study was conducted over an extended period of 210 days. Photon Correlation Spectroscopy (PCS) and Vibrating Sample Magnetometry (VSM) are used to determine effect of aging on the colloidal stability and magnetic properties of MZ fluids.

Chapter 6 aims to evaluate colloidal stability of magnetic fluids under accelerated thermal aging and its correlation with hydrodynamic size and magnetic properties of the magnetic fluids. In this chapter, effect of accelerated thermal aging on the dispersion stability and magnetic properties have been evaluated by photon correlation spectroscopy and vibration sample magnetometry, respectively on MZ fluids that are aged at 50 °C to 150 °C for 0 – 72 h. A correlation between hydrodynamic size of nanoparticles, its polydispersity and colloidal stability of fluids have been established. Effect of influence of degree of Zn substitution on the stability of MZ fluids under accelerated thermal aging has also been evaluated.

Chapter 7 summarises important findings of this work and scope for the future work.

CHAPTER 1

INTRODUCTION

1.1 MAGNETIC FLUIDS

Magnetic fluids are the colloidal suspension of superparamagnetic nanoparticles dispersed in carrier liquid, which responds to an applied external magnetic field as if the fluid itself possesses magnetic characteristics [1-3]. It combines both fluidic and magnetic properties in a single system. Magnetic fluids are generally composed of 5% magnetic nanoparticles, 10% chemically adsorbed surfactant and 85% liquid carrier [4]. Magnetic nanoparticles dispersed in fluids have diameter of the order of 10 nm. They undergo translational and rotational Brownian motion, which avoid the settling of particles under the gravitational and magnetic fields. High surface energy (due to small size) of nanoparticles and relatively strong Van der Waals forces between magnetic particles can cause their aggregation. To inhibit this agglomeration, nanoparticles are stabilized by steric or ionic stabilization process [5]. Based on the type of stabilization, magnetic fluids are classified into following two subclasses:

1.1.1 Sterically Stabilized Magnetic Fluids
1.1.2 Ionically Stabilized Magnetic Fluids

1.1.1 Sterically Stabilized Magnetic Fluids

Sterically stabilized magnetic fluids are prepared by coating magnetic nanoparticles with surfactants to prevent aggregation of nanoparticles. Surfactants are made up of polar organic molecules, whose structure comprised of a short functional group (alkali, acid, etc.) and long tail chain (hydrocarbon, fluorocarbon, etc.). Steric repulsion caused by this polymeric chains of surfactants between nanoparticles acts as a physical barrier, which keeps the magnetic nanoparticles floating in the fluid and stabilizes the colloid [5]. If nanoparticles are dispersed in a non-polar medium like oils, a monolayer of hydrophobic surfactant is sufficient to provide steric repulsion against the magnetic and Van der Waals attraction between nanoparticles. The polar head of the surfactant is attached to the particle surface through chemi-adsorption and the carbon chain is floating in the carrier liquid. On the other hand, if the nanoparticles needs to dispersed in a polar median like water, a double layer of surfactant is required to form a hydrophilic layer around the nanoparticle surface. The polar head of a

surfactant can be cationic, anionic or non-ionic. Sketches of sterically stabilized magnetic nanoparticles dispersible in non-polar medium (like oil) and polar medium (like water) is shown in **Fig. 1.1.**

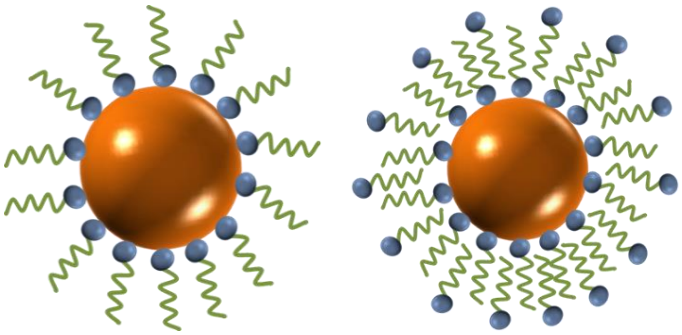

(a) (b)

Fig. 1.1. Sterically stabilized magnetic nanoparticles coated with (a) monolayer of surfactant (dispersible in oil) and (b) double-layer of surfactant (dispersible in water).

1.1.2 Ionically Stabilized Magnetic Fluids

In ionically stabilized magnetic fluids, colloidal stability of nanoparticles is achieved by decorating the surface of nanoparticles with ions [6, 7]. Magnetic nanoparticles when prepared by chemical precipitation method, an acid-alkaline reaction keeps the surface of nanoparticles electrically charged [8, 9]. Usually water is used as liquid carrier and pH of the solution vary between 2 to 12, depending on the sign of the surface charge of the particles. Acidic ionic magnetic fluid (pH < 7) have positive charge on the surface of nanoparticles, and alkaline ionic magnetic fluid (pH > 7) have negative charge on the surface of nanoparticles. The surface charge density of the particles is typically of the order of 10 $\mu C/cm^2$ [10]. Ionic citrated or tartrated magnetic fluids provide both the steric and electrostatic repulsion to prevent aggregation of nanoparticles in magnetic fluids. In case of citrated magnetic fluids, nanoparticles are coated with small chain molecules, such as 3-carboxy-3-hydroxypentanedicarboxylic acid (COOH-CH_2-COH-COOH-CH_2-COOH). In the presence of water, these molecules ionize. Besides the steric repulsion, there is also an electrostatic interaction. The sketches of a nanoparticles of acidic and alkaline magnetic fluids are shown in **Fig. 1.2.**

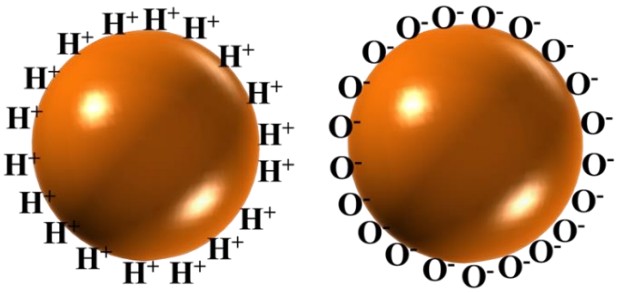

(a) (b)

Fig. 1.2. Ionically stabilized nanoparticles in (a) acidic magnetic fluid (pH < 7) and (b) alkaline magnetic (pH > 7).

1.2 PROPERTIES OF MAGNETIC FLUIDS

1.2.1 Magnetic properties

Magnetic fluids contains ferro or ferrimagnetic nanoparticles. Magnetic fluids do not show ferromagnetism as they do not retain residual magnetization, when the external magnetic field is removed. Magnetic nanoparticles dispersed in fluids are superparamagnetic and possess high magnetic susceptibility. When the size of ferro or ferrimagnetic particle decreases below its domain size, nanoparticles transform from polydomain to single-domain [11-13]. The critical size of a single-domain particle depends on its shape, temperature and magnetic anisotropy of the crystal. When the particle size reduces below this critical limit, the thermal energy is sufficient to randomize the magnetic dipoles [14, 15]. Such small particles have no intrinsic net magnetic moment in the absence of external magnetic field, but in the presence of external field, they show strong magnetism owing to their high magnetic susceptibility. These particles behave identical to paramagnets in the absence of external magnetic field and they show spontaneous magnetization like ferromagnets when subject external magnetic field [14-16]. Ferrites are used to prepare magnetic fluids [17-19]. Magnetic properties of ferrite nanoparticles are strongly correlated with the characteristics of nanoparticles such as size, size distribution, shape, surface chemistry, cationic distribution, etc. [20].

1.2.1.1 Size effect

Magnetic properties of nanoparticles depends on the size of nanoparticles. As the size of the magnetic nanoparticles decreases, the magnetic anisotropy energy per nanoparticle also decreases. Magnetic anisotropy energy is the energy that keeps the magnetic moment in a

particular orientation. At a particular size called the characteristic size of nanoparticles, the anisotropy energy equals to the thermal energy, which allows the random flipping of the magnetic moments [21]. This flipping occurs when the size of the nanoparticles decreases below the characteristic size (r_o). Below this size, each magnetic nanoparticles display superparamagnetism. The saturation magnetization (M_s) of nanoparticles also strongly depends on the size of the nanoparticles **(eq. (1.1))** [22]. Magnetic nanoparticles possess disordered spin structure on its surface which is known as 'magnetic dead layer'. When the size of the nanoparticles is relatively small (< 5 nm), the ratio of thickness of disordered spin layer (dead layer) to the radius of the magnetic nanoparticle becomes significant. Surface spin disorder thus lead to the reduction in saturation magnetization. The correlation between saturation magnetization and nanoparticle size can be given by [22]

$$M_s = M_{sb}\,[(r - d)/r]^3 \qquad (1.1)$$

where r is the radius of nanoparticles, d is thickness of the magnetic nanoparticles surface exhibiting disordered spins, M_{sb} is saturation magnetization of bulk sample and M_s represents saturation magnetization of magnetic nanoparticles of radius r.

1.2.1.2 Structural properties

Magnetic properties of ferrites are directly related to the chemical composition and distribution of the cations between tetrahedral and octahedral lattice sites in spinel crystal structure of ferrites. Generally, chemical composition of ferrites can be expressed by AB_2O_4, where; A and B refer to the tetrahedral and octahedral cation sites, respectively **(Fig. 1.3.)**. In normal spinel lattice, all the bivalent (M^{+2}) metal ions occupy the tetrahedral sites while all the octahedral sites are occupied by the trivalent (Fe^{+3}) metal ions. In inverse spinel, half of the trivalent (Fe^{+3}) metal ions and all the bivalent (M^{+2}) metal ions occupy the octahedral sites while the other half of the trivalent (Fe^{+3}) metal ions occupies the tetrahedral sites. In mixed metal ferrites, both bivalent and trivalent metal ions occupy both the tetrahedral and octahedral sites. Type of cations and their distribution between the two interstitial sites in the spinel unit cell determine their intrinsic magnetic properties [23, 24]. The cation distribution between A and B sites depends on the ionic radii of the cations [25]. Since the magnetic moments of the cations at the octahedral sites are parallel to the magnetic field, and the magnetic moments at the tetrahedral sites are antiparallel, the vector sum of the magnetic moments between sub-lattice A and B gives the magnetic moment of the crystal.

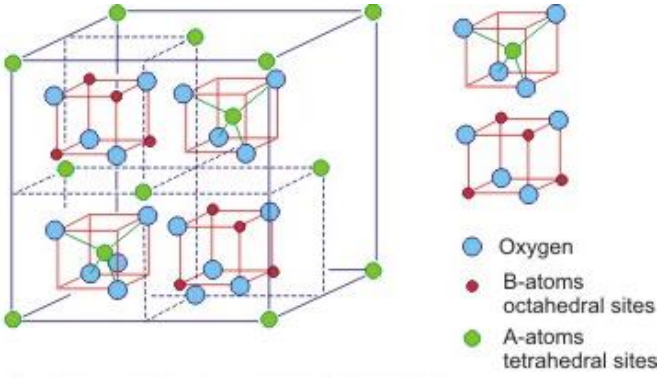

Fig. 1.3. Crystal structure of AB_2O_4 spinel ferrites [26].

Saturation magnetization of nanoparticles depends on the net magnetic moment of the crystal and exchange interactions between magnetic ions occupying the tetrahedral A–sites and octahedral B–sites. In normal spinel, all bivalent metal ions (M^{2+}) occupies the tetrahedral A–sites and Fe^{3+} ions occupies the octahedral B–sites. The structural formula can be represented as:

$$A \quad [\ B\ ]$$

$$M^{2+}\ [Fe^{3+}]\ O^{2-}{}_4$$

$$\downarrow \quad \uparrow \quad 0$$

In the inverse spinel structure, half of the Fe^{3+} ions occupy the tetrahedral A–sites and another half is at octahedral B–sites. All the bivalent metal ions (M^{2+}) occupies the B–sites. Magnetic moments of Fe^{3+} at A and B sites mutually compensates each other and net moment of the nanoparticles is because of the magnetic moments of bivalent cations (M^{2+}) at the octahedral B–sites. The structural formula for the inverse spinel structure can be represented as

$$A \quad [\quad B \quad]$$

$$Fe^{3+}\ [M^{2+}\ Fe^{3+}]\ O^{2-}{}_4$$

$$\downarrow \quad \uparrow \quad \uparrow \quad 0$$

In mixed spinel, bivalent metal ions M^{2+} and Fe^{3+} ions occupies both the A and B–sites. The structural formula for such mixed spinel is

A [B]

$M^{2+}_{1-\delta} Fe^{3+}_{\delta} [M^{2+}_{\delta} Fe^{3+}_{1-\delta} Fe^{3+}] O^{2-}_{4}$

↓ ↓ ↑ ↑ ↑ 0

where δ is the degree of inversion. It represents the fraction of Fe^{3+} presents at the tetrahedral A–sites.

Interaction between A and B sub-lattices in spinel structures consist of inter sub-lattice (A–B) super-exchange interactions and intra sub-lattice (A–A) and (B–B) exchange interactions. Amongst these, the inter sub-lattice (A– B) interaction is the strongest. (A–A) is relatively weak as compared to (A–B) interaction. In general, (A–A) interaction is ten times weaker than the (A–B) interaction. (B–B) interaction is the weakest amongst all [27, 28]. These exchange interactions effects the magnetization and hence the Curie temperature of AB_2O_4 ferrites. Therefore any deviation from the normal cation distribution as explained above can lead to the cation site disorder resulting into the drastic changes in the magnetic properties of nanoparticles.

1.2.2 Polydispersity in size

Magnetic fluids contains magnetic nanoparticles as dispersed phase. These magnetic nanoparticles are polydispersed in size and follow the log-normal particle size distribution [29, 30]. Polydispersity in size of magnetic nanoparticles plays an important role in the magnetic properties of fluids. Progressive alignment of magnetic moments in an applied magnetic field for polydisperse magnetic nanoparticles is different from that of the monodisperse magnetic nanoparticles. This different characteristic is due to the dependence of magnetic dipole moment on the size distribution of magnetic nanoparticles. Particles with larger size orientates at low magnetic fields while smaller particles require stronger fields.

1.2.3 Inter-particle interactions in magnetic fluids

The classical Langevin theory for paramagnetism has often been applied for interpreting the M–H data of magnetic fluids by comparing the individual magnetic moments of particles. Here each magnetic moment is considered to be non-interacting like gas molecules. Magnetic fluid contains non-interacting single-domain particles. The magnetization of assembly of such isolated superparamagnetic nanoparticles can be described by the Langevin's theory [31]. This

model assumes spherical shape of particles, dominance of thermal energy over the anisotropy energy, polydispersed nature of particles that usually obeys log-normal size distribution function and average domain magnetization (M_d) of the particles that remains constant for a given size distribution. The inter-particle interactions are neglected in this model.

$$M = M_s \int_0^\infty f(D)\, L\,(\alpha) dD \tag{1.2}$$

where M_s is the saturation magnetization of nanoparticles and $L(\alpha) = \coth\alpha - 1/\alpha$ is the Langevin function. The Langevin parameter $\alpha = \mu H / k_B T$. μ is the magnetic moment of individual spin cluster, H is applied external magnetic field. f(D)dD is the log-normal cluster diameter distribution function with mean cluster diameter D_m and width σ.

$$f(D)\, dD = \frac{1}{\sqrt{2\pi D}} exp\left(\frac{-ln\left(D/D_m\right)^2}{2\sigma^2}\right) dD \tag{1.3}$$

If inter-particle interaction is taken into the consideration then classical Langevin's theory is modified with the mean field theory in which Langevin parameter α is defined as [32, 33];

$$\alpha = \frac{\mu(H+H_{int})}{k_B T} \tag{1.4}$$

Here, $H_{int} = \lambda M_1$; λ is mean field constant (dimensionless) and M_1 is the internal field acting on each particle/cluster.

$$M = M_s \int_0^\infty f(D)\, L\, \left(\frac{\mu(H+H_{int})}{k_B T}\right) dD \tag{1.5}$$

1.3 APPLICATIONS OF MAGNETIC FLUIDS

Applications of magnetic fluids can be broadly classified into two categories:

1.3.1 Biomedical applications

1.3.2 Engineering Applications

1.3.1 Biomedical applications

1.3.1.1 Magnetic drug targeting

Magnetic drug targeting is a proposed therapy which can be used to treat malignant tumours by targeting chemotherapeutics drugs tagged with magnetic carriers by means of external magnetic field. The principle of magnetic drug targeting is to deliver the drug to the tumour region without harming healthy tissues. Magnetic fluids loaded with anticancer drugs are injected into the tumour and localized by means of external magnetic field at the targeted site. In this therapy, the amount of drug required is much lower than that required in conventional chemotherapy. When the magnetic field is turned off, the drug along with magnetic nanoparticle carrier disperses in blood and eventually removed from the blood stream by the plasma proteins **(Fig. 1.4.)** [34]. Since the total amount of drug to be delivered is very small, there is very little or no side effects of this therapy [34].

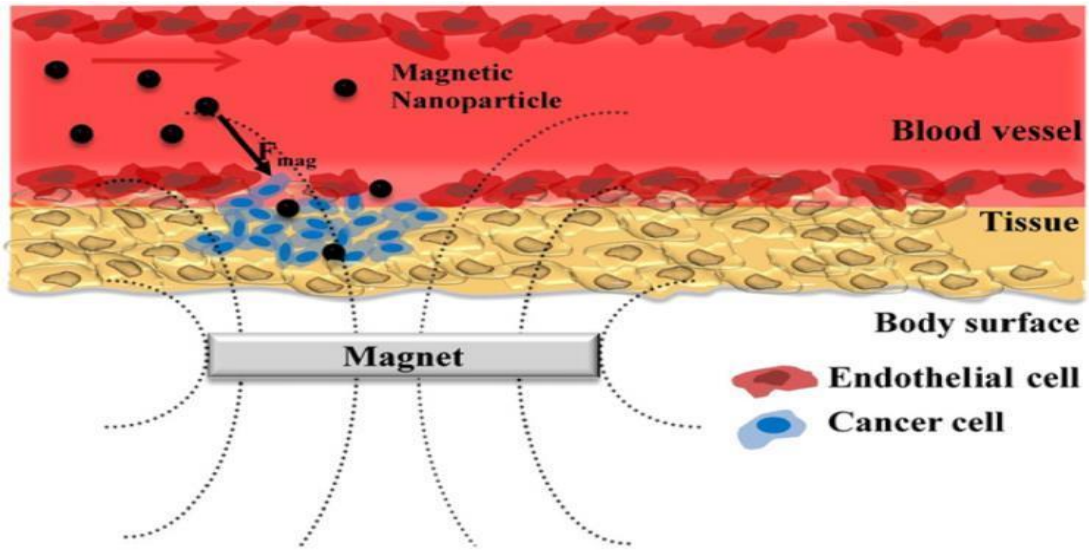

Fig. 1.4. Schematic diagram representing the concept of magnetic drug targeting [35].

1.3.1.2 Magnetic cell separation

The separation of target cells from the untargeted cells, and the maintenance of the membranes of target cells and untargeted cells, are particularly important in biomedicine. Magnetic cell separation using biocompatible nanoparticles is one way to achieve this. This process involves

- Labelling / tagging of specific cells with magnetic nanoparticles coated with polymers like dextran or polyvinyl alcohol.
- Separating out of these labelled entities via a fluid-based magnetic separation device, which is made by passing it through a region in which there is a magnetic field gradient which can immobilize the tagged material by external magnetic field (**Fig. 1.5.)** [36].

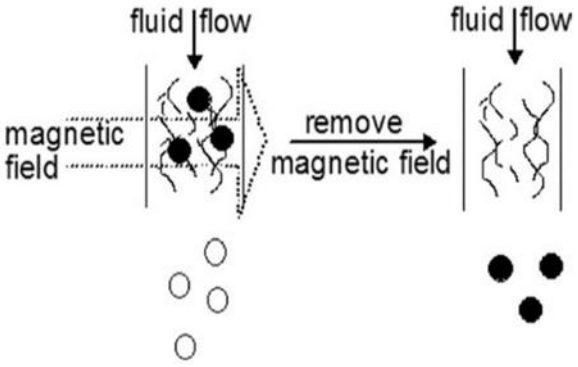

Fig. 1.5. Schematic representation of magnetic cell separation [36].

Cell separation can be used to clean up bone marrow from cancer infected samples. In this case, magnetic nanospheres coated with monoclonal antibodies having affinity towards tumour cells are used. When marrow removed from the patient, it is put in contact with the coated spheres in a liquid solution, the tumour cells selectively attach to the surface of the spheres, which are then magnetically separated from the solution [34]. The clean bone marrow is then reintroduce into the patient.

1.3.1.3 Hyperthermia

Magnetic hyperthermia is a proposed treatment option for cancer, which is under active research. It is based on the idea that magnetic nanoparticles can generate heat in AC magnetic field, which can cause cell apoptosis in localized cancer region. In this method, magnetic fluids containing magnetic nanoparticles dispersed in a carrier liquid are targeted to the tumour site. Once localized, these magnetic nanoparticles are subject to an AC magnetic field **(Fig. 1.6.)**. Magnetic nanoparticles generate heat due to hysteresis loses, which kills the cells in the surrounding cancerous tissues. For hyperthermia treatments temperature profile in the malignant tissue region is very important. The ideal temperature profile is one where the body temperature in healthy tissue is maintained, while the therapeutic temperature of 42 °C inside the tumour is achieved by choosing appropriate biocompatible magnetic fluids containing magnetic

nanoparticles having their Curie temperature in the vicinity of therapeutic temperature of 42 – 45 °C [37].

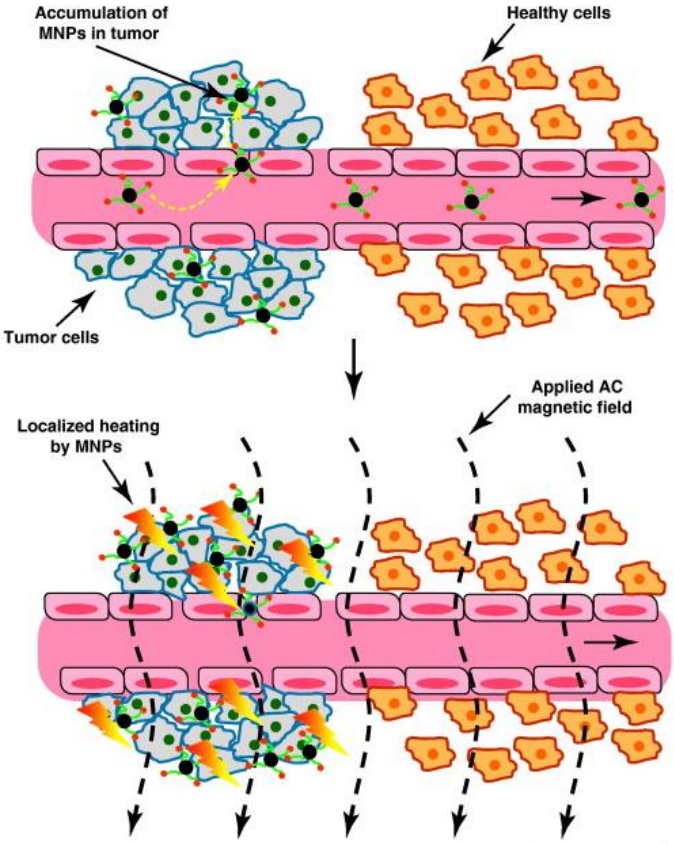

Fig. 1.6. Schematic representation of magnetic hyperthermia [38].

1.3.1.4 Contrast enhancement for Magnetic Resonance Imaging

Magnetic resonance imaging (MRI) is used to examine and diagnose variety of disorders in internal body structures. In conventional MRI, the contrast between the object under investigation and its surrounding medium is poor as it depends on the difference of relaxation time of H^+ in two mediums. Generally, this difference is not strong enough to render well resolved images. If magnetic nanoparticles from a biocompatible magnetic fluid are selectively absorbed by tissues, they give sharp contrast in the MRI image. Further, uptake of magnetic nanoparticles by various tissues will be different and hence their relaxation times also differs, thus providing MRI images with improved contrast [39].

1.3.2 Engineering Applications

1.3.2.1 Dynamic sealing

Computer hard disks operates in a hermetically closed box as powder or smoke can destroy the reading and writing process. Hence it is required to seal hermetically the hole through which the axle passes. It is done by introducing the magnetic fluid in between the magnet and the shaft (**Fig. 1.7.)**. The presence of external magnetic field keeps the fluid in the grooves, which blocks the passage of the foreign impurities. Presence of fluid provides frictionless motion to the shaft under hermetically sealed condition [40].

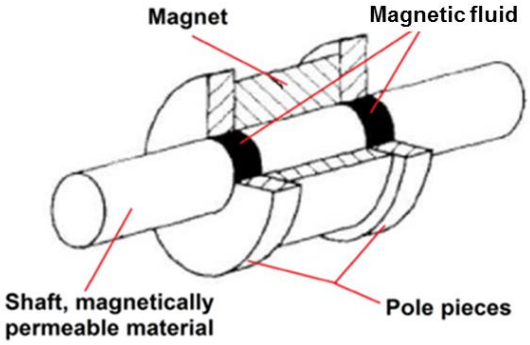

Fig. 1.7. Schematic diagram of dynamic seal using magnetic fluid [40].

1.3.2.2 Transformer cooling

Power transformers are usually cooled by mineral oils. As the oil is heated, it experiences decrease in the density. Oil in contact with the transformer coils absorbs highest amount of heat and as a result it becomes least dense and starts rising relative to the surrounding oil. The rising oil makes contact with the walls of the housing, transfers the heat to the walls and ultimately to the exterior environment. The cooled oil moves downward and replace the heated oil, which is rising from the windings. This natural convection, caused by the interplay between the gravity and heat induced density variation, represents the cooling mechanism most commonly used in commercial high power transformers [41].

Gravitational forces that circulate the oil are relatively weak. Temperature gradients across the oil reservoirs are often observed to be quite large, which results into poor heat transfer. Hence, to improve heat transfer, magnetic fluid can be used instead of the mineral oils

that surrounds the windings and core of the transformer. Magnetic fluid can improve the cooling efficiency of transformers by enhancing the fluid circulation within windings because of the magnetically driven fluid flow. Magnetic field surrounds the windings and core of the transformer. This "leakage field" because of the current in the windings reflects imperfect channelling of magnetic flux into the core (**Fig. 1.8.)** [42, 43]. Its strength is highest in the immediate vicinity of the core and windings and falls of rapidly with increasing distance. This magnetic field gradient draws the magnetic fluid towards the core. Since the core and windings generate heat, the temperature of the fluid rises as it approaches towards the core, resulting into the loss of magnetic properties and decrease in the density. Magnetic fluid starts rising as the gravitational effect of density reduction begins to overcome the weakening of magnetic attraction. Movement of hot magnetic fluid is assisted by the attraction exerted by the core and windings on cooler more intense magnetic fluid, which displaces the hot rising fluid as it moves towards the core. Movement away from the heat source and contact with the walls of the housing causes the hot magnetic fluid to cool and reacquire magnetization. This convection cycle driven by the magnetic and gravitational forces involves much faster fluid flow and therefore greater cooling efficiency can be achieved with thermomagnetic cooling [42].

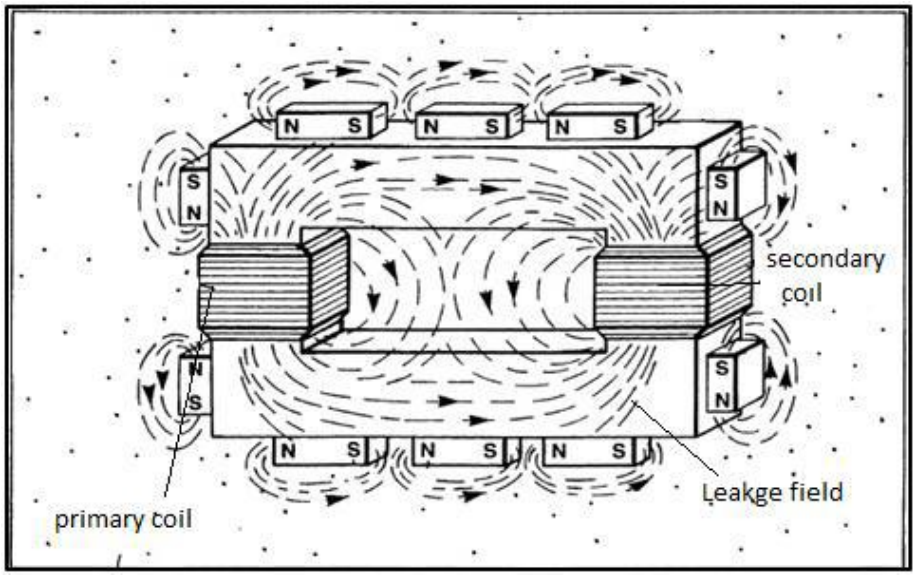

Fig. 1.8 Schematic representation of thermomagnetic cooling in power transformers [42].

1.4 TEMPERATURE SENSITIVE MAGNETIC FLUIDS

To use magnetic fluids in heat exchange devices, they should possess large thermomagnetic coefficient and suitable Curie temperature, which should be matching with the operating

temperature of transformer. Temperature sensitive magnetic fluids suitable for cooling applications in high power transformers should have Curie temperature between 70 °C to 300 °C [42]. Ferrites are generally used to prepare temperature sensitive magnetic fluids [42 - 44]. Magnetic properties can be tuned by choice of bivalent (M^{2+}) metal ions, which may be a single metal species or a combination of two or more species. The variable parameters include particle size, shape, surface properties, Curie temperature and saturation magnetization. Most substituted ferrites used in the preparation of magnetic fluids tend to have Curie temperatures that are too high for practical use in transformers. Curie temperature of mixed metal ferrites lie between 100 °C to 200 °C **(Table 1.1).** In addition, some ortho ferrites and rare-earth garnets have low Curie temperatures. Amongst them $Mn_{1-x}Zn_xFe_2O_4$ (MZ) ferrite nanoparticles are well suited for thermomagnetic cooling, because of their moderate saturation magnetization and tunable Curie temperature [1, 45].

Table 1.1: Curie temperature of various ferrite nanoparticles [42].

Ferrite nanoparticles	Curie Temperature (°C)
$Zn_{0.6}Co_{0.5}Fe_{1.9}O_4$	115
$Mg_{0.5}Zn_{0.5}Fe_2O_4$	120
$Ni_{0.3}Zn_{0.7}Fe_2O_4$	130
$Ni_{0.2}Zn_{0.6}Fe_{2.2}O_4$	145
$Mn_{0.5}Zn_{0.5}Fe_2O_4$	150
$MnFe_2O_4$	300

1.5 STABILITY OF TEMPERATURE SENSITIVE MAGNETIC FLUIDS

Stability of temperature sensitive magnetic fluids play an important role for cooling applications in power transformers. Magnetic particles needs to be dispersed in carrier fluids with high colloidal stability for long periods without significant aggregation [19, 46]. Particles in dispersion may adhere together and form aggregates of larger size and random shapes which may settle down under gravity. Stability denotes that the particles do not aggregate at a significant rate. The agglomeration of magnetic nanoparticles in fluids can cause clogging of

microchannel in transformers. Particle agglomeration also decreases the thermal conductivity of magnetic fluids. One of the important parameter that effects the stability of the magnetic fluids is the size of nanoparticles and its distribution. Small size nanoparticles and narrow size distribution is essential to prepare stable magnetic fluids [1].

1.6 AGING OF TEMPERATURE SENSITIVE MAGNETIC FLUIDS

In temperature sensitive magnetic fluids; magnetization of fluid strongly depends on the fluid temperature. When exposed to temperature gradient, they exhibit magnetic convection in addition to natural convection caused by the density gradient. This additional drag force enhances the cooling efficiency of the fluid and thus improves their performance in transformers. Magnetic nanoparticles dispersed in transformer oil should be able to withstand the device's operating temperature without any loss in their dispersity [19]. One of the important parameter that effects the stability of the magnetic fluids at elevated temperature is agglomeration of nanoparticles. The presence of surfactant coated magnetic nanoparticles helps in improving the heat dissipation of the magnetic fluids by preventing the particle agglomeration even when a strong magnetic field is present. When fluids subject to high temperatures for long period, thermal stress reduce the surfactant capping [47]. Another parameter that effects the stability of the magnetic fluids is the size of nanoparticles and its distribution. Nanoparticles in fluids when subjected to accelerated thermal aging can have enhance temperature induced aggregation of nanoparticles. This temperature dependent aggregation could significantly reduce cooling efficiency of magnetic fluids in transformers. Hence, it is essential to prepare magnetic fluids having high colloidal stability at elevated temperatures.

References

1. R. E. Rosensweig, *Ferrohydrodynamics*, Dover Publications, Inc., New York, (1997).
2. R. V. Mehta, R.V. Upadhyay, *Current Science* **76** (1999) 305.
3. B. Berkovski and V. Bashtovoy, *Magnetic Fluids and Applications Handbook*, Begell House, Wallingford (1996).
4. T. Albrecht, C. Buchrer, *Appl Phys A Mater Sci Process* **65** (1997) 215.
5. S. W. Charles and J. Popplewell, *Ferromagnetic Material*, E. P. Wohfarth, North-Holland Publishing Company **2** (1980).
6. R. Massart, *IEEE Trans. Magn*. **17** (1981) 1247.
7. J. Depeyrot, G. J. Silva, C. R. Alves, E. C. Sousa, M. Magalhaes, A. M. Figueiredo Neto, M. H. Sousa, F.A. Tourinho, *Braz. J. Phys*. **31** (2001) 390.
8. R. Massart, E. Dubois, V. Cabuil, E. Hasmonay, *J. Magn. Magn. Mater.* **149** (1995) 1.
9. E. Dubois, *PhD. Thesis*, Université Pierre et Marie Curie, Paris **6** (1997).
10. E. Hasmonay, *PhD. Thesis*, Université Pierre et Marie Curie, Paris **6** (1998).
11. A. Joseph, S. Mathew, *Chem Plus Chem.* **79** (2014) 1382.
12. M. Faraji, Y. Yamini, and M. Rezaee, *J. Iran. Chem. Soc.* **7** (2010) 1.
13. U. Jeong, X. Teng, Y. Wang, H. Yang, Y. Xiaet, *Adv. Mater.* **19** (2007) 33.
14. M. Mahmoudi, S. Sant, B. Wang, S. Laurent, T. Senet, 2011, *Adv Drug Deliv Rev* **63** (2011) 24.
15. J. Vicente, D. J. Klingenberg, R. Hidalgo-Alvarez, *Soft Matter* **7** (2011) 3701.
16. M. T. Lopez-Lopez, A. Gomez-Ramirez, L. Rodriguez-Arco, *Langmuir* **28** (2012) 6232.
17. A.Yu. Zubarev, L.Yu. Iskakova, *Physica A* **335** (2004) 314.
18. A. O. Ivanov, S. S. Kantorovich, *Phys. Rev. E.* **70** (2004) 021401.
19. K. Parekh, RV Upadhyay, *Indian J. Eng. Mater. Sci.* **11** (2004) 262.
20. K. Rana, P. Thakur, P. Sharma, M. Tomar, V.Gupta, A. Thakur, *Ceram. Int.* **41** (2015) 4492.
21. V. Skumeyev, S. Stoyanov, Y. Zhang, G. Hadjipanayis, D. Givord, J. Nogues, *Nature* **423** (2003) 850.
22. Y. W. Jun, J. W. Seo, J. Cheon, *Acc. Chem. Res.* **41** (2008) 179.
23. S. Jauhar, J. Kaur, A. Goyal, S. Singhal, *RSC Adv.,* **6** (2016) 97694.
24. W. H. Lin, S. K. J. Jean, C. S. Hwang, *J. Mater. Res.* **14** (1999) 204
25. N. M. Deraz, A. Alarifi, *Int. J. Electrochem. Sci.* **7** (2012) 6501.
26. J. H. Lee, Y. M. Huh, Y. W. Jun, J. W. Seo, J. T. Jang, H. T. Song, S. Kim, E. J. Cho, H. G. Yoon, J. S. Suh, *J. Cheon, Nat. Med*. **13** (2006) 95.
27. M. Atif, S. K. Hasanian, M. Nadeem, *Solid State Commun.* **138** (2006) 416.
28. S. Ammar, N. Jouini, F. Fievet, Z. Beji, L. Smiri, P. Moline, M. Danot, J. M. Greneche, *J. Phys.: Condens. Matter* **18** (2006) 9055.
29. L. Vekas, *Adv Sci Tech* **54** (2008)127.
30. S. Odenbach, *Magnetoviscous Effects in Ferrofluids*, Springer-Verlag: Berlin, Heidelberg. (2002).
31. M. Knobel, W. C. Nunes, A. L. Brand, J. M. Vargas, L. M. Socolovsky, D. Zanchet, *Physica B* **354** (2004) 80.

32. B. D Cullity, *Introduction to magnetic materials,* Reading, Mass., Addison-Wesley Pub. Co. (1972).
33. M. D. Mukadam, S. M. Yusuf, P. Sharma, S. K. Kulshreshtha, *J. Magn. Magn. Mater*. **269** (2004) 317.
34. R. E. Rosensweig, *Conceptual applications of magnetic fluids,* Chapter in Magnetic fluids and applications handbook, (1996) 589.
35. A. Grillone, G. Ciofani, *Chem. Eur. J.* **23** (2017) 16109.
36. Q. A. Pankhurst, J. S. Connolly, S. K. Jones, J. Dobson, *J. Phys. D: Appl. Phys*. **3** (2003) R167.
37. S. Laurent, S. Dutz, U. O. Hafeli, M. Mahmoudi, *Adv. Colloid Interface Sci.* **166** (2011) 8.
38. A. J. Cole, V. C. Yang, A. E. David, *Trends Biotechnol.* **29** (2011) 323.
39. Q. A. Pankhurst, J. Connolly, S. K. Jones, J. Dobson, *J. Phys. D: Appl. Phys.* **36** (2003) R167
40. K. Raj, R. Moskowitz, *J. Magn. Magn. Mater.* **85** (1990) 233.
41. *Transformer Cooling System Improvements: Analysis and Recommendations*. EPRI, Palo Alto, CA: 1010585 (2005).
42. K. Raj, R. Moskowitz, US Patent No. 5,462,685 (1995).
43. T. Cader, S. Bernstein, Clayton Crowe, US Patent No. 5898353 (1999).
44. W. C. Elmore, *Phys. Rev*, **54** (1938) 309.
45. C. L. Sansom, P. Jones, R. A. Dorey, C. Beck, A. Stanhope-Bosumpim, J. Peterson, *J. Magn. Magn. Mater.* **335** (2013) 159.
46. U. Banerjee, P. Bit, R. Ganguly, S. Hardt, *Microfluid Nanofluid* **13** (2012) 565.
47. B. Venkatraman, J. Kumar, O. Kumar, S. V. Ramagopal, *J. Mat. Sci. Mech. Eng.* **1** (2014) 131.

CHAPTER 2

LITERATURE REVIEW

2.1 INTRODUCTION

Magnetic nanoparticles of iron, nickel, cobalt and manganese, their alloys and their oxides are used for the synthesis of magnetic fluids [1-3]. The choice magnetic nanoparticles for fluids depends on their application. In order to use magnetic fluid for transformer cooling applications, it requires large pyromagnetic coefficient i.e. fluid with high saturation magnetization and low Curie temperature. Therefore, synthesis of magnetic nanoparticles with tunable magnetization and Curie temperature is of great interest. Ferrites are widely used in the preparation of temperature sensitive magnetic fluids [4-7]. Amongst them Zn-containing spinel ferrites ($M_{1-x}Zn_xFe_2O_4$) are most attractive because it is possible to tune their magnetic properties by small variation in the content of Zn.

Physical and chemical properties of ferrite nanoparticles largely depends on the synthesis method and preparation conditions. Several techniques have been developed to synthesize ferrite nanoparticles. In this literature review we compare the influence of synthesis methods and conditions of synthesis on the properties of $Mn_{1-x}Zn_xFe_2O_4$ (MZ) nanoparticles. The literature survey is also focused on the effect of synthesis variables on the size and size distribution of nanoparticles and their correlation with the magnetic properties. This chapter also cover literature available on the preparation of magnetic fluids. A brief review is also presented on the structural and magnetic properties of magnetic nanoparticles. In the last section of this chapter, a limited literature on colloidal stability and thermal aging of magnetic fluids are presented.

2.2 SYNTHESIS OF MZ NANOPARTICLES

This section reviews literature on synthesis of MZ nanoparticles. MZ nanoparticles are generally synthesized by high energy ball-milling [8], hydrothermal method [9], auto-combustion method [10], sol-gel process [10], micro-emulsion technique [12], and co-precipitation method [13].

Arcos et al. [14] introduced **high energy ball-milling process** for preparation of MZ nanoparticles. MZ nanoparticles with particle size in the range of 40 – 51 nm were obtained. It

was observed that the particles obtained by ball-milling process were large and non-uniform. Ball-milling also introduce strain into the crystal lattice of nanoparticles.

Rath et al. [15] proposed **hydrothermal process** to synthesize ultra-fine and relatively strain free MZ nanoparticles with narrow size distribution. $Mn_{0.65}Zn_{0.35}Fe_2O_4$ nanoparticles with size 9 – 12 nm were synthesized by controlling the pH of precipitation. Although the particles were small, but were not superparamagnetic. The cation distribution in the nanoparticles was different from the normal spinel structure observed in bulk ferrites. Rath et al. [16] have studied the influence of cation distribution on magnetic properties (H_c, M_s and T_c) and size of MZ nanoparticles. They have observed that the particle size decreases with increasing Zn content. MZ nanoparticles synthesized by hydrothermal route contains hematite (α-Fe_2O_4). The presence of this secondary phase makes the correlation difficult between microstructure and magnetic properties of MZ nanoparticles. Wang et al. [17] have synthesized MZ nanoparticles by hydrothermal method. They have concluded that the magnetic properties of spinel ferrite nanoparticles depends on the occupancy of bivalent metal ion at tetrahedral A–sites in spinel matrix. Aggregation of nanoparticles are usually observed when synthesized by hydrothermal route. This method is also very costly and not suitable for bulk production of nanoparticles.

Mangalaraja et al. [8] proposed low cost **auto-combustion method** for the synthesis of MZ nanoparticles. They have synthesized $Mn_{0.8}Zn_{0.2}Fe_2O_4$ nanoparticles with moderate crystallinity. Deraz et al. [18] reported synthesis of $Mn_{0.5}Zn_{0.5}Fe_2O_4$ nanoparticles by auto-combustion method by using mixture of glycine and ammonium nitrate. Synthesized nanoparticles possess high saturation magnetization (85 emu/g), the remnant magnetization (22 emu/g) and coercivity (58 Oe) owing to their large size. Ping Hu et al. [19] studied effect of heat treatment on the structural and magnetic properties of MZ nanoparticles prepared by auto-combustion method. When annealed at 550 °C, it decomposes into Fe_2O_3 and Mn_2O_3. Angadi et al. [20] reported synthesis of spinel MZ nanoparticle with average crystallite size of 25 – 30 nm. It was prepared by solution combustion method using mixture of urea and glucose. They have observed that lattice parameter, cell volume, saturation magnetization, remanence magnetization and magneton number decreases with increase in Zn^{2+} concentration in MZ nanoparticles. This method yields nanoparticles with improved phase, large size and broad size distribution. Clustering of nanoparticles is difficult to control. Yield is also low and process is difficult to scale-up.

Limin et al. [21] proposed **sol-gel method** for the synthesis of MZ nanoparticles. The average crystallite size of nanoparticles was 60 – 90 nm. This method was simple, fast and produced MZ nanoparticles at low temperature. They have studied effect of calcination temperature on the grain size of nanoparticles. The grain size increases with increase in the calcination temperature. Azadmanjiri et al. [22] synthesized $Mn_{0.8}Zn_{0.2}Fe_2O_4$ nanoparticles with particle size 70 – 80 nm by sol-gel method using nitrate citrate gel and studied the effect of sintering temperature on the magnetic properties of MZ nanoparticles. They observed that nanoparticles did not show saturation in magnetization even at high magnetic fields. Chand et al. [23] synthesized Mn substituted Zn ferrite ($Mn_xZn_{1-x}Fe_2O_4$) nanoparticles by sol-gel method using glycol. They have observed high agglomeration of nanoparticles with relatively less saturation magnetization (13 – 25 emu/g) as compared to bulk and high coercivity (127- 320 Oe).

Dahotre et al. [24] synthesized MZ nanoparticles by sol-gel method using citric and ethylene glycol. They reported formation of Fe_2O_4 and MZ phases. Saturation magnetization, remnant magnetization and coercivity; all decreases with increase in the Zn content in MZ nanoparticles. They attributed these changes in magnetic properties to the variation in cationic stoichiometry and occupancies at interstitial sites. They also reported formation of magnetic dead layer on the surface of nanoparticles i.e. existence of spin canting is responsible for the observed decrease in magnetization with reduction in particle size. Winiarska et al. [25] have studied effect of precursor on the properties of MZ nanoparticles. They have reported that MZ nanoparticles obtained from the hydroxide precursor had larger crystallite size (35.6 nm) and heterogonous structure, whereas MZ nanoparticles obtained from the oxalate precursor had smaller crystallite size (29.6 nm) with heavy agglomeration. MZ nanoparticles prepared with citric acid and ethylenediaminetetraacetic acid (EDTA) had large crystallite size (40 nm) and loose sponge-like structure with fewer aggregation [26]. Sol-gel method is easy and economical, yield is acceptable and process can be scale-up without much pain. However difficulty in control over the size, aggregation and poor tunability of magnetic properties of MZ nanoparticles obtained by sol-gel method limits its utility.

Liu et al. [27] proposed **micro-emulsion technique** to synthesize nanocrystalline $MnFe_2O_4$ nanoparticles with narrow size distribution and negligible agglomeration. Superparamagnetic $MnFe_2O_4$ nanoparticles having size 4 to 15 nm were obtained by water-in-toluene reverse micelles formed by sodium dodecylbenzenesulfonate (NaDBS) surfactant. Morrison et al. [28] carried out the comparative study of MZ nanoparticles synthesized by

micro-emulsion and ball-milling process. They reported that the nanoparticles synthesized by ball-milling possess broad distribution of particle sizes, whereas micro-emulsion technique provides better control over size and morphology. Makovec et al. [29] studied the influence of particle size on specific magnetization of MZ nanoparticles. They reported the size controlled synthesis of $Mn_{0.5}Zn_{0.5}Fe_2O_4$ nanoparticles in water-CTAB-hexanol micro-emulsion. They concluded that the specific magnetization of the nanoparticles depends on the size of magnetic nanoparticles. The same group in another study [30] concluded that the pH after the precipitation should be > 8, as pH < 8 favors formation of nonmagnetic α-FeOOH phase. Micro-emulsion technique can produce nanocrystalline MZ nanoparticles with narrow size distribution and low agglomeration. However, the major limitation of this method is low yield.

Auzans et al. [31] proposed size controlled synthesis of MZ nanoparticles by **co-precipitation method**. Ultrafine MZ nanoparticles with particle size 6 – 19 nm were obtained by co-precipitation method. Arulmurugan et al. [11] reported synthesis of MZ nanoparticles having size < 12 nm by co-precipitation method. They have observed that saturation magnetization and Curie temperature of MZ nanoparticles decreases with increase in Zn content. Lan et al. [32] reported effect of Zn substitution on magnetic properties of MZ nanoparticles in terms of cation distribution. $Mn_{1-x}Zn_xFe_2O_4$ (x = 0 - 0.7) with particle size 8 – 19 nm were synthesized by co-precipitation method. They have observed that the Curie temperature of $Mn_{1-x}Zn_xFe_2O_4$ nanoparticles decreases with increase in Zn content, which was due to the substitution of non-magnetic Zn^{2+} at A–sites, which reduces the (A–B) inter lattice exchange interaction. Kareem et al. [33] reported effect of Zn substitution on structural properties of MZ nanoparticles synthesized by co-precipitation method. Zn substitution in MZ nanoparticles changes its crystal structure from normal spinel structure to inverse spinel or mixed spinel depending on the degree of Zn substitution. Zn substitution did not affect the morphology of nanoparticles but their particle size decreases with increase in Zn substitution.

Amongst all methods of MZ nanoparticle's synthesis, chemical co-precipitation method is economical, reproducible and easy to scale-up. Hence, **chemical co-precipitation method** is widely explored for the synthesis of MZ nanoparticles.

2.3 PREPARATION OF MAGNETIC FLUID

This section reviews existing literature on preparation of magnetic fluids. The first study on preparation of water based magnetic fluids was reported by Elmore [34] in 1938. Intensive

research on magnetic fluids did not start until 1960. Pappel et al. [35] in 1965 synthesized first stable magnetic fluid by grinding magnetite in ball-mill with oleic acid and heptane. This magnetic fluid was stable for more than six months. The major disadvantage of this method was its long production time, low productivity, contamination and broad size distribution. In 1973, Khalafalla and Reimers first proposed a chemical method for the preparation of Fe_3O_4 based sterically stabilized magnetic fluid by using nonmagnetic precursor such as suboxide of iron compounds [36].

Zins et al. [37] in 1999 reported synthesis of charge stabilized aqueous magnetic fluid without stabilizing agent. They synthesized aqueous magnetic fluids by chemical method and studied their stability as a function of pH. They observed that the particle size of magnetic nanoparticles is most critical parameter as far as its stability is concerned.

Bica et al. [2] proposed the synthesis of concentrated magnetic fluids with polar liquids, C_3–C_{10} (propanol, .., decanol) alcohols as carriers and double layer steric stabilization with oleic acid and dodecylbenzensulphonic acid. High colloidal stability of magnetic fluids with hydrodynamic volume fraction ~0.65 was observed in polar medium while in aqueous medium this stability starts falling as the volume fraction of magnetic particles increases.

Xing-ping Qiu et al. [38] proposed the stabilization of magnetic fluids by using organic solvents. They reported synthesis of polyvinyl alcohol (PVA) and dextran stabilized Fe_2O_4 nanoparticles based magnetic fluids. Particle size increases with increase in PVA concentration, while particle size decreases with increase in dextran concentration. Lin et al. [39] prepared magnetic fluids with Fe_2O_4 nanoparticles which are coated with poly (acrylic acid) (PAA). The PAA oligomers provides both the electrostatic and steric repulsion against particle aggregation. Wang et al. [40] synthesized γ-Fe_2O_3 nanoparticles based aqueous magnetic fluids. It was observed that the magnetic fluids were stable over the pH range of 4 – 12. Mandel et al. [41] also reported that steric stabilization in water based magnetic fluids was lost above pH 12. Ramimoghadam et al. [42] synthesized magnetic fluids in which Fe_3O_4 nanoparticles were coated with dodecanoic acid. It was observed that dodecanoic acid increases the dispersion stability of magnetite nanoparticles and reduces their polydispersity. These fluids were stable in pH range from 4 to 12.

Jacintho et al. [43] proposed synthesis of magnetic fluids having ferrite nanoparticles coated with fatty acids of raw vegetable oils such as soybean and castor oil and dispersed them

in cyclohexane. These raw fatty acids stabilized magnetic fluids were stable and readily usable in nonpolar media. Sahoo et al. [44] reported synthesis of magnetic fluids by stabilizing the magnetite nanoparticles with oleic acid (OA), lauric acid, dodecyl phosphonate, hexadecyl phosphonate, and dihexadecyl phosphate. It was reported that alkyl phosphonates and phosphates can be used for obtaining thermodynamically stable dispersions of magnetic ferrite nanoparticles. It was also observed that the phosphonate / phosphate coated particles suffered from lower dispersibility as compared to oleic acid coated nanoparticles. Oleic acid coated nanoparticles were readily dispersible in nonpolar solvent, while lauric acid coated nanoparticles were partially dispersed in non-polar solvents.

Sartoratto et al. [45] synthesized maghemite nanoparticles based temperature sensitive magnetic fluids. Nanoparticles were coated with either oleate or decanoate and dodecanoate. Colloidal stability at 90 °C was highest for oleate-grafted maghemite-based magnetic fluid, whereas decanoate and dodecanoate-grafted fluids were unstable. Yue-hua et al. [46] studied the effect of cation on the dispersibility of oleate coated magnetite nanoparticle based magnetic fluids with sodium chloride, calcium chloride and aluminium chloride. It was observed that magnetic fluids with sodium chloride gives better colloid dispersibility. They have also studied effect of anions on the dispersibility of oleate coated magnetite based magnetic fluids by using sodium chloride, sodium sulphate and sodium phosphate. It was concluded that aqueous magnetic fluid with sodium oleate as dispersant show better dispersibility in acidic medium.

Caruntu et al. [47] reported synthesis of magnetic fluids with particles coated with oleates and dispersed in polyols. It was observed that increase in inter-particle distance with dilution led to a higher anisotropy which, in turn, led to substantial increase in the coercivity and blocking temperature. Maity et al. [48] reported synthesis of magnetic fluids with superparamagnetic nanoparticles suspended in aqueous and non-aqueous media by coating nanoparticles with single and bilayer of oleic acid. Better dispersion of nanoparticles was observed in non-aqueous media. Lopez-Lopez et al. [49] reported synthesis of magnetic fluids with oleate coated magnetite nanoparticles in different organic solvents with dielectric constant, ranging from 1.8 to 9. It was observed that magnetic fluids prepared in liquids like kerosene, mineral oil, dodecane, carbon tetrachloride, and chloroform with low dielectric constant ($\varepsilon_r < 5$) were stable. They demonstrated from thermodynamic analysis that stability of the suspensions in liquids with low dielectric constant ($\varepsilon_r < 5$) was well correlated with the low lyophobic attraction between the particles, which can easily surmounted by thermal agitation, since the

van der Waals attraction was negligible. In contrast, for liquids with $\varepsilon_r > 5$ like CH_2Cl_2 and water, the suspensions become unstable because of the combined action of the Van der Waals and lyophobic attractions, the latter being dominant for strong polar solvents.

Parekh et al. [50] synthesized Fe–Zn ferrite magnetic fluids having low Curie temperature and moderate saturation magnetization for use in energy conversion devices. They observed that magnetization of fluids decreases with increase in the Zn content. Arulmurugan et al. [51] reported synthesis of Co–Zn magnetic fluid. Curie temperature of the fluid decreases from 415 °C to 267 °C with increase in Zn substitution in ferrite nanoparticles. Vaidyanathan et al. [52] reported synthesis of temperature sensitive Co–Zn magnetic fluid using transformer oil as carrier. The magnetic particle size and saturation magnetization decreases with increase in zinc substitution.

Upadhyay et al. [53] synthesized Gd substituted Mn–Zn ferrite based temperature sensitive magnetic fluids. Saturation magnetization, Curie temperature and pyromagnetic coefficient, all increases with Gd substitution. Ortiz et al. [54] reported the synthesis of Gd and Eu substituted Mn–Zn magnetic fluid. Curie temperature increases with Gd substitution and it decreases with Eu substitution in $Mn_{0.8}Zn_{0.2}Fe_2O_4$. Arulmurugan et al. [55] synthesized Mn–Zn ferrite based temperature sensitive magnetic fluid in heptane by using oleic acid as surfactant. The Curie temperature decreases from 360 °C to 160 °C and specific magnetization decreases from 148 G to 120 G with the increase in zinc substitution.

2.4 PROPERTIES OF TEMPERATURE SENSITIVE MAGNETIC FLUIDS

2.4.1 Structural properties

Chikazumi et al. [56] have shown that magnetic nanoparticles form chain-like clusters due to dipole-dipole interaction in magnetic fluids. They observed that when a weak field was applied, particles tend to form micro-clusters elongated parallel to the field. Further increase in magnetic field causes growth of clusters, resulting into the formation of macrostructures.

Horng et al. [57] revealed that two separate chains merge and elongate under higher magnetic field. They observed that chains also tend to elongate when the particle concentration was increased. They have also reported that magnetic fluids prepared with polydispersed particles forms needle like structure while fluids prepared with monodispersed nanoparticles

form column like structures [58]. Butter et al. [59] reported the presence of linear clusters in magnetic fluids even in zero magnetic field. They observed that the chains grow larger in the field direction as well as in direction perpendicular to the magnetic field. Zubarev et al. [60] studied the formation of chain like structures in polydispersed magnetic fluids. They have observed that the magnetic interaction decreases the chain length while steric interaction increase the chain length. Rajnak et al. [61] reported the formation of visually observable patterns in dilute low-polarity magnetic fluids when exposed to external electric field. The presence of space charge and its motion towards electric field gradients was assumed to be a trigger for the colloidal cloud formation. They revealed that electrical forces due to space charge and permittivity variation induced the pattern formation in magnetic fluids.

2.4.2 Magnetic properties

Blums et al. [62] performed the magnetogranubmetric analysis of magnetic fluids by using Langevin model of non-interacting subdomain particles. They have observed that instead of log-normal particle size distribution, it follows a more complex distribution of magnetic moments. They have reported that decrease in magnetization of small particles was due to the presence of canted spin structure on the surface of nanoparticles. Maiorov et al. [63] studied the magnetic properties of MZ magnetic fluids. They have used high field approximation and decompose the magnetization curve into a spectrum of Langevin functions having different magnetic moments to estimate the spontaneous magnetization of the fluid. Desai et al. [64] used the modified Langevin's theory by incorporating inter-particle interactions to fit the virgin curve of particle magnetization. It was observed that mean field constant decreases with increase in the particle size and saturation magnetization. Further, with decrease in Zn-content in MZ magnetic fluids, their particle size, domain magnetization and Curie temperature increases linearly [65]. They have reported that this linear variation in saturation magnetization and Curie temperatures were function of cationic distribution and occupancies of octahedral and tetrahedral sites, which in turn affects the inter (J_{AB}) and intra magnetic interactions (J_{AA}, J_{BB}).

Ivanov et al. [66] reported the process of finding particle size distribution from the experimental magnetization curves for polydispersed magnetite magnetic fluid at various concentrations by using modified mean field theory of second order. To check the consistency, extensive molecular dynamics and Monte Carlo simulations were performed for systems with different particle size distributions. A perfect match between experimental, theory and computer simulations proved that the modified mean field theory of second order is an effective tool for

the magnetogranulometric analysis of magnetic fluids with wide range of concentrations. Solovyova et al. [67] studied the effect of polydispersity on the magnetostatic properties of magnetic fluids by using extended second-order modified mean-field theory. The theoretical predictions were tested rigorously against results from Monte Carlo simulations of monodisperse, bidisperse, and polydisperse magnetic fluids. Comparisons were made between systems with the same Langevin susceptibility and the same saturation magnetization. For initial susceptibility, second-order modified mean-field theory was most accurate for the monodisperse model, while the new theory worked best for polydisperse systems with a significant proportion of large particles.

2.5 COLLOIDAL STABILITY OF MAGNETIC FLUIDS

Mendenhal et al. [68] demonstrated that short term stability of magnetic fluids was independent of the nature of surfactant and long-term stability of magnetic fluids was function of the pH of the medium, surfactant concentration and its molecular weight. Yerin [69] reported that that when magnetic fluids were diluted, their colloidal stability was distributed by the formation of aggregate macrostructures. It was observed that these aggregated nanoparticles got dispersed in 2 – 4 days. Jozefczak et al. [70] reported effect of temperature on particle size distribution of transformer oil-based magnetic fluids. Samples with different volume concentrations of magnetite nanoparticles were prepared by subsequent dilution. They have observed that with increase in the temperature, larger structures split into aggregates consisting of two or more nanoparticles.

Pop et al. [71] reported long term stability of magnetic fluids under low gradient magnetic fields. They have observed that exposure of magnetic fluids to low gradient magnetic fields for long term led to the formation of clusters. Kudelcik et al. [72] studied structural changes in magnetic fluids with external magnetic field and temperature. They observed that when magnetic field was increased, the interaction between external magnetic field and the magnetic moments of the nanoparticles resulted into aggregation of magnetic nanoparticles followed by cluster formation. At temperatures above 30 °C the influence of external magnetic field on cluster formation was negligible as the thermal energy exceeds the magnetic energy. Thirupathi et al. [73] reported formation of chains in magnetic fluids with increasing magnetic field. Formation and destruction of magnetically induced structures influences the interactions between magnetic nanoparticles and hence the formation of aggregates. Hornowski et al. [74] had observed formation of chain like aggregates in diluted magnetic fluids and homogeneous

drop-like structures in dense magnetic fluids. Durdureanu-Angheluta et al. [75] studied the colloidal stability of magnetic fluid with aging by calculating % age weight loss with time. They have reported that magnetic fluids were stable upto 90 days.

2.6 ACCELERATED THERMAL AGING OF MAGNETIC FLUIDS

Effect of elevated temperature on physical and insulating properties of magnetic fluids was studied by Segal et al. [76]. Transformer oil based magnetic fluid sample was subject to thermal aging. Studies carried out for 34 and 50 weeks at 185 °C have shown little degradation in the thermal and colloidal stability of magnetic fluids. It was concluded that the magnetic fluids' integrity was not affected by long term exposure to elevated temperatures (185 °C). No change was observed in the dielectric properties of magnetic fluids as well. In another study, they have reported that magnetic fluids retain their colloidal stability and its initial magnetic susceptibility even at very low magnetization when exposed to magnetic field gradients for long time [76, 77].

In recent reports by Patel et. al. [78 , 79], they have estimated normal life expectancy of MZ magnetic fluids by using Arrhenius rate equation by measuring winding temperature of transformer submerged in magnetic fluid which was subjected to normal load and over load conditions. Patel et al. showed that under over loading condition for about 24 h, the insulation degradation reduced the normal life of a transformer by 27 days when it is immersed in transformer oil, whereas in case of magnetic fluid normal life reduced by only 3 days.

From the Literature surveys following gaps in study have been identified:

Gaps in the study

- Mixed metal ferrite nanoparticles having Curie temperature that is covering the entire operating range of transformers are not available.
- Application of magnetic fluids for heat transfer applications also depends on factors like particle size, shape, size distribution, etc., which needs to be understood before optimizing the magnetic fluid system.
- Very little information is available on the properties of temperature sensitive magnetic fluids at elevated temperatures, which are generally prevailing inside the power transformers.

- Colloidal stability of temperature sensitive magnetic fluids under accelerated aging is a major concern and it poorly understood.

Based on these shortcomings, following objectives have been defined for this assignment.

Objectives

1. Synthesis of stable temperature sensitive magnetic fluids from magnetic particle system ($Mn_{1-x}Zn_xFe_2O_4$), with requisite Curie temperature.
2. Investigate the effect of particle size and size distribution on stability and thermomagnetic properties of magnetic fluids.
3. Photon Correlation Spectroscopy (PCS) and Vibrating Sample Magnetometry (VSM) characterizations of as-synthesized and aged magnetic fluids to understand the effect of accelerated thermal aging on the stability of magnetic fluids.

References

1. K. Raj, L. M. Aziz, US Patent No. 5,958,282 (1999).
2. D. Bica, L. Vekas, M. Rasa, *J. Magn. Magn. Mater.* **252** (2002) 10.
3. L. Vekas, D. Bica, O. Marinica, M. Rasa, V. Socoliuc, F. D. Stoian, *J. Magn. Magn. Mater.* **289** (2005) 50.
4. K. Raj, R. Moskowitz, US Patent No. 5,462,685 (1995).
5. T. Cader, S. Bernstein, C. Crowe, US Patent No. 5,898,353 (1999).
6. R. V. Mehta, R.V. Upadhyay, *Current Science* **76** (1999) 305.
7. K. Parekh, R. V. Upadhyay, *Indian J. Eng. Mater. Sci.* **11** (2004) 262.
8. R. V. Mangalaraja, S. Ananthakmar, P. Manohar, F. D. Gnanam, M. Awano, *Mater. Sci. Eng. A.* **367** (2004) 301.
9. A. Thakur, P. Mathur, M. Singh, *J. Phys. Chem. Solids.* **68** (2007) 378.
10. P. K. Roy, B. B. Nayak, J. Bera, *J. Magn. Magn. Mater.* **320** (2008) 1128.
11. R. Arulmurugan, B. Jeyadevan, G. Vaidyanathan, S. Sendhilnatha. *J. Magn. Magn. Mater.* **288** (2005) 470.
12. W. H. Lin., S. K. J. Jean, C. S. Hwang, *J. Mater. Res.* **14** (1999) 204.
13. S. K. Pradhan, S. Bid, M. Gateshki, V. Petkov, *Mater. Chem. Phys*. **93** (2005) 224.
14. D. Arcos, R. Valenzuela, M. Vazquez, M. Vallet-Regi, *J. Solid State Chem.* **141** (1998) 10.
15. C. Rath, K. K. Sahu, S. Anand, S. K. Date, N. C. Mishra, R. P. Das, *J. Magn. Magn. Mater*. **202** (1999) 77.
16. C. Rath, S. Anand, R. P. Das, K. K. Sahu, S. D. Kulkarni, S. K. Date, N. C. Mishra, *J. Appl. Phys*. **91** (2002) 2211.
17. J. Wang, C. Zeng, Z. Peng, Q. Chen, *Physica B* **349** (2004) 124.
18. N. M. Deraz, A. Alarifi, *Int. J. Electrochem. Sci.*, **7** (2012) 5828.
19. P. Hua, H. Yang, D. Pan, H. Wang, J. Tian, S. Zhang, X. Wang, A. A. Volinsky, *J. Magn. Magn. Mater.* **322** (2010) 173.
20. V. J. Angadi, B. Rudraswamy, K. Sadhana, K. Praveena, *J. Magn. Magn. Mater.* **409** (2016) 111.
21. D. Limin, H. Zhidong, Z. Yaoming, W. Ze, Z. Xianyou, *J Rare Earth.* **24** (2006) 54.
22. J. Azadmanjiri, *J. Non-Cryst. Solids*, **353** (2007) 4170.
23. M. Chand, A. Kumar, Annveer, S. Singh, A. Shankar, R. P. Pant, *Indian J. Eng. Mater. Sci*. **18** (2011) 385.
24. S. G. Dahotre, L. N. Singh, *Arch Phys Res* **2** (2011) 81.
25. K. Winiarska, I. Szczygiel, R. Klimkiewicz, *Ind. Eng. Chem. Res.* **52** (2013) 353.
26. I. Szczygiel, K. Winiarska, *J. Therm. Anal. Calorim.* **115** (2014) 471.
27. C. Liu, B. Zou, A. J. Rondinone, Z. J. Zhang, *J. Phys. Chem. B.* **104** (2000) 1141.
28. S. A. Morrison, C. L. Cahill, E. E. Carpenter, S. Calvin, V. G. Harris, *J. Appl. Phys*. **93** (2003) 7489.
29. D. Makovec, A. Kosak, M. Drofenik, *Nanotechnology* **15** (2004) S160.
30. A. Kosak, D. Makovec, M. Drofenik, A. Znidarsic, *J. Magn. Magn. Mater.* **272–276** (2004) 1542.
31. E. Auzans, D. Zins, E. Blums, R. Massart, *J. Mater. Sci*. **34** (1999) 1253.
32. N. T. Lan, T. D. Hien, N. P. Duong, D. V. Truong, *J. Korean Chem. Soc.* **52** (2008) 1522.

33. S. H. Kareem, Y. K. Ooi, S. S. Abdulnoor, M. Shamsuddin, S. L. Lee, *Jurnal Teknologi (Sciences & Engineering)* **69** (2014) 103.
34. W. C. Elmore, *Phys. Rev*. **54** (1938) 309.
35. S. S. Papell, US Patent No. 3,215,572 (1965)
36. S. E. Khalafalla, G. W. Reimers, US Patent No. 3,764,540 (1973).
37. D. Zins, V. Cabuil, R. Massart, *J. Mol. Liq.* **83** (1999) 217.
38. X. P. Qiu, F. Winnik, *Chin. J. Polym. Sci.* **18** (2000) 535.
39. C. L. Lin, C. F. Lee, W. Y. Chiu, *J. Colloid Interface Sci.* **291** (2005) 411.
40. N. Jain, Y. Wang, S. K. Jones, B. S. Hawkett, G. G. Warr, *Langmuir* **26** (2010) 4465.
41. K. Mandel, F. Huttera, C. Gellermann, G. Sextl, *Colloids Surf. A: Physicochem. Eng. Aspects* **390** (2011) 173.
42. D. Ramimoghadam, S. Bagheri, S. B. A. Hamid, *J. Magn. Magn. Mater.* **379** (2015) 74.
43. G. V. M. Jacintho, A. G. Brolo, P. Corio, P. A. Z. Suarez, J. C. Rubim, *J. Phys. Chem. C* **113** (2009) 7684.
44. Y. Sahoo, H. Pizem, T. Fried, D. Golodnitsky, L. Burstein, C. N. Sukenik, G. Markovich, *Langmuir* **17** (2001) 7907.
45. P. P. C. Sartoratto, A. V. S. Neto, E. C. D. Lima, A. L. C. Rodrigues de Sa, P. C. Morais, *J. Appl. Phys.* **97** (2005) 917.
46. H. Yue-hua, L. Jian-ping, X. Jing, W. Dian-zuo, *J. Cent. South Univ. Technol.* **15** (2008) 663.
47. D. Caruntu, G. Caruntu, C. J. O. Connor, *J. Phys. D: Appl. Phys.* **40** (2007) 5801.
48. D. Maity, D. C. Agrawal, *J. Magn. Magn. Mater.* **308** (2007) 46.
49. M. T. Lopez-Lopez, J. D. G. Duran, A. V. Delgado, F. Gonzalez-Caballero, *J. Colloid Interface Sci.* **291** (2005) 144.
50. K. Parekh, R. V. Upadhyay, R. V. Mehta, *J. Magn. Magn. Mater.* **252** (2002) 35.
51. R. Arulmurugan, G. Vaidyanathan, S. Sendhilnathan, B. Jeyadevan, *Physica B* **363** (2005) 225.
52. G. Vaidyanathan, S. Sendhilnathan, *J. Magn. Magn. Mater.* **320** (2008) 803.
53. R. V. Upadhyay, R. V. Mehta, K. Parekh, D. Srinivas, R. P. Pant, *J. Magn. Magn. Mater.* **201** (1999) 129.
54. E. C. Ortiz, O. P. Perez, P. Voyles, G. Gutierrez, M. S. Tomar, *Microelectron. J.* **40** (2009) 677.
55. R. Arulmurugan, G. Vaidyanathan, S. Sendhilnathan, B. Jeyadevan, *J. Magn. Magn. Mater.* **298** (2006) 83.
56. S. Chikazumi, S. Taketomi, M. Ukita, M. Mizukami, H. Miyajima, M. Setogawa, Y. Kurihara, *J. Magn. Magn. Mater.* **65** (1987) 245.
57. H. E. Horng, C. Y. Hong, S. Y. Yang, H. C. Yang, *J. Phys. Chem. Solids.* **62** (2001)1749.
58. C. Y. Hong, H. E. Horng, F. C. Kuo, S. Y. Yang, H. C. Yang, J. M. Wu, *Appl. Phys. Lett.* **75** (1999) 2196.
59. K. Butter, P. H. Bomans, P. M. Frederik, G. J. Vroege, A. P. Philipse, *J. Phys.: Condens. Matter* **15** (2003) S1451.
60. A. Y. Zubarev, L.Y. Iskakova, *Physica A.* **335** (2004) 314.
61. M. Rajnak, V. I. Petrenko, M. V. Avdeev, O. I. Ivankov, A. Feoktystov, B. Dolnik, J. Kurimsky, P. Kopcansky, M. Timko, Appl. Phys. Lett. **107** (2015) 073108.

62. E. Blums, M. M. Maiorov, G. Kronkalns, *IEEE Trans. Magn.* **29** (1993) 3267.
63. M. Maiorov, E. Blums, M. Hanson, C. Johanson, *J. Magn. Magn. Mater.* **201** (1999) 95.
64. R. Desai, V. Davariya, K. Parekh, R. V. Upadhyay, *Pramana - J Phys.* **73** (2009) 765.
65. R. Desai, R. V. Upadhyay, V. Davariya, R. V. Mehta, *Phys Procedia* **9** (2010) 6.
66. A. O. Ivanov, S. S. Kantorovich, E. N. Reznikov, C. Holm, A. F. Pshenichnikov, A. V. Lebedev, A. Chremos, P. J. Camp, *Magnetohydrodynamics*, **43** (2007) 393.
67. A.Y. Solovyova, E. A. Elfimova, A. O. Ivanov, *Phys. Rev. E,* **96** (2017) 052609.
68. G. D. Mendenhall, Y. Geng, J. Hwang, *J. Colloid Interface Sci.* **184** (1996) 519.
69. C. V. Yerin, *J. Magn. Magn. Mater.* **431** (2017) 27.
70. A. Jozefczak, T. Hornowski, A. Skumiel, *Int J Thermophys* **32** (2011) 795.
71. L. M. Pop, C. D. Buioca, V. Iusan, M. Zimnicaru, *J. Magn. Magn. Mater.* **252** (2002) 46.
72. J. Kudelcik, P. Bury, J. Drga, P. Kopcansky, V. Zavisova, M. Timko, *J. Magn. Magn. Mater.* **326** (2013) 75.
73. G. Thirupathi, R. Singh, *Physica B* **448** (2014) 346.
74. T. Hornowski, A. Jozefczak, B. Kolodziejczyk, M. Timko, A. Skumiel, M Rajnak, *J. Phys. D: Appl. Phys.* **48** (2015) 175303.
75. A. D. Angheluta, L. Pricop, I. Stoica, C. A. Peptu, A. Dascalu, N. Marangoci, F. Doroftei, H. Chiriac, M. Pinteala, B. C. Simionescu, *J. Magn. Magn. Mater.* **322** (2010) 2956.
76. V. Segal, D. Nattrass, K. Raj, D. Leonard, *J. Magn. Magn. Mater.* **201** (1999) 70.
77. V. Segal, A. Hjortsberg, A. Rabinovich, D. Nattrass, K. Raj, Conference Record of the *IEEE International Symposium on Electrical Insulation*, Arlington, Virginia, USA, **10** (1998).
78. J. Patel, K. Parekh, R.V. Upadhyay, *Int J Therm Sci.* **103** (2016) 35.
79. J. Patel, K. Parekh, R.V. Upadhyay, *Int J Therm Sci.* **114** (2017) 64.

CHAPTER 3

SYNTHESIS AND CHARACTERIZATION OF $Mn_{1-x}Zn_xFe_2O_4$ NANOPARTICLES

3.1 INTRODUCTION

$Mn_{1-x}Zn_xFe_2O_4$ (MZ) nanoparticles can be used for the synthesis of temperature sensitive magnetic fluids. Synthesis of MZ nanoparticles with desired magnetic properties and tunable Curie temperature is quite challenging. These properties depends on the degree of Zn-ion substitution in spinel lattice, synthesis method used and conditions of preparation. Hence, it is desirable to optimize processing parameters affecting the Curie temperature and magnetic properties of nanoparticles. Factors that needs to be taken into the account for description of magnetic properties are distribution of particle sizes and magnetic interaction among the particles as well as distribution of magnetic ions between the tetrahedral A–sites and octahedral B–sites.

Several techniques have been developed to synthesize MZ nanoparticles. This includes high-energy ball milling, micro-emulsion [1, 2], sol-gel [3], hydrothermal [4] and co-precipitation techniques [5]. Amongst them co-precipitation method is a promising approach for the synthesis of MZ nanoparticles because of the simplicity of the method. In the first part of this chapter, protocols for the synthesis of uniform MZ nanoparticles with tunable magnetic properties by chemical co-precipitation method have been described. A series of $Mn_{1-x}Zn_xFe_2O_4$ ($x = 0 – 1$) nanoparticles are synthesized by chemical co-precipitation method. Optimize synthesis conditions have been established by controlling the degree of Zn-ion substitution, reaction pH, reaction temperature and reaction time to prepare superparamagnetic MZ nanoparticles with tunable magnetic properties.

As-synthesized MZ nanoparticles needs to be characterized for their structural and magnetic properties in order to understand their dependence on synthesis conditions. MZ nanoparticles are characterized by X-ray diffraction. Structural investigation of nanoparticles have been carried out on PAN analytical X'pert PRO powder X-ray diffractometer. The X-ray diffraction patterns are recorded at room temperature by using monochromatic CuK_α radiation ($\lambda = 1.5405$ nm) in the 2θ range of 28° to 70°. The X-ray diffraction patterns are further refined by Rietveld refinement technique using "Fullprof suite" program. Magnetization and Curie temperature measurements of MZ nanoparticles are carried out on Lake Shore 7404 vibrating

sample magnetometer (VSM). M–H loops are measured at 25 ºC in the magnetic field range of 0 to 5 KOe. High temperature M–T measurements are carried out on Lake Shore 7404 VSM with 74035 single stage cryostat oven assembly from 300K to 700K.

3.2 SYNTHESIS OF $Mn_{1-x}Zn_xFe_2O_4$ (x = 0 - 1) NANOPARTICLES

3.2.1 Materials

AR grade $FeCl_3$ was obtained from S.D. fine-chem Ltd., $MnCl_2.4H_2O$ was purchased from LOBA chemicals. $ZnSO_4.7H_2O$, NaOH and acetone were purchased from Merck, India. All chemicals were used as-received without any purification. Aqueous solutions were prepared in Milli-Q ultrapure water (ρ = 18.2 MΩ).

3.2.2 Synthesis procedure

A series of $Mn_{1-x}Zn_xFe_2O_4$ (x = 0 – 1) nanoparticles has been synthesized by chemical co-precipitation of Fe^{3+}, Mn^{2+} and Zn^{2+} from their aqueous salt solutions with NaOH base [6, 7]. Synthesis of MZ nanoparticles are summarized as a flow chart in **Fig. 3.1** and described in detail in **Annexure–I (A1).**

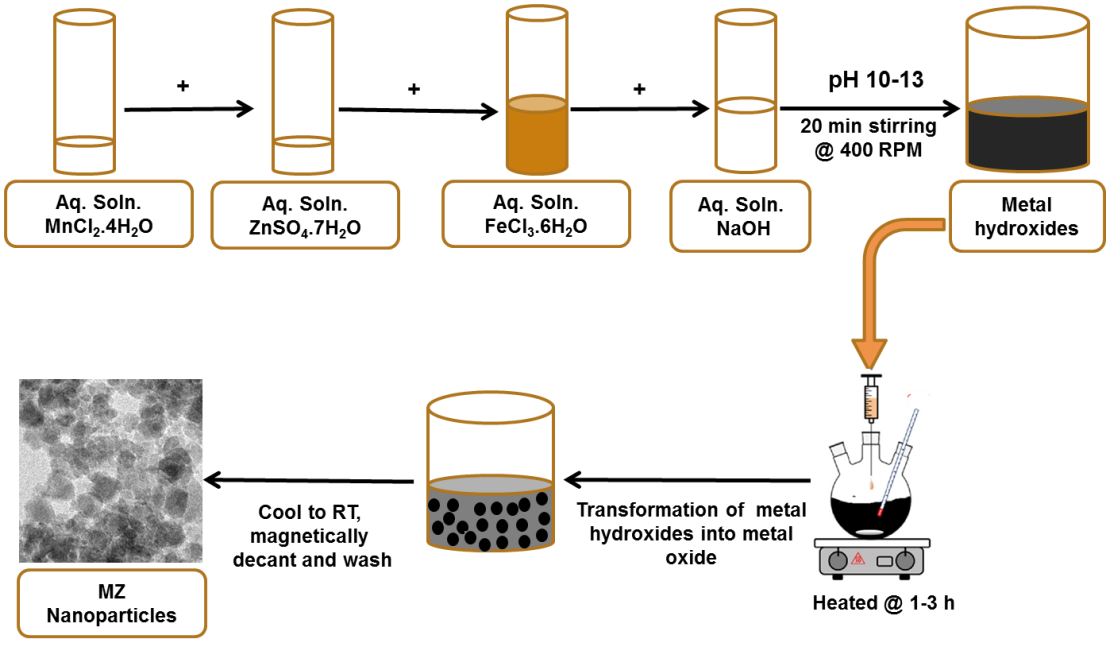

Fig. 3.1. Schematic diagram of synthesis protocols used for the preparation of MZ nanoparticles.

Aqueous solutions (100 mL each) of $MnCl_2.4H_2O$, $ZnSO_4.H_2O$ and $FeCl_3$ were prepared by dissolving appropriate quantities of reactants in distilled water. The pH of the solution was adjusted to < 2 with dilute HCl. It was then added into aqueous NaOH (100 mL) under constant mechanical stirring at 400 RPM. The molar ratio of ($MnCl_2.4H_2O$ + $ZnSO_4.7H_2O$) : $FeCl_3$: NaOH was maintained as 1 : 2 : 8. The solution pH was adjusted to 10 – 13 with 1 M NaOH under constant stirring. The colour of the solution immediately turned brown-black indicating the precipitation of solid phase. These precipitates were constantly stirred at 400 RPM for 20 min. After 20 min of mechanical stirring metal salts get converted into their hydroxides. These metal hydroxides were then subjected to constant heating at 80 – 100 ºC for 1 – 4 h. During this time hydroxides transform to nanoparticles of metal oxides [8]. Magnetic nanoparticles were then cooled to room temperature and decanted with permanent magnet. Nanoparticles were then washed 3 − 4 times with warm distilled water followed by an acetone wash and dried overnight at 100 °C. Sample codes and compositions of as-synthesized MZ nanoparticles are summarized in **Table 3.1**.

Table 3.1 Sample codes and composition of MZ nanoparticles.

Sample code	Composition of MZ nanoparticles
MZ0	$Mn_{1.0}Zn_{0.0}Fe_2O_4$
MZ2	$Mn_{0.8}Zn_{0.2}Fe_2O_4$
MZ4	$Mn_{0.6}Zn_{0.4}Fe_2O_4$
MZ6	$Mn_{0.4}Zn_{0.6}Fe_2O_4$
MZ8	$Mn_{0.2}Zn_{0.8}Fe_2O_4$
MZ10	$Mn_{0.0}Zn_{1.0}Fe_2O_4$

3.3 EFFECT OF Zn–ION SUBSTITUTION ON STRUCTURAL PROPERTIES OF MZ NANOPARTICLES

Magnetic properties of MZ nanoparticles depend on the degree of Zn-ion substitution and distribution of bivalent metal ions between tetrahedral A–sites and octahedral B–sites in spinel

lattice of MZ nanoparticles. To probe this structural dependence, powder X-ray diffractograms of MZ nanoparticles were recorded. **Fig. 3.2** shows the Rietveld refined X-ray diffractograms of as-synthesized MZ nanoparticles. In each diffractogram six peaks were observed, which are indexed well with the cubic spinel structure having Fd3m space group [9, 10].

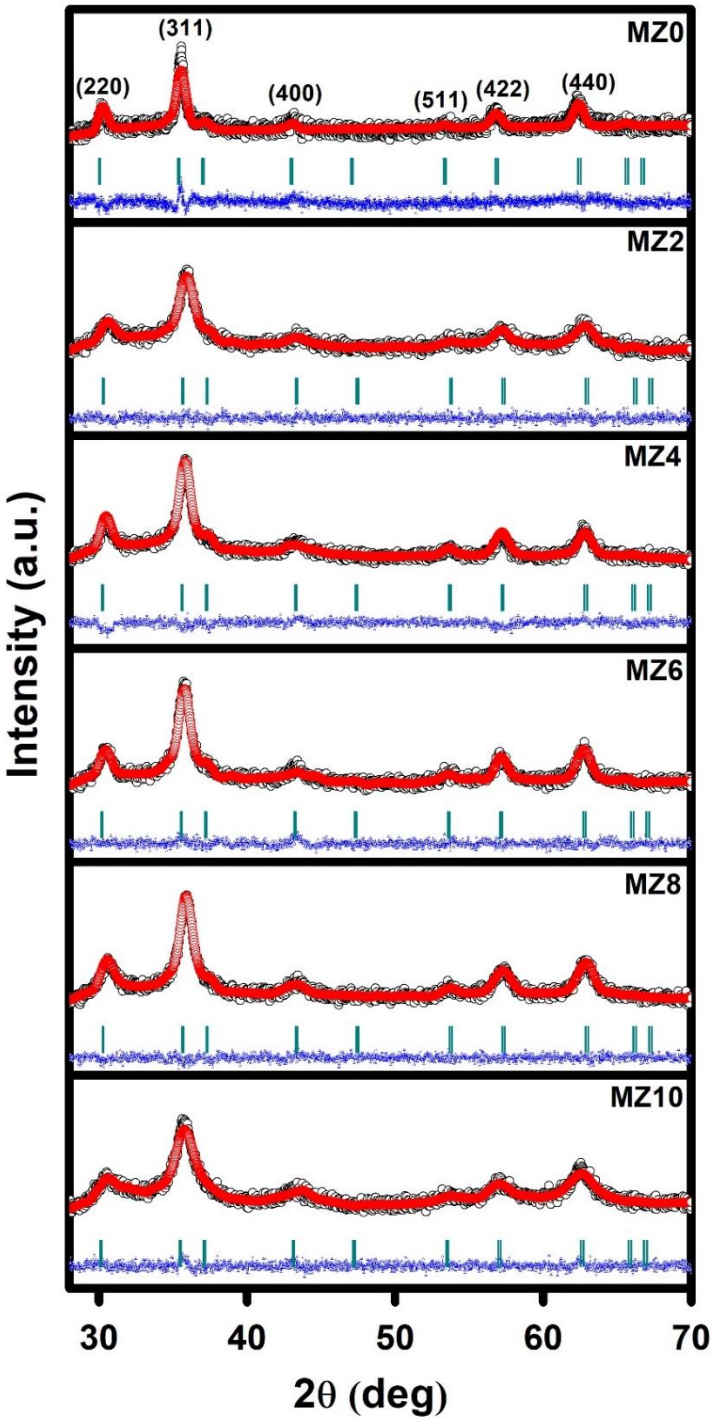

Fig. 3.2. Rietveld refined X-ray diffraction patterns of MZ nanoparticles.

Rietveld refinement uses a least square approach to refine a theoretical line profile until it matches the measured profile [11]. Obtained best fit values of various structure factors and goodness of fit parameters (χ^2, R_p, R_{wp}) are reported in **Table 3.2.** In normal spinel lattice, all the bivalent metal ions occupy the tetrahedral A–sites while all the octahedral B–sites are occupied by the trivalent metal ions. In the inverse spinel structure half of the trivalent metal ions occupy the tetrahedral A–sites while rest of them occupies the octahedral B–sites and all the bivalent metal ions occupy the remaining vacant octahedral B–sites. In mixed metal ferrites, both bivalent and trivalent metal ions occupy both the tetrahedral A–sites and octahedral B–sites with random occupancies [12]. Occupancies of Mn^{2+}, Zn^{2+}, Fe^{3+} in MZ nanoparticles as obtained from the Rietveld refinement are reported in **Table 3.2**.

It is observed from refined data that the lattice parameter "a" of MZ nanoparticles increases with increasing Zn-content. This might be because of the difference in the ionic radii of bivalent and trivalent metal ions occupying the tetrahedral A–sites and octahedral B–sites in spinel lattice leading to strained lattice. The ionic radius of Mn^{2+}, Zn^{2+} and Fe^{3+} are 0.81 A°, 0.74 A° and 0.68 A° respectively, which are higher than the void size of tetrahedral A–sites (0.28 A°) and octahedral B–sites (0.52 A°). Hence, occupation of A–sites and B–sites by Mn^{2+}, Zn^{2+} and Fe^{3+} ions results into strained lattice. Amongst the bivalent (Zn^{2+}, Mn^{2+}) metal ions, Zn^{2+} ions occupy the tetrahedral A–sites, due to their smaller radius. Mn^{2+} ions which are supposed to occupy the tetrahedral A–sites only, now also partially occupies the octahedral B–sites. The fraction of octahedral B–sites occupied by the Mn^{2+} ions or fraction of tetrahedral A–sites occupied by the Fe^{3+} ions, referred as the degree of inversion 'δ' is responsible for this observed changes in lattice parameters. Rath et al. [13] have previously reported decrease in lattice parameter with increasing Zn ion substitution. They have attributed this decrease to the replacement of Mn^{2+} cations having larger ionic radii (r = 0.082 nm) by the Zn^{2+} cations, which are having smaller ionic radii (r = 0.074 nm). However, they have not evaluated distributions of occupancies of bivalent and trivalent metal ions between tetrahedral A–sites and octahedral B–sites to support their conclusion. An opposite trend in the lattice parameter variation viz-a-viz to the substitution of Zn-ions in spinel matrix was observed in this study. It may be because of the partial compensation of decrease in lattice strain by the corresponding increase in the degree of inversion **(Table 3.3)** [14].

To further probe the effect of Zn substitution on the particle size and magnetic properties of MZ nanoparticles, analysis of peak broadening in each diffractogram was performed by adopting the Williamson-Hall (W–H) approach [15]. According to the W–H approach, crystallite size and lattice strain contributes to the X-ray line broadening ($\beta_{1/2}$). X-ray line broadening is the sum of the broadening caused by the crystallite size and lattice strain i.e.

$$\beta_{1/2} = \beta_{size} + \beta_{strain} \quad (3.1)$$

where $\beta_{size} = \lambda/(L \cos\theta)$ and

$\beta_{strain} = 4\eta\tan\theta$

$$\beta_{1/2}\cos\theta = 4\eta\sin\theta + \lambda/L \quad (3.2)$$

where λ is the wavelength of X-rays, L is the full-width half maximum (FWHM) of each diffraction peaks, θ is the angle of diffraction, η represent the lattice strain and $\beta_{1/2}$ is the average crystallite size of nanoparticles. If $\beta_{1/2}\cos\theta$ is plotted against $\sin\theta$, the slope of the line and intercept will provide estimation of the lattice strain and crystallite size of the nanoparticles, respectively.

The variation in crystallite size of MZ nanoparticles obtained from W–H plot as a function of degree of Zn-ion substitution (x) is shown in **Fig. 3.3.** The highest crystallite size (19 nm) was observed for x = 1, which is within the superparamagnetic limit of 25 nm for MZ nanoparticles [15, 16]. Crystallite size of MZ nanoparticles decreases with increase in Zn substitution in the spinel matrix of $Mn_{1-x}Zn_xFe_2O_4$. Crystallite size varies between 9 – 19 nm. This decrease in crystallite size of MZ nanoparticles with increasing Zn-ion substitution indicates that Zn also acts as grain growth inhibitor during the growth of MZ nanoparticles [17]. These results are in good agreement with those reported in literature by Gopalan et al. [9].

Table 3.2. Structural parameters obtained from the Rietveld refinement of X-ray diffraction patterns of MZ nanoparticles.

Sample	Lattice Parameter (Å)	Atom	Atomic positons				R_{Bragg}	R_f	X^2
			x	y	z	Occ.			
MZ0	8.41838	Mn	0.62500(0)	0.62500(0)	0.62500(0)	0.781(32)	18.5	17.5	1.39
		Mn	0.00000(0)	0.00000(0)	0.00000(0)	0.111(0)			
		Fe	0.62500(0)	0.62500(0)	0.62500(0)	0.219(32)			
		Fe	0.00000(0)	0.00000(0)	0.00000(0)	0.889(0)			
		O	0.24119(16)	0.24119(16)	0.24119(16)	1.000(0)			
MZ2	8.35689	Mn	0.62500(0)	0.62500(0)	0.62500(0)	0.483(0)	1.40	1.12	1.11
		Mn	0.00000(0)	0.00000(0)	0.00000(0)	0.159(0)			
		Zn	0.62500(0)	0.62500(0)	0.62500(0)	0.200(0)			
		Fe	0.62500(0)	0.62500(0)	0.62500(0)	0.317(0)			
		Fe	0.00000(0)	0.00000(0)	0.00000(0)	0.341(0)			
		Fe	0.00000(0)	0.00000(0)	0.00000(0)	0.500(0)			
		O	0.27388(0)	0.27388(0)	0.27388(0)	1.000(0)			
MZ4	8.36746	Mn	0.62500(0)	0.62500(0)	0.62500(0)	0.519(0)	17.1	12.7	1.36
		Mn	0.00000(0)	0.00000(0)	0.00000(0)	0.141(0)			
		Zn	0.62500(0)	0.62500(0)	0.62500(0)	0.400(0)			
		Fe	0.62500(0)	0.62500(0)	0.62500(0)	0.281(0)			
		Fe	0.00000(0)	0.00000(0)	0.00000(0)	0.342(0)			
		Fe	0.00000(0)	0.00000(0)	0.00000(0)	0.500(0)			
		O	0.27486(11)	0.27486(11)	0.27486(11)	1.000(0)			
MZ6	8.37792	Mn	0.62500(0)	0.62500(0)	0.62500(0)	0.254(0)	4.04	2.92	1.18
		Mn	0.00000(0)	0.00000(0)	0.00000(0)	0.073(0)			
		Zn	0.62500(0)	0.62500(0)	0.62500(0)	0.600(0)			
		Fe	0.62500(0)	0.62500(0)	0.62500(0)	0.146(0)			
		Fe	0.00000(0)	0.00000(0)	0.00000(0)	0.427(0)			
		Fe	0.00000(0)	0.00000(0)	0.00000(0)	0.500(0)			
		O	0.27308(48)	0.27308(48)	0.27308(48)	1.000(0)			
MZ8	8.357486	Mn	0.62500(0)	0.62500(0)	0.62500(0)	0.01537	4.15	3.62	1.17
		Mn	0.00000(0)	0.00000(0)	0.00000(0)	0.09232			
		Zn	0.62500(0)	0.62500(0)	0.62500(0)	0.80000			
		Fe	0.62500(0)	0.62500(0)	0.62500(0)	0.18464			
		Fe	0.00000(0)	0.00000(0)	0.00000(0)	0.40768			
		Fe	0.00000(0)	0.00000(0)	0.00000(0)	0.50000			
		O	0.252(10)	0.252(10)	0.252(10)	1.00000			
MZ10	8.39503	Zn	0.62500(0)	0.62500(0)	0.62500(0)	1.000(0)	1.95	1.64	1.17
		Fe	0.00000(0)	0.00000(0)	0.00000(0)	0.500(0)			
		Fe	0.00000(0)	0.00000(0)	0.00000(0)	0.500(0)			
		O	0.24742(0)	0.24742(0)	0.24742(0)	1.000(0)			

Table 3.3. Degree of inversion (δ) of MZ nanoparticles.

Sample	Degree of inversion (δ)
MZ0	0.22
MZ2	0.32
MZ4	0.28
MZ6	0.15
MZ8	0.19
MZ10	0.00

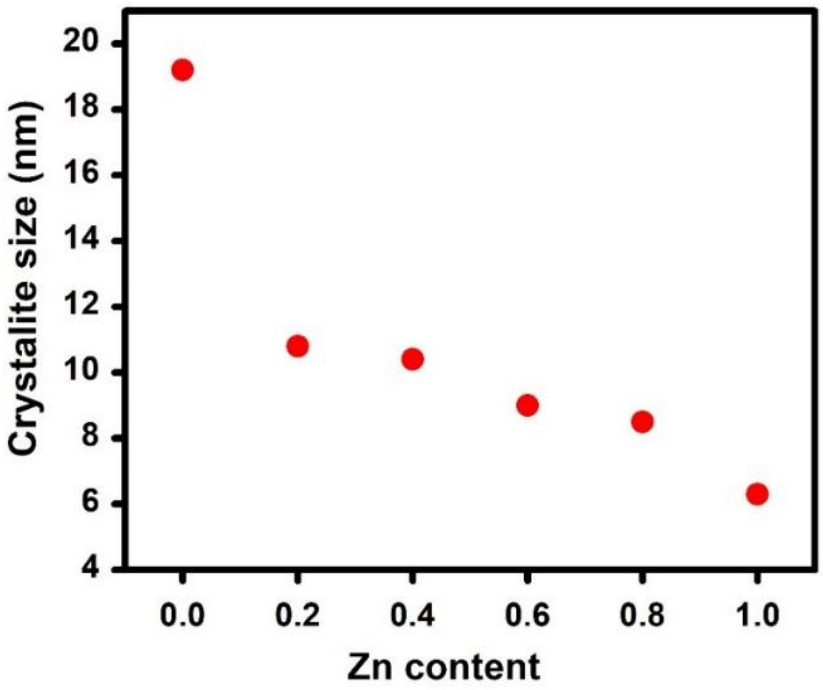

Fig. 3.3. Effect of Zn substitution on crystallite size of MZ nanoparticles.

Morphology of the nanoparticles is another critical parameter that has significant influence on both the magnetic properties and their colloidal dispersion. Transmission electron micrographs of as-synthesized MZ nanoparticles are shown in **Fig. 3.4** along with their size distribution histograms. As can be seen in the TEM micrographs, synthesized nanoparticles possess near spherical morphology. Significant clustering of nanoparticles can also be observed in the micrographs. This might be caused by the strong dipole-dipole interaction between

magnetic nanoparticles [14]. Each size distribution histograms in **Fig. 3.4** was fitted with log-normal particle size distribution function,

$$P(D) = \frac{1}{D\sigma(2\pi)^{1/2}} e^{\frac{-\ln\left(\frac{D}{D_o}\right)^2}{2\sigma^2}} \quad (3.3)$$

where, σ is the standard deviation, D is particle diameter and ln (D_o) a mean of ln (D) [18]. From the fit, mean physical size and polydispersity of nanoparticles were obtained, which are shown in **Fig 3.5.** The mean physical size of nanoparticles are in good agreement with the crystallite size determined from X-ray diffraction studies. With respect to particle size distribution, a parameter used to define the size range of the nanoparticles is called the "polydispersity index". The term "polydispersity" is used to describe the degree of non-uniformity of a size distribution of particles. A relatively higher value of polydispersity index (σ) indicates that the synthesized nanoparticles are polydispersed, which is expected when nanoparticles are prepared by chemical co-precipitation method [19].

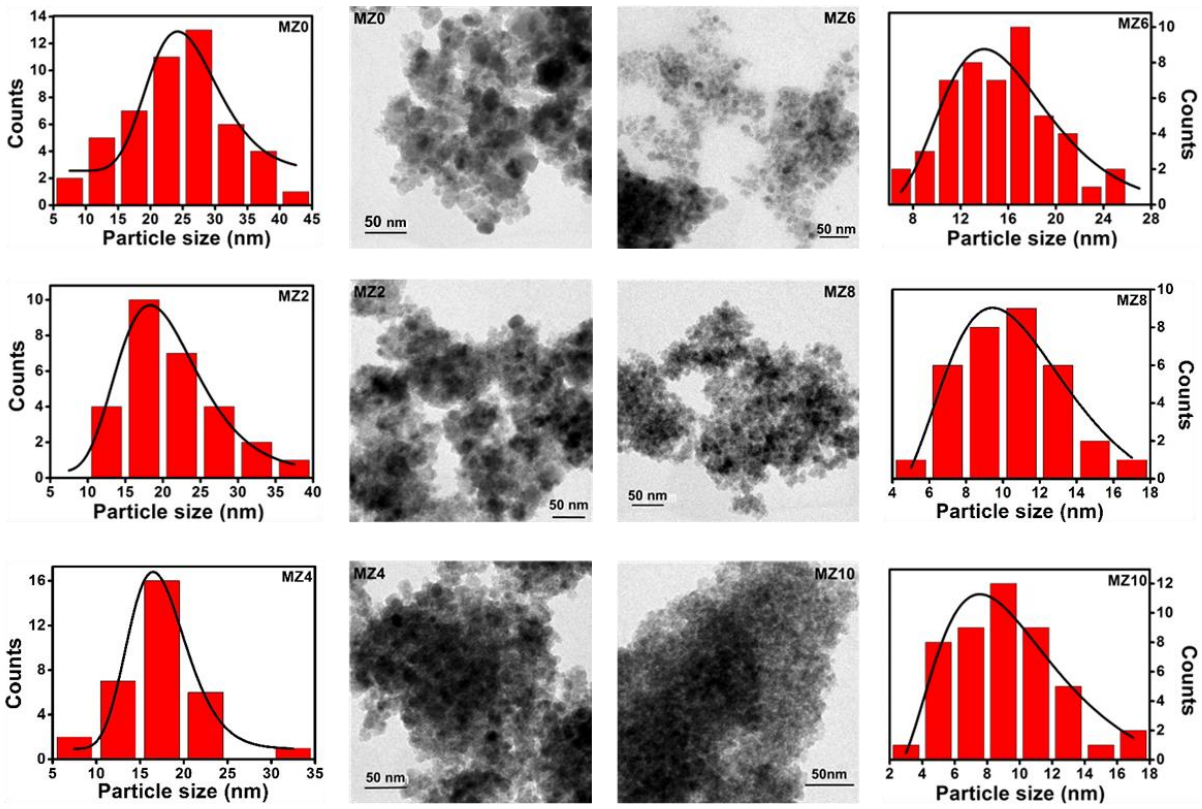

Fig. 3.4. TEM images of MZ nanoparticles and corresponding size distribution histograms obtained from TEM micrographs.

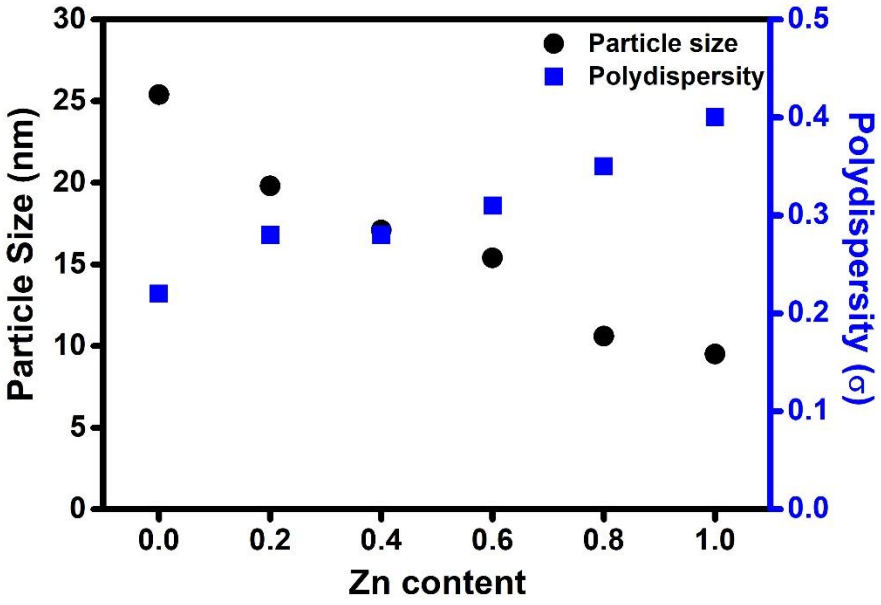

Fig. 3.5. Effect of Zn-ion substitution on particle size and polydispersity of MZ nanoparticles.

3.4. EFFECT OF Zn-ION SUBSTITUTION ON MAGNETIC PROPERTIES OF MZ NANOPARTICLES

Specific magnetization curves of as-synthesized MZ nanoparticles are shown in **Fig. 3.6(a).** No hysteresis is observable in any of the samples irrespective of the degree of Zn-ion substitution i.e., each sample exhibits superparamagnetism. Superparamagnetic behavior of nanoparticles is further confirmed from their 'near zero' remanence and coercivity values **(Fig 3.6 (b)).**

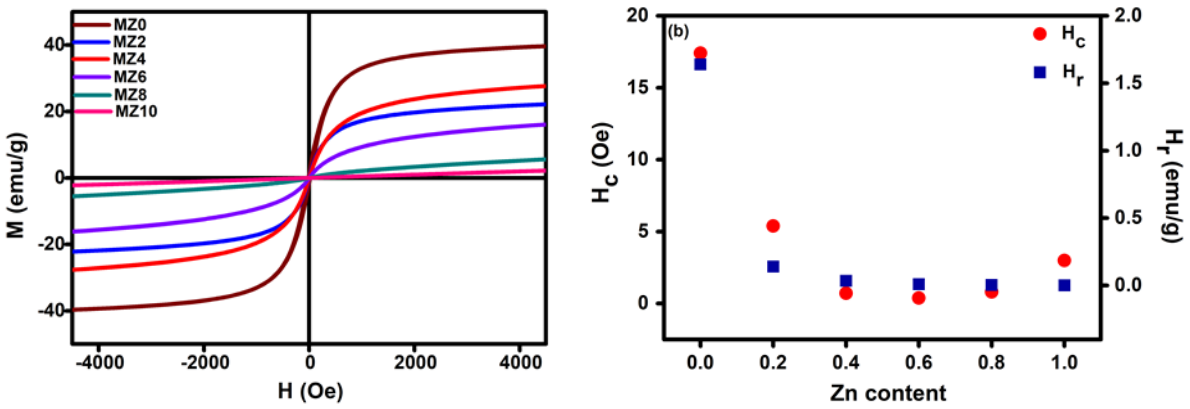

Fig. 3.6. (a) M–H loops of MZ nanoparticles, (b) coercivity (H_c) and remanence (H_r) of MZ nanoparticles as a function of degree of Zn-ion substitution. Here 1 emu/g = 1 Am^2/Kg and 1 Oe = 79.61 A/m.

Magnetization of an assembly of isolated superparamagnetic nanoparticles can be described by Langevin's theory [20]. This model assumes (i) spherical shape of particles, (ii) dominance of thermal energy over the anisotropy energy, (iii) polydispersed nature of magnetic nanoparticles that usually obeys log-normal size distribution function and (iv) average domain magnetization (M_d) of the particles that remains constant for a given size distribution. Inter-particle interactions are also neglected in this model. As per Langevin's theory, magnetization (M) of nanoparticles can be defined as,

$$M = M_s \int_0^\infty f(D)\, L(\alpha) dD \tag{3.4}$$

where M_s is the saturation magnetization of nanoparticles and $L(\alpha) = \coth\alpha - 1/\alpha$ is the Langevin function. The Langevin parameter $\alpha = \mu H / k_B T$. μ is the magnetic moment of individual spin cluster, H is applied external magnetic field. f(D) dD is log-normal cluster diameter distribution function with mean cluster diameter D_m and width σ.

$$f(D)dD = \frac{1}{\sqrt{2\pi D}} exp\left(\frac{-ln\left(D/D_m\right)^2}{2\sigma^2}\right) dD \tag{3.5}$$

If inter-particle interaction is taken into the consideration then classical Langevin's theory is modified with the mean field theory in which Langevin's parameter α is defined as [21, 22];

$$\alpha = \frac{\mu(H+H_{int})}{k_B T} \tag{3.6}$$

$H_{int} = \lambda M_1$; λ is mean field constant (dimensionless) and M_1 is the internal field acting on each particle/cluster

$$M = M_s \int_0^\infty f(D)\, L\left(\frac{\mu(H+H_{int})}{k_B T}\right) dD \tag{3.7}$$

When the magnetization data are fitted with Langevin's **eq. (3.7);** they did not fit well. A representative M–H curve of MZ4 nanoparticles fitted with the mean field theory **eq. (3.7)** is shown in **Fig. 3.7 (a).** To improve this fitting, **eq. (3.7)** is modified with extra linear term of H [23]

$$M = M_s \int_0^\infty f(D)\, L\left(\frac{\mu(H+H_{int})}{k_B T}\right) dD + \chi H \tag{3.8}$$

Where χ is the susceptibility of nanoparticles having size greater than the superparamagnetic limit. When M–H data of MZ4 nanoparticles are fitted with this modified Langevin's **eq. (3.8)**, a better fit is observed **(Fig. 3.7 (b)).**

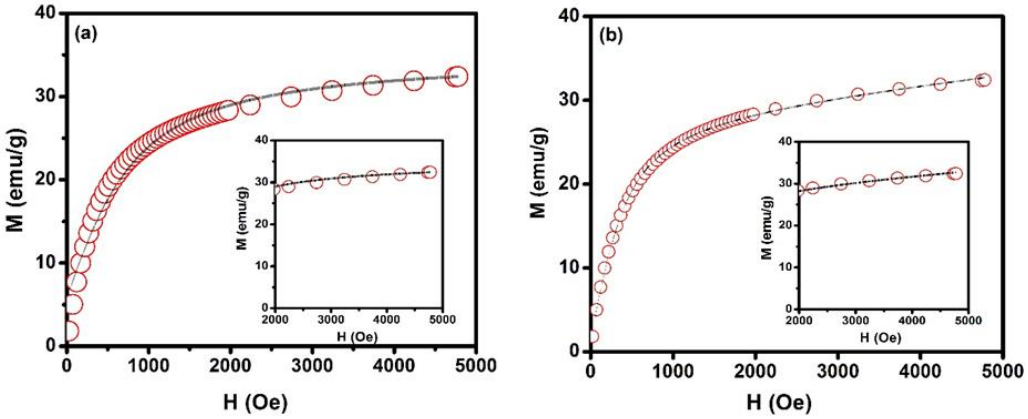

Fig. 3.7. (a) M–H curve of MZ4 nanoparticles fitted with modified mean field theory **eq. (3.7).** Inset shows enlarge image of high field region where fitting is poor, (b) M–H curve of MZ4 nanoparticles fitted with modified Langevin's **eq. (3.8).** Inset show enlarge image of high field region where fitting was poor in initial fit **(Fig. 3.7 (a)).** Here 1 emu/g = 1 Am^2/Kg and 1 Oe = 79.61 A/m.

All M–H curves (1st quadrant of **Fig. 3.6 (a)**) of MZ nanoparticle are fitted with modified Langevin's theory **eq. (3.8).** These fitted M–H curves are shown in **Fig. 3.8 (a).** Fitting parameters derived from these fits are reported in **Table 3.4**. It has been observed that both the saturation magnetization and magnetic diameter decreases with increase in the Zn substitution **(Table 3.4)**. Variation in the saturation magnetization (M_s) of MZ nanoparticles as a function of degree of Zn substitution is plotted in **Fig. 3.8 (b).**

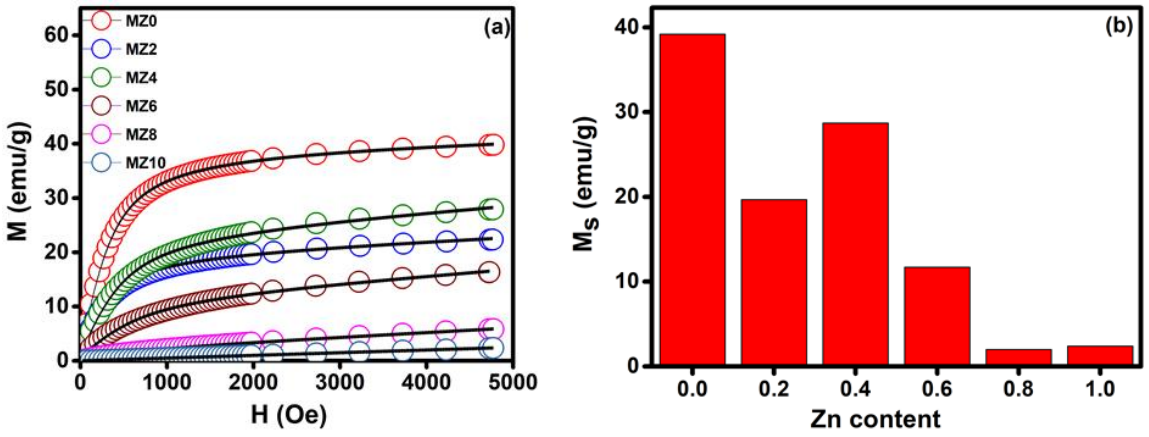

Fig. 3.8. (a) Magnetization fitted data for MZ nanoparticles (x = 0 – 1) with modified Langevin theory using mean field approximation **(eq. (3.8)),** (b) their saturation of magnetization as a function of Zn content. Here 1 emu/g = 1 Am^2/Kg and 1 Oe = 79.61 A/m.

From this plot it can be observed that the saturation magnetization of MZ nanoparticles strongly dependents on the degree of Zn substitution (x). For smaller values of x i.e. x = 0.2 - 0.4, the M_s of the MZ nanoparticles increases with increase in the degree of Zn substitution. However, M_s of MZ nanoparticles decreases with further increase in the degree of Zn substitution (x > 0.4).

Table 3.4. Magnetic parameters of MZ nanoparticles obtained from the fits of M–H data with modified Langevin theory **(eq. (3.8)).** Here 1 emu/g = 1 Am^2/Kg and 1 Oe = 79.61 A/m.

Sample	**M_s (emu/g)**	**μ ($\times 10^4 \mu_B$)**	**σ**	**D_m (nm)**	**λ**	**M_1 (Oe)**	**χ ($\times 10^{-4}$)**
MZ0	39.19	2.40	0.22	22.4	24.80	0.82	4.27
MZ2	19.66	2.50	0.24	13.9	22.39	1.35	7.36
MZ4	28.70	2.20	0.29	11.7	22.00	1.33	10.5
MZ6	11.70	1.30	0.23	9.3	30.74	1.86	11.7
MZ8	1.98	1.18	0.23	9.0	34.32	2.08	8.43
MZ10	2.40	0.70	0.23	7.0	33.00	2.00	4.96

Saturation magnetization of MZ nanoparticles depends on the magnetic moments of M^{2+} and Fe^{3+} ions and exchange interaction between them. In normal spinels bivalent metal ions (M^{2+}) occupies all the tetrahedral A–sites and Fe^{3+} ions occupies the octahedral B–sites.

A [B]

M^{2+} $[Fe^{3+}]$ $O^{2-}{}_4$

↓ ↑ 0

In the inverse spinel, half of the Fe^{3+} ions occupy the tetrahedral A–sites and rest occupies the octahedral B–sites. Since, their magnetic moments are mutually compensated, the resulting moment of the nanoparticles is because of the magnetic moments of bivalent metal cations (M^{2+}) occupying the octahedral B–sites.

A [B]

$Fe^{3+}\,[M^{2+}\,Fe^{3+}]\,O^{2-}{}_4$

↓ ↑ ↑ 0

In mixed spinels bivalent metal ions M^{2+} and Fe^{3+} occupy both the tetrahedral A–sites and octahedral B–sites.

A [B]

$M^{2+}{}_{1-\delta}\,Fe^{3+}{}_{\delta}\,[Mn^{2+}{}_{\delta}\,Fe^{3+}{}_{1-\delta}\,Fe^{3+}]\,O^{2-}{}_4$

↓ ↓ ↑ ↑ ↑ 0

Here δ is the degree of inversion. It represents fraction of Fe^{3+} ions occupying the tetrahedral A–sites. Interaction between A and B sub-lattices in spinel matrix consist of inter sub-lattice (A–B) super-exchange interactions and intra sub-lattice (A–A) and (B–B) exchange interactions. Amongst these, the inter sub-lattice (A–B) interaction is the strongest. (A–A) is relatively weak as compared to (A–B) interaction [24]. It is generally ten times weaker than (A–B) interaction [24]. (B–B) interaction is weakest amongst these three interactions [24, 25].

Bulk MZ0 is expected to have normal spinel structure. When the size of $MnFe_2O_4$ decreases to several nanometers, its normal spinel structure transforms into mixed spinel structure with degree of inversion, δ = 0.1-0.3 [26]. From the Rietveld refinement of X-ray diffraction data, the degree of inversion (δ) is determined, which is 0.22 **(Table 3.3)** for MZ0 nanoparticles. This means that in MZ0 nanoparticles, some of the Fe^{3+} ions which otherwise occupies the octahedral B–sites in bulk now occupies the tetrahedral A–sites.

A [B]

$Mn^{2+}{}_{0.78}\,Fe^{3+}{}_{0.22}\,[Mn^{2+}{}_{0.18}\,Fe^{3+}{}_{0.78}\,Fe^{3+}]\,O^{2-}{}_4$

↓ ↓ ↑ ↑ ↑ 0

Occupation of tetrahedral A–sites by Fe^{3+} ions results into strong Fe_A^{3+} – Fe_B^{3+} inter lattice super - exchange interaction. As the (A–B) interactions are much stronger as compared to Mn_A^{2+}– Fe_B^{3+} interactions and other (A–A) and (B–B) interactions, this would result into highest saturation magnetization amongst the studied MZ0 nanoparticles [27]. However, the observed saturation magnetization of 40 emu/g is much lower than the M_s value of bulk MZ0, which is 80 emu/g [28]. This decrease in saturation magnetization of MZ0 nanoparticles viz-a-viz to their bulk counterparts ascribed to the formation of canted spin magnetic dead layer on the surface of nanoparticles [29, 30].

Partial substitution of Zn^{2+} ions at tetrahedral A–sites increases the diamagnetic contribution and reduces the Mn^{2+} ions at A–sites. This weakens the Fe_A^{3+} – Fe_B^{3+} and Mn_A^{2+}– Fe_B^{3+} inter lattice exchange interactions. This results into decrease in M_s (21.5 emu/g) of MZ2 nanoparticles.

A [B]

$$Zn^{2+}_{0.2}\, Mn^{2+}_{0.48}\, Fe^{3+}_{0.32}\, [Mn^{2+}_{0.32}\, Fe^{3+}_{0.68}\, Fe^{3+}]\, O^{2-}_{4}$$

0 ↓ ↓ ↑ ↑ ↑ 0

Further increase in Zn substitution (x = 0.4) increases the saturation magnetization from 21.5 emu/g to 26.6 emu/g. This increase in M_s is because of two competitive processes. Increase in Zn-content increases the diamagnetic contribution, which decrease the overall magnetization of MZ4 nanoparticles. At the same time, this decrease in M_s is compensated by the corresponding increase in Fe_A^{2+}– Fe_B^{3+} inter lattice exchange interactions.

A [B]

$$Zn^{2+}_{0.4}\, Mn^{2+}_{0.32}\, Fe^{3+}_{0.28}\, [Mn^{2+}_{0.28}\, Fe^{3+}_{0.72}\, Fe^{3+}]\, O^{2-}_{4}$$

0 ↓ ↓ ↑ ↑ ↑ 0

Increase in the Zn^{2+} ions at A-site lead to an increased Mn_A^{2+}–Fe_B^{3+} interaction. This enhanced A-B interaction dominates over the decreasing (A–A) interaction and thus lead to an enhancement in the overall magnetization of MZ4 nanoparticles. Similar results have been previously reported by Anantharaman et al. [31].

With further increase in Zn ($x > 0.4$), the M_s of MZ nanoparticles decreases. Similar trend was observed by Anantharaman et al. [31]. They have attributed this reversal in trend to the transformation of mixed spinel structure to the inverse spinel structure. However, they did not support their hypothesis with concrete experimental evidence. Contradictory to their claim, we have observed no such deviation from mixed spinel structure (except for MZ10, which is normal spinel) as previously concluded from X-ray analysis. We attribute this decrease in M_s of MZ nanoparticles with increasing Zn substitution at tetrahedral A–sites to the enhanced diamagnetic contribution of Zn and to the weakening A–B and A–A interactions.

In MZ10 nanoparticles ($x = 1$); there is no (A–B) or (A–A) interactions. The only possible interaction is the very weak (B–B) interaction between two Fe^{3+} ions present at the B–sites. As this interaction is very week, MZ10 shows a typical paramagnetic behavior **(Fig. 3.8(a)).**

A [B]

$Zn^{2+}[Fe^{3+}\ Fe^{3+}]O_4^{2-}$

0 ↑ ↑ 0

In some cases small magnetism is reported in MZ10 [32, 33]. For example, after fast quenching, a small part of Zn^{2+} may remain at the B–site and corresponding part of Fe^{3+} at the A–site. Typical degree of inversion 'δ' reported in literature is of the order of 0.1 [34]. This type of $ZnFe_2O_4$ manifests non-compensated ferri or antiferromagnetism, however this study did not find any such evidence of non-compensated spins.

Another important magnetic property of MZ nanoparticles that too depend on the degree of Zn substitution is their Curie temperature (T_c). Curie temperatures of MZ nanoparticles have been determined from high temperature VSM measurements. **Fig. 3.9** shows the $M \rightarrow T$ curves of MZ nanoparticles. Linear region of $M \rightarrow T$ curves are extrapolated and its intercept on the x-axis provides an estimation of the Curie temperature. T_c of MZ nanoparticles as a function of zinc substitution (x) is also shown in **Fig. 3.10.**

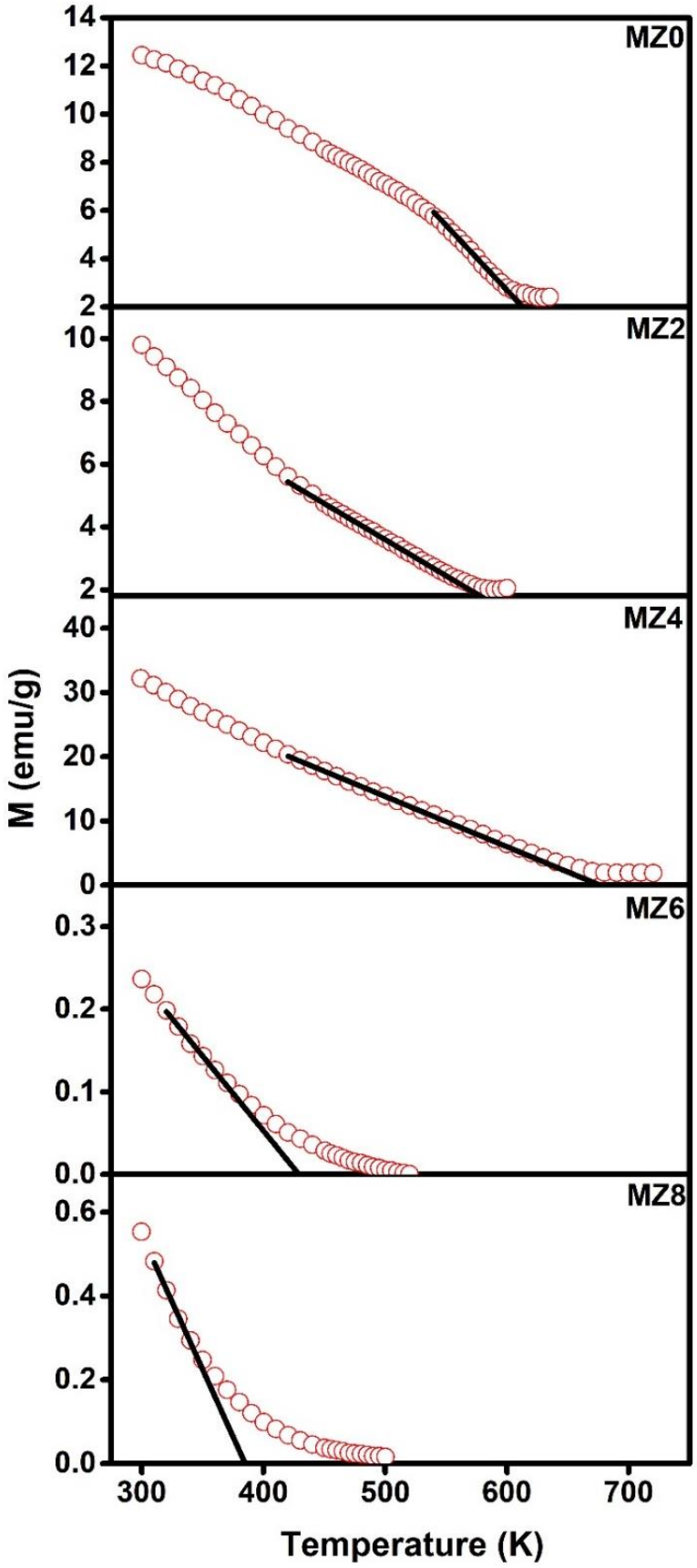

Fig. 3.9. M → T plots of MZ nanoparticles. Here 1 emu/g = 1 Am^2/Kg.

Curie temperature of MZ4 nanoparticles is highest (675 K), which monotonously decreases with further increase in the Zn content **(Fig. 3.10).** The T_c of MZ nanoparticles drops to 384 K for x = 0.8. MZ nanoparticles having lower Zn content (x ≤ 0.4) have stronger (A–B) exchange interaction. This strong interaction is responsible for their high T_c and M_s. As the degree of Zn substitution increases in MZ nanoparticles, the (A–B) intra-lattice exchange interaction weakens leading to the decrease in their Curie temperature. Pyromagnetic coefficients of MZ nanoparticles are calculated from (**∂**M/**∂**T) at T=Tc. Pyromagnetic coefficient ranges between 11 – 118 A/mK.

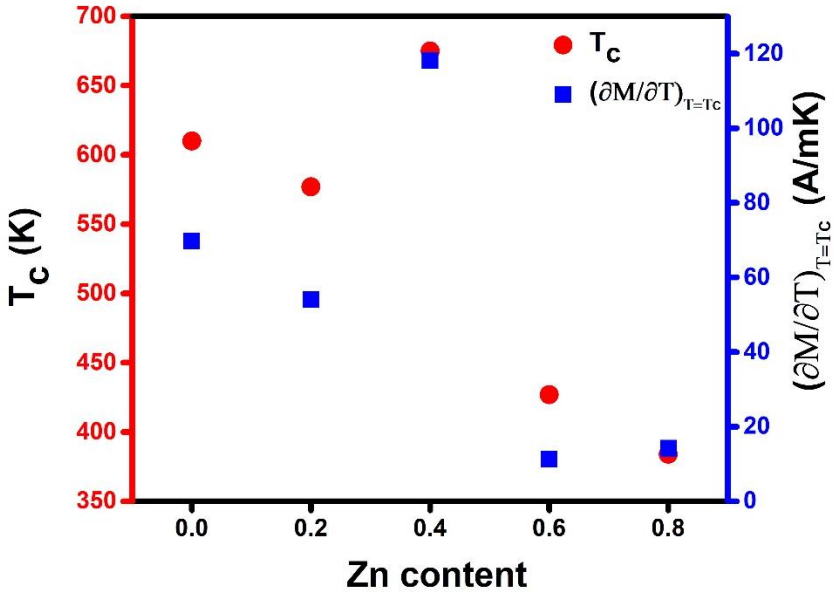

Fig. 3.10. Effect of Zn content on the Curie temperature (Tc) and pyromagnetic coefficient ((**∂**M/**∂**T)$_{T=Tc}$) of MZ nanoparticles.

Amongst all synthesized MZ nanoparticles, MZ4 nanoparticles have suitable crystallite size, magnetization and Curie temperature, therefore MZ4 nanoparticles has been chosen for further investigation.

3.5 EFFECT OF REACTION PARAMETERS ON STRUCTURAL PROPERTIES OF MZ4 NANOPARTICLES

To understand the effect of reaction parameters (pH, temperature, time) on the structural properties of MZ4 nanoparticles, a series of MZ4 nanoparticles have been synthesized by chemical co-precipitation method by following the protocols as described in **Annexure–I (A2).** Sample codes of as-synthesized MZ4 nanoparticles and their preparation conditions are summarized in **Table 3.5.**

Table 3.5. Sample codes and preparation conditions of MZ4 nanoparticles.

Sample code	Preparation conditions		
	pH	**Reaction time (h)**	**Reaction temperature (ºC)**
S-1	10.0	3	90
S-2	10.5	3	90
S-3	11.0	3	90
S-4	11.5	3	90
S-5	12.0	3	90
S-6	12.5	3	90
S-7	13.0	3	90
S-8	11.0	1	90
S-9	11.0	2	90
S-10	11.0	3	90
S-11	11.0	4	90
S-12	11.0	3	80
S-13	11.0	3	90
S-14	11.0	3	100

X-ray diffraction patterns of MZ4 nanoparticles prepared as a function of reaction pH, reaction time and reaction temperature are shown in **Fig. 3.11.** In each diffractogram six peaks were observed, which are indexed well with the spinel structure. Each diffraction pattern is refined by the Rietveld method by assuming Fd3m space group. Obtained best fit values of structure factors and goodness of fit parameters (χ^2, R_p, R_{wp}) are reported in **Table 3.6** for reaction pH, in **Table 3.7** for reaction time and in **Table 3.8** for reaction temperature.

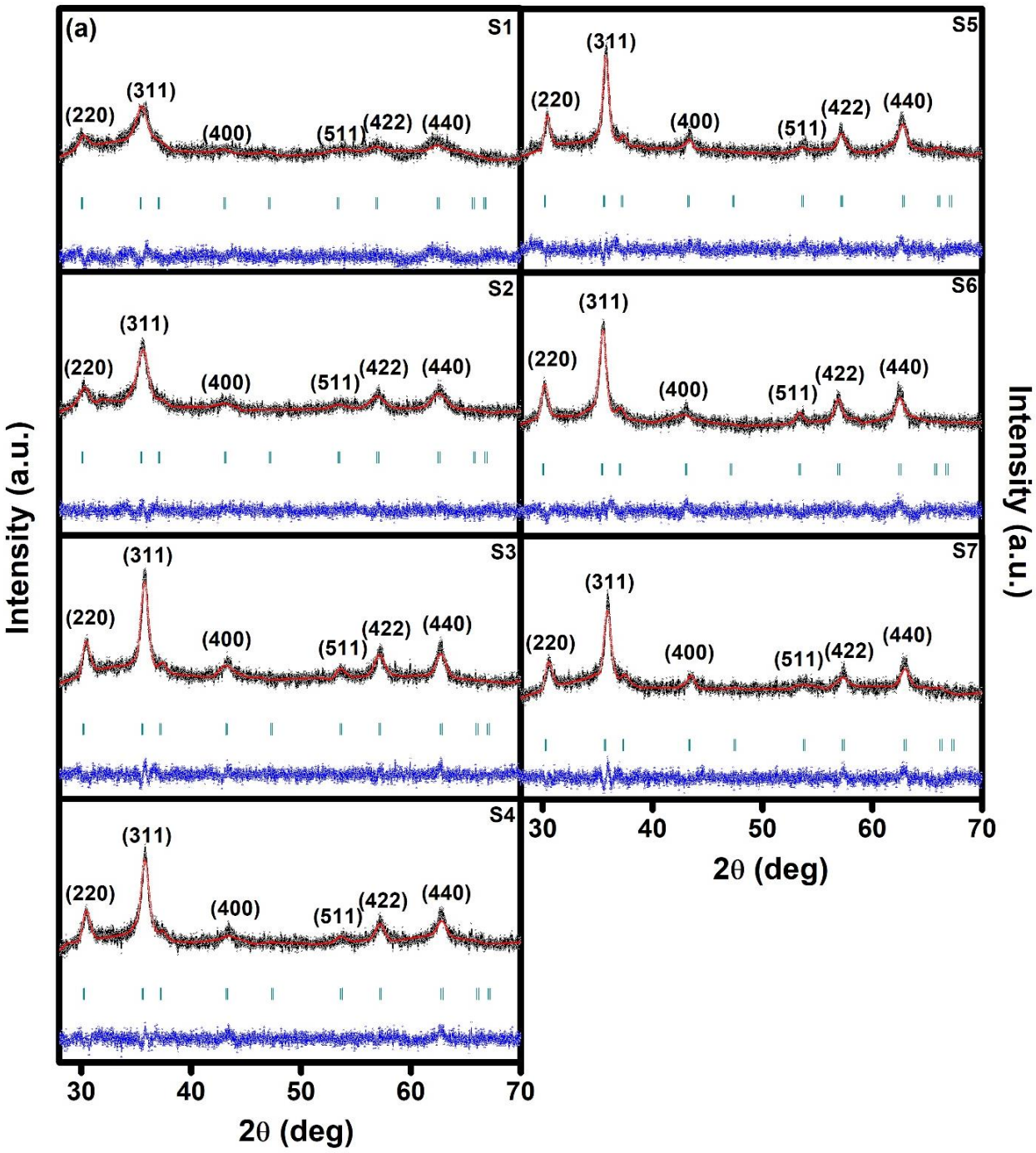

Fig. 3.11. (a) Rietveld refined X-ray diffraction patterns of MZ4 nanoparticles synthesized as a function of reaction pH.

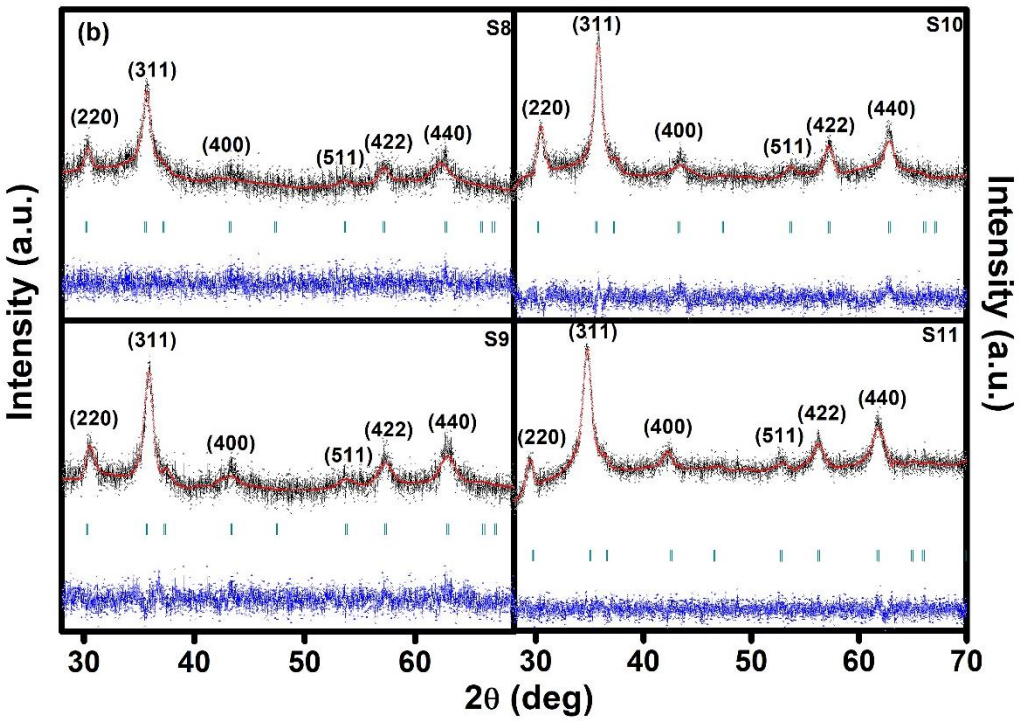

Fig. 3.11. (b) Rietveld refined X-ray diffraction patterns of MZ4 nanoparticles synthesized as a function of reaction time.

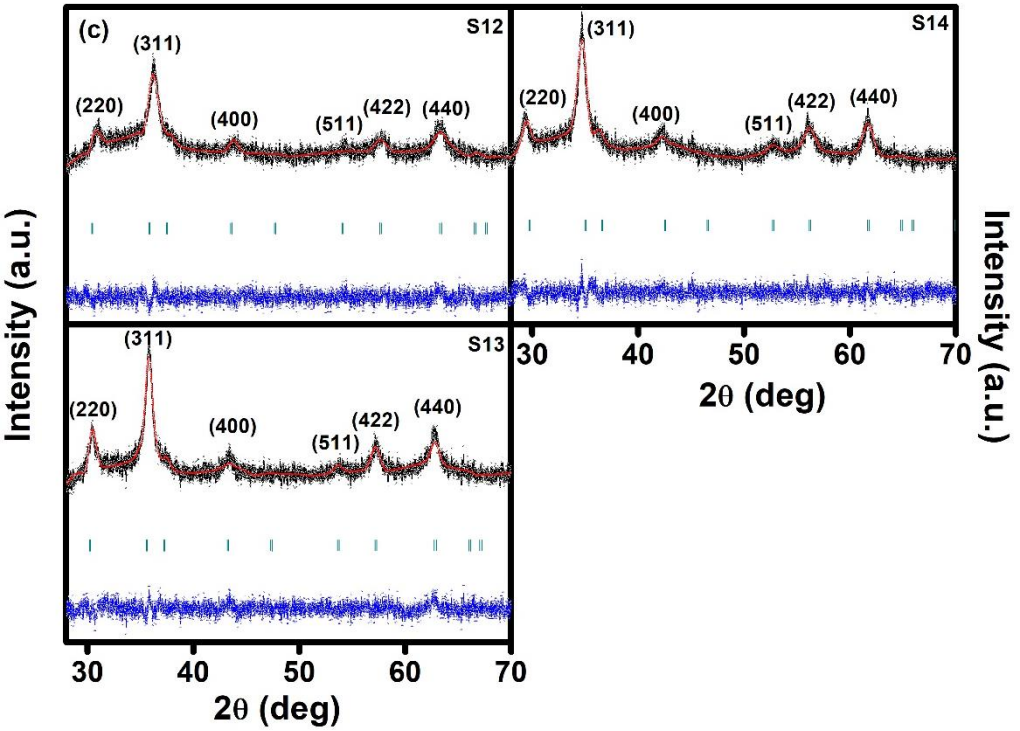

Fig. 3.11. (c) Rietveld refined X-ray diffraction patterns of MZ4 nanoparticles synthesized as a function of reaction temperature.

Table 3.6. Structural parameters of MZ4 nanoparticles prepared as a function of reaction pH.

Sample Code / pH	Lattice Parameter (Å)	Atom	Atomic positons				R_{Brag}	R_f	X^2
			x	y	z	Occ.			
S1/pH 10.0	8.313(10)	Mn	0.62500(0)	0.62500(0)	0.62500(0)	0.27014	23.4	19.6	1.21
		Mn	0.00000(0)	0.00000(0)	0.00000(0)	0.14701			
		Zn	0.62500(0)	0.62500(0)	0.62500(0)	0.43861			
		Fe	0.62500(0)	0.62500(0)	0.62500(0)	0.29125			
		Fe	0.00000(0)	0.00000(0)	0.00000(0)	0.35319			
		Fe	0.00000(0)	0.00000(0)	0.00000(0)	0.49980			
		O	0.2783(10)	0.2783(10)	0.2783(10)	1.00000			
S2/pH 10.5	8.358(7)	Mn	0.62500(0)	0.62500(0)	0.62500(0)	0.33240	3.70	3.44	1.11
		Mn	0.00000(0)	0.00000(0)	0.00000(0)	0.17067			
		Zn	0.62500(0)	0.62500(0)	0.62500(0)	0.38692			
		Fe	0.62500(0)	0.62500(0)	0.62500(0)	0.28068			
		Fe	0.00000(0)	0.00000(0)	0.00000(0)	0.32953			
		Fe	0.00000(0)	0.00000(0)	0.00000(0)	0.49980			
		O	0.247(5)	0.247(5)	0.247(5)	0.89435			
S3/pH 11.0	8.386(4)	Mn	0.62500(0)	0.62500(0)	0.62500(0)	0.38987	5.17	6.15	1.15
		Mn	0.00000(0)	0.00000(0)	0.00000(0)	0.18949			
		Zn	0.62500(0)	0.62500(0)	0.62500(0)	0.32895			
		Fe	0.62500(0)	0.62500(0)	0.62500(0)	0.28118			
		Fe	0.00000(0)	0.00000(0)	0.00000(0)	0.30999			
		Fe	0.00000(0)	0.00000(0)	0.00000(0)	0.50052			
		O	0.242(3)	0.242(3)	0.242(3)	1.20145			
S4/pH 11.5	8.364(4)	Mn	0.62500(0)	0.62500(0)	0.62500(0)	0.31005	9.13	11.4	1.19
		Mn	0.00000(0)	0.00000(0)	0.00000(0)	0.15514			
		Zn	0.62500(0)	0.62500(0)	0.62500(0)	0.40803			
		Fe	0.62500(0)	0.62500(0)	0.62500(0)	0.28192			
		Fe	0.00000(0)	0.00000(0)	0.00000(0)	0.34490			
		Fe	0.00000(0)	0.00000(0)	0.00000(0)	0.49996			
		O	0.2270(13)	0.2270(13)	0.2270(13)	1.00000			
S5/pH 12.0	8.333(3)	Mn	0.62500(0)	0.62500(0)	0.62500(0)	0.35332	7.50	5.66	1.64
		Mn	0.00000(0)	0.00000(0)	0.00000(0)	0.12601			
		Zn	0.62500(0)	0.62500(0)	0.62500(0)	0.36554			
		Fe	0.62500(0)	0.62500(0)	0.62500(0)	0.28114			
		Fe	0.00000(0)	0.00000(0)	0.00000(0)	0.37408			
		Fe	0.00000(0)	0.00000(0)	0.00000(0)	0.49991			
		O	0.250(4)	0.250(4)	0.250(4)	1.00000			
S6/pH 12.5	8.377(4)	Mn	0.62500(0)	0.62500(0)	0.62500(0)	0.34996	9.32	20.6	1.19
		Mn	0.00000(0)	0.00000(0)	0.00000(0)	0.12381			
		Zn	0.62500(0)	0.62500(0)	0.62500(0)	0.36785			
		Fe	0.62500(0)	0.62500(0)	0.62500(0)	0.28219			
		Fe	0.00000(0)	0.00000(0)	0.00000(0)	0.31647			
		Fe	0.00000(0)	0.00000(0)	0.00000(0)	0.49972			
		O	0.238(3)	0.238(3)	0.238(3)	1.08934			
S7/pH 13.0	8.373(4)	Mn	0.62500(0)	0.62500(0)	0.62500(0)	0.34620	12.5	11.4	1.20
		Mn	0.00000(0)	0.00000(0)	0.00000(0)	0.11217			
		Zn	0.62500(0)	0.62500(0)	0.62500(0)	0.39145			
		Fe	0.62500(0)	0.62500(0)	0.62500(0)	0.28235			
		Fe	0.00000(0)	0.00000(0)	0.00000(0)	0.34354			
		Fe	0.00000(0)	0.00000(0)	0.00000(0)	0.49429			
		O	0.245(2)	0.245(2)	0.245(2)	0.97655			

Table 3.7. Structural parameters of MZ4 nanoparticles prepared as a function of reaction time.

Sample Code/ Time (h)	Lattice Parameter (Å)	Atom	Atomic positons				R_{Bra}	R_f	X^2
			x	y	z	Occ.			
S8/ 1	8.344(14)	Mn	0.62500(0)	0.62500(0)	0.62500(0)	0.40156	13.3	21.0	1.08
		Mn	0.00000(0)	0.00000(0)	0.00000(0)	0.09666			
		Zn	0.62500(0)	0.62500(0)	0.62500(0)	0.39321			
		Fe	0.62500(0)	0.62500(0)	0.62500(0)	0.20523			
		Fe	0.00000(0)	0.00000(0)	0.00000(0)	0.40255			
		Fe	0.00000(0)	0.00000(0)	0.00000(0)	0.49979			
		O	0.275(4)	0.275(4)	0.275(4)	1.00000			
S9/2	8.358(7)	Mn	0.62500(0)	0.62500(0)	0.62500(0)	0.41682	10.9	21.1	1.07
		Mn	0.00000(0)	0.00000(0)	0.00000(0)	0.09711			
		Zn	0.62500(0)	0.62500(0)	0.62500(0)	0.38082			
		Fe	0.62500(0)	0.62500(0)	0.62500(0)	0.20236			
		Fe	0.00000(0)	0.00000(0)	0.00000(0)	0.40393			
		Fe	0.00000(0)	0.00000(0)	0.00000(0)	0.49996			
		O	0.238(7)	0.238(7)	0.238(7)	1.00000			
S10/3	8.386(4)	Mn	0.62500(0)	0.62500(0)	0.62500(0)	0.38987	5.17	6.15	1.15
		Mn	0.00000(0)	0.00000(0)	0.00000(0)	0.18949			
		Zn	0.62500(0)	0.62500(0)	0.62500(0)	0.32895			
		Fe	0.62500(0)	0.62500(0)	0.62500(0)	0.28118			
		Fe	0.00000(0)	0.00000(0)	0.00000(0)	0.30999			
		Fe	0.00000(0)	0.00000(0)	0.00000(0)	0.50052			
		O	0.242(3)	0.242(3)	0.242(3)	1.20145			
S11/4	8.502(9)	Mn	0.62500(0)	0.62500(0)	0.62500(0)	0.25602	3.91	3.67	1.04
		Mn	0.00000(0)	0.00000(0)	0.00000(0)	0.05(3)			
		Zn	0.62500(0)	0.62500(0)	0.62500(0)	0.40456			
		Fe	0.62500(0)	0.62500(0)	0.62500(0)	0.28529			
		Fe	0.00000(0)	0.00000(0)	0.00000(0)	0.34701			
		Fe	0.00000(0)	0.00000(0)	0.00000(0)	0.50102			
		O	0.2354(0)	0.2354(0)	0.2354(0)	1.00000			

Table 3.8. Structural parameters of MZ4 nanoparticles prepared as a function of reaction temperature.

Sample/ Temp. (ºC)	Lattice Parameter (Å)	Atom	Atomic positons				R_{Bragg}	R_f	X^2
			x	y	z	Occ.			
S12/ 80	8.343(9)	Mn	0.62500(0)	0.62500(0)	0.62500(0)	0.30149	1.93	0.895	1.11
		Mn	0.00000(0)	0.00000(0)	0.00000(0)	0.16769			
		Zn	0.62500(0)	0.62500(0)	0.62500(0)	0.41620			
		Fe	0.62500(0)	0.62500(0)	0.62500(0)	0.28231			
		Fe	0.00000(0)	0.00000(0)	0.00000(0)	0.33224			
		Fe	0.00000(0)	0.00000(0)	0.00000(0)	0.50007			
		O	0.2299(14)	0.2299(14)	0.2299(14)	0.90240			
S13/ 90	8.358(7)	Mn	0.62500(0)	0.62500(0)	0.62500(0)	0.38987	10.9	21.1	1.07
		Mn	0.00000(0)	0.00000(0)	0.00000(0)	0.18949			
		Zn	0.62500(0)	0.62500(0)	0.62500(0)	0.32895			
		Fe	0.62500(0)	0.62500(0)	0.62500(0)	0.28118			
		Fe	0.00000(0)	0.00000(0)	0.00000(0)	0.30999			
		Fe	0.00000(0)	0.00000(0)	0.00000(0)	0.50052			
		O	0.242(3)	0.242(3)	0.242(3)	1.20145			
S14/ 100	8.355(6)	Mn	0.62500(0)	0.62500(0)	0.62500(0)	0.30639	0.68	0.42	1.26
		Mn	0.00000(0)	0.00000(0)	0.00000(0)	0.15427			
		Zn	0.62500(0)	0.62500(0)	0.62500(0)	0.40263			
		Fe	0.62500(0)	0.62500(0)	0.62500(0)	0.29098			
		Fe	0.00000(0)	0.00000(0)	0.00000(0)	0.35025			
		Fe	0.00000(0)	0.00000(0)	0.00000(0)	0.49548			
		O	0.2680(9)	0.2680(9)	0.2680(9)	1.00000			

Variation in crystallite size of MZ4 nanoparticles synthesized as a function of reaction pH, time and temperature is shown in **Fig. 3.12.** Crystallite size of MZ4 nanoparticles increases with increase in the co-precipitation pH, reaction time and reaction temperature. A similar observation was also reported by Desai et al. [35]. The crystallite size of all the synthesized MZ4 nanoparticles are well within the superparamagnetic limit of 25 nm [15, 16]. Reaction temperature could not be kept below 80 ºC as, co-precipitation reaction below this temperature yields amorphous nanoparticles.

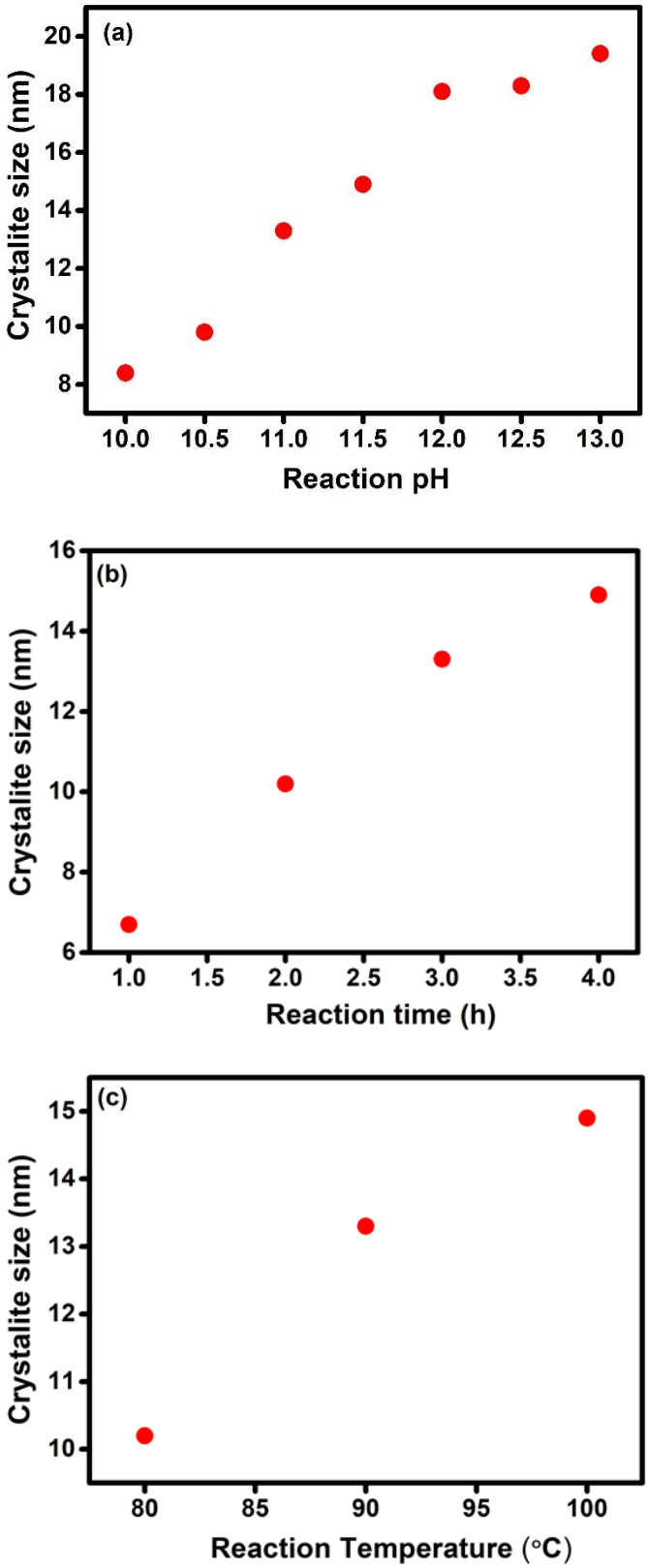

Fig. 3.12. Effect of (a) reaction pH, (b) reaction time and (c) reaction temperature on the crystallite size of MZ4 nanoparticles.

3.6. EFFECT OF REACTION PARAMETERS ON THE MAGNETIC PROPERTIES OF MZ4 NANOPARTICLES

Magnetization curves of MZ4 nanoparticles synthesized as a function of reaction pH, reaction and reaction temperature are shown in **Fig. 3.13.** With increase in magnetic field, the magnetization of MZ4 nanoparticles increases because of progressive alignment of ensemble of magnetic nanoparticles along the external field direction. All samples exhibit superparamagnetic behavior i.e. near zero remanence and zero coercivity **(Fig. 3.14, Table 3.9).** It has been observed from the fits of MZ4 nanoparticles with modified Langevin's **eq. (3.8)** that the magnetic diameter increases with increase in reaction pH, reaction time and reaction temperature **(Table 3.10).** Mean field constant (λ) and mean internal field (M_1) decreases with increasing particle size **(Table 3.10).** Saturation magnetization (M_s) also increases with increase in the particle size at lower pH. Highest saturation magnetization (28.7 emu/g) was observed when magnetic particle size was ~12 nm. Beyond 12 nm, magnetization of MZ4 nanoparticles decreases with increase in the particle size [36].

This variation in magnetization can be explained in terms of the site occupancy of cations (Mn^{2+}) at tetrahedral A–sites and B–sites. MZ4 nanoparticles possess mixed spinel structure ($Zn^{2+}_{0.4}\, Mn^{2+}_{0.4}\, Fe^{3+}_{0.2}\, [Mn^{2+}_{0.2}\, Fe^{3+}_{0.8}\, Fe^{3+}]\, O^{2-}_{4}$). A–A interactions in mixed spinel is weak as compared to A–B interactions. Thus changes in the occupancy of Mn^{2+} ions at A–sites **(Table 3.6)** are responsible for the observed trend of saturation magnetization. Occupancy of Mn^{2+} ions at B–sites increases with increase in reaction pH upto 11. With further increase in reaction pH, occupancy of Mn^{2+} at B–sites decreases. Accordingly, the saturation magnetization of MZ4 nanoparticles increases with the reaction pH (upto 11) and with further increase in the pH; saturation magnetization of nanoparticles decreases. This may be because of decrease in the occupancy of Mn^{2+} ions at B–sites, which further weakens inter lattice A–B interactions. Similarly with increase in reaction time and reaction temperature upto 3h and 90 ºC respectively, the saturation magnetization increases with increase in the occupancy of Mn^{2+} ions at B–sites. Further increase in reaction time or reaction temperature lead to the decrease in saturation magnetization of nanoparticles. This is because of decrease in the occupancy of Mn^{2+} ions at the B–sites **(Table 3.7 and 3.8).**

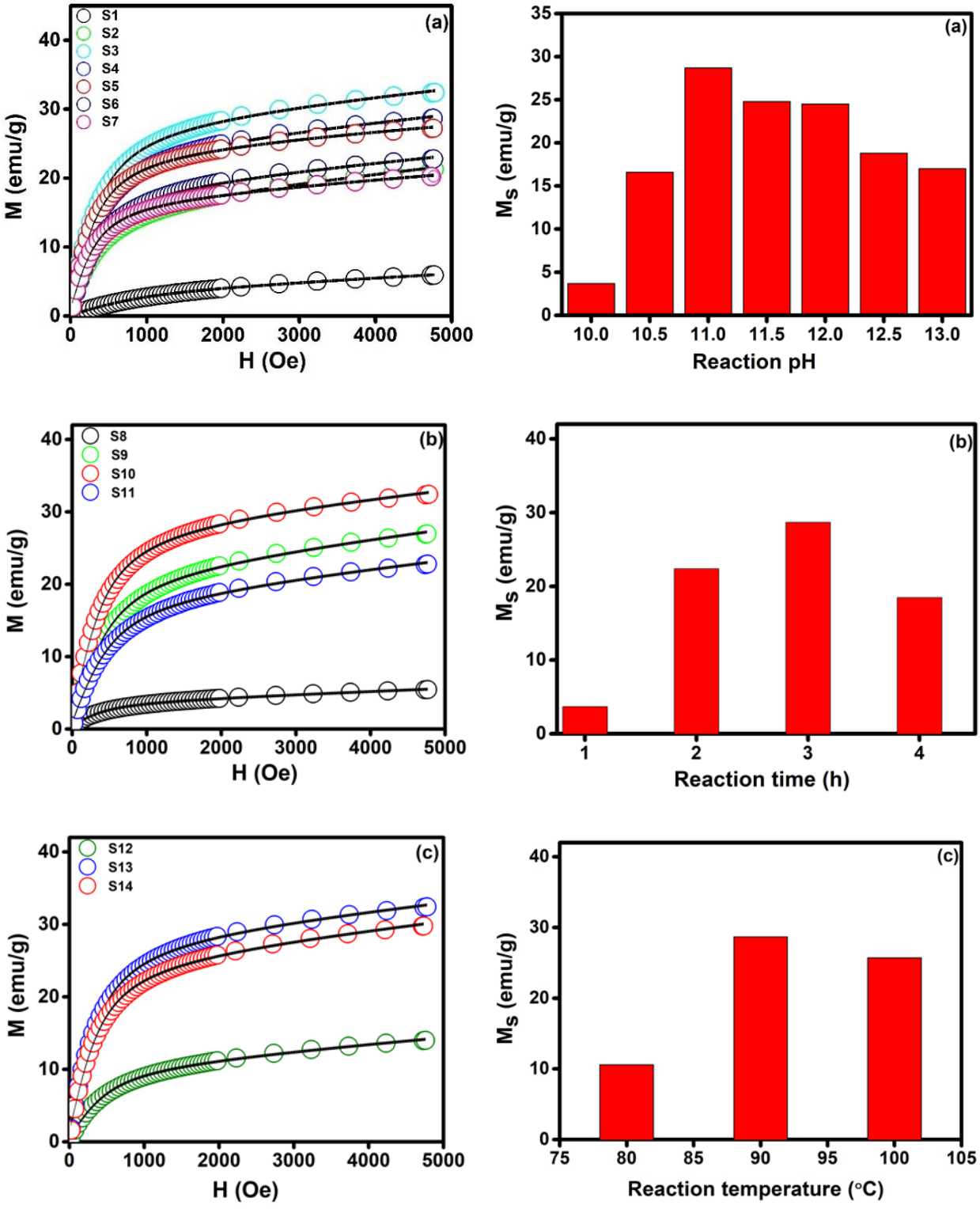

Fig. 3.13. Magnetization curves and corresponding saturation magnetization (M_s) of MZ4 nanoparticles synthesized as a function of reaction of (a) reaction pH, (b) reaction time and (c) reaction temperature. Here 1 emu/g = 1 Am^2/Kg and 1 Oe = 79.61 A/m.

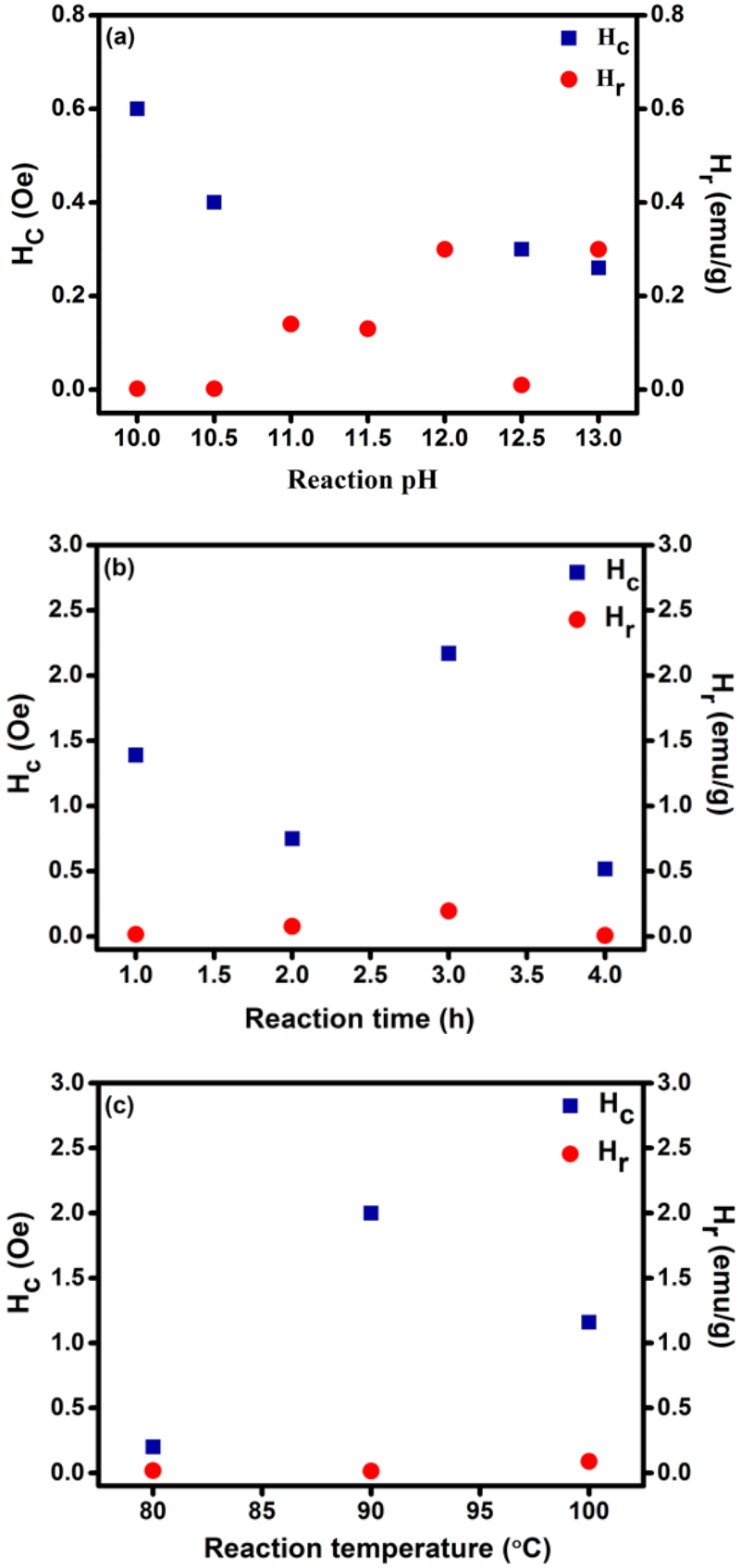

Fig. 3.14. Coercivity and remanence of MZ4 nanoparticles as a function of (a) reaction pH, (b) reaction time and (c) reaction temperature. Here 1 emu/g = 1 Am^2/Kg and 1 Oe = 79.61 A/m.

Table 3.9. Effect of reaction pH, reaction time and reaction temperature on structural (crystallite size) and magnetic properties (Coercivity (H_c), Remanence (M_r), Curie temperature (T_c)) of MZ4 nanoparticles. Here 1 emu/g = 1 Am^2/Kg and 1 Oe = 79.61 A/m.

Sample	Crystallite Size (nm)	H_c (Oe)	M_r (emu/g)	T_c (K)
S1	08.4	0.60	0.002	392
S2	09.8	0.40	0.002	547
S3	13.3	2.00	0.140	665
S4	14.9	2.20	0.130	611
S5	18.1	4.70	0.300	589
S6	18.3	0.30	0.010	574
S7	19.4	0.20	0.300	557
S8	06.7	1.39	0.016	428
S9	10.2	0.75	0.077	543
S10	13.3	2.17	0.196	665
S11	14.9	0.51	0.007	573
S12	10.2	0.20	0.018	464
S13	13.3	2.00	0.014	665
S14	14.9	1.16	0.090	566

Curie temperature of MZ4 nanoparticles has been determined from high temperature VSM measurements. The M $\rightarrow$ T curves of MZ4 nanoparticles prepared as a function of reaction pH, reaction time and reaction temperature are shown in **Fig. 3.15.** The linear region of M $\rightarrow$ T curves have been extrapolated and intercept of each of this extrapolation on x-axis provides an estimation of the Curie temperature of nanoparticles. T_c of MZ4 nanoparticles are also reported in **Table 3.9.** T_c of MZ4 nanoparticles increase with increase in the pH from 10 to 11 and then decreases with further increase in the pH **(Table 3.9).** For larger size nanoparticles (d > 13), the demagnetization effect appears at higher temperature and this effect disappears for size d < 13 nm because of lower saturation magnetization of these nanoparticles **(Fig. 3.16)** [37]. This size dependence of Curie temperature of MZ4 nanoparticles can be explained in terms of the site occupancy of cations (Mn^{2+}) in the spinel lattice [38].

Table 3.10. Magnetic parameters of MZ4 nanoparticles derived from the modified Langevin theory **(eq. (3.8))** for particle systems synthesized as a function of reaction pH, reaction time and reaction temperature. Here 1 emu/g = 1 Am^2/Kg and 1 Oe = 79.61 A/m.

Sample	**M_s (emu/g)**	**μ ($\times 10^4\ \mu_B$)**	**σ**	**D_m (nm)**	**λ**	**M_1**	**χ ($\times 10^{-4}$)**
S-1	03.7	0.9	0.30	04.4	33.0	1.80	05.4
S-2	16.6	2.2	0.32	07.7	29.7	1.48	11.6
S-3	28.7	2.2	0.29	11.7	22.0	1.33	10.5
S-4	24.8	2.3	0.26	12.3	22.0	1.30	10.4
S-5	24.5	2.5	0.27	15.0	20.2	1.20	07.7
S-6	18.8	2.2	0.29	17.2	20.0	1.20	10.3
S-7	17.0	2.8	0.30	17.8	19.0	1.10	07.9
S-8	03.7	2.0	0.25	04.4	32.5	1.86	03.9
S-9	22.4	1.8	0.29	08.6	25.1	1.43	12.3
S-10	28.7	2.2	0.29	11.7	22.0	1.33	10.5
S-11	18.5	1.8	0.26	12.2	21.2	1.30	11.2
S-12	10.6	1.8	0.31	9.3	24.0	1.60	10.3
S-13	28.7	2.2	0.29	11.7	22.0	1.33	10.5
S-14	25.7	2.2	0.26	12.2	20.8	1.30	11.1

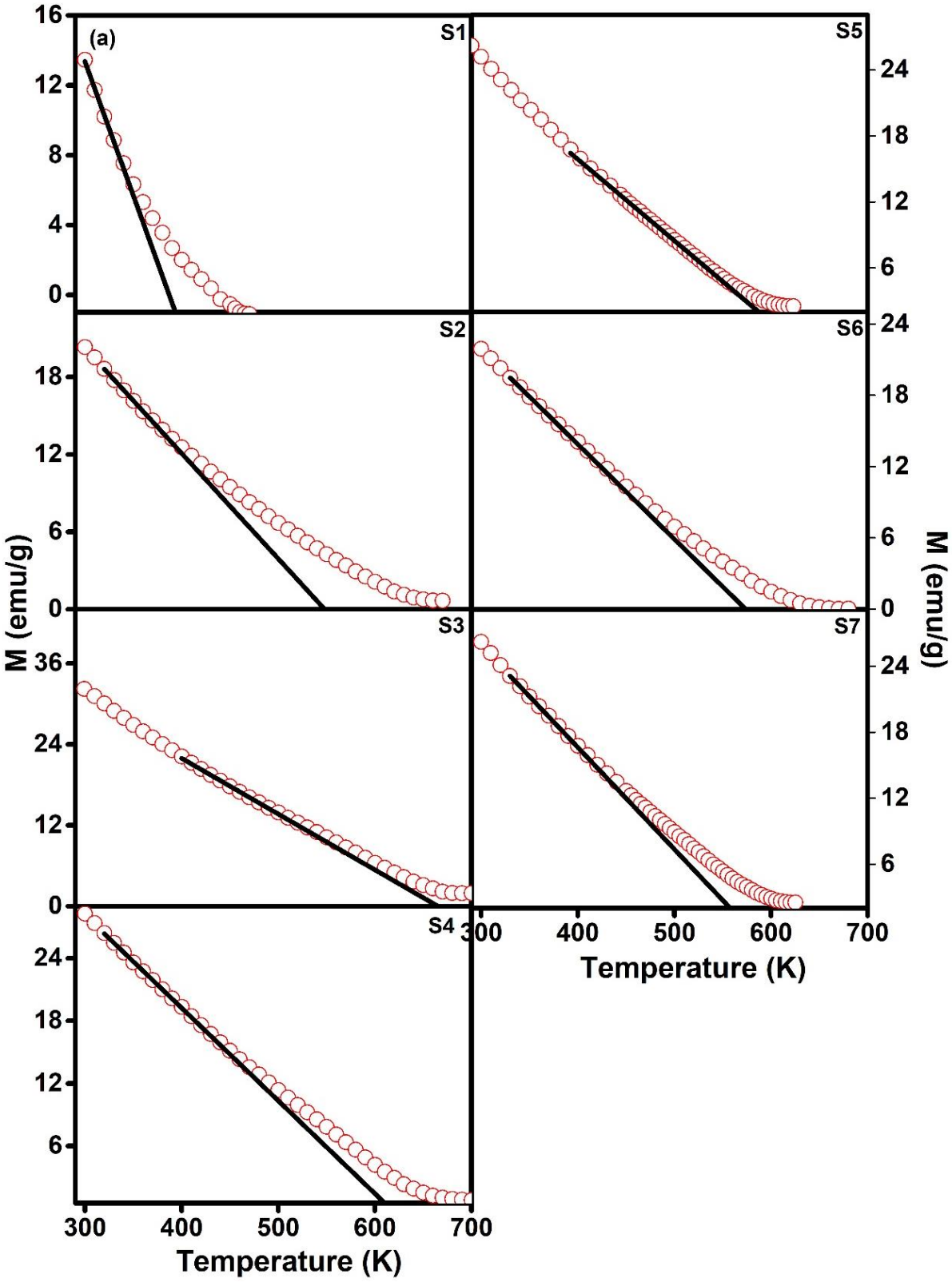

Fig. 3.15. (a) M → T plots of MZ4 nanoparticles synthesized as a function of reaction pH. Here 1 emu/g = 1 Am^2/Kg.

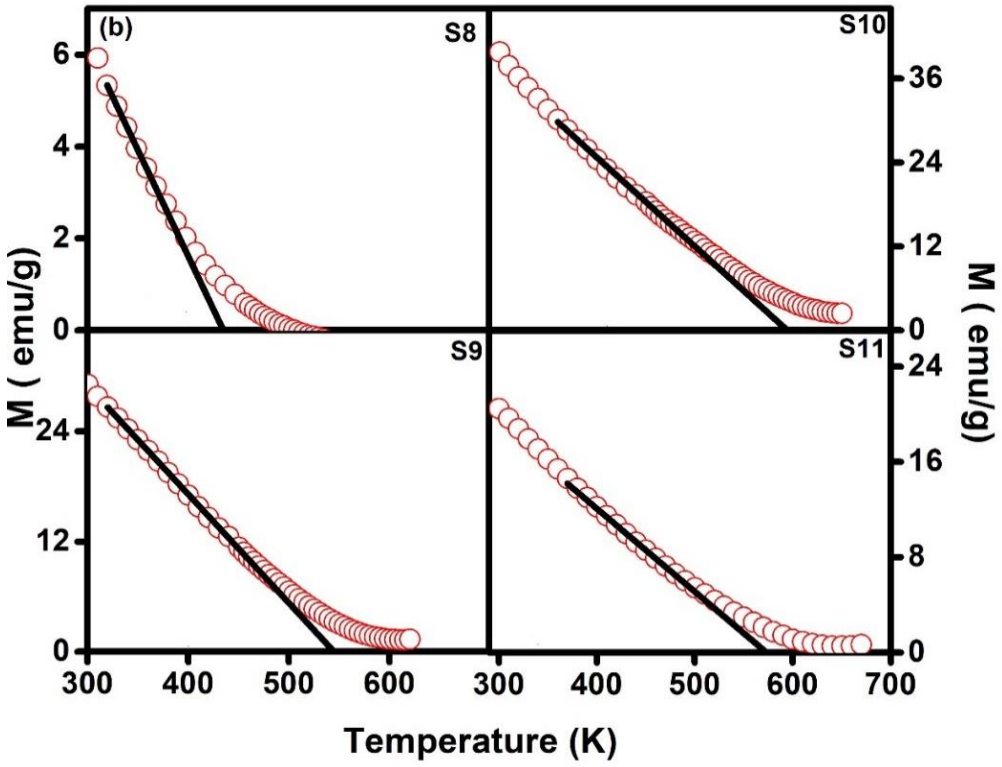

Fig. 3.15. (b) M → T plots of MZ4 nanoparticles synthesized as a function of reaction time. Here 1 emu/g = 1 Am^2/Kg.

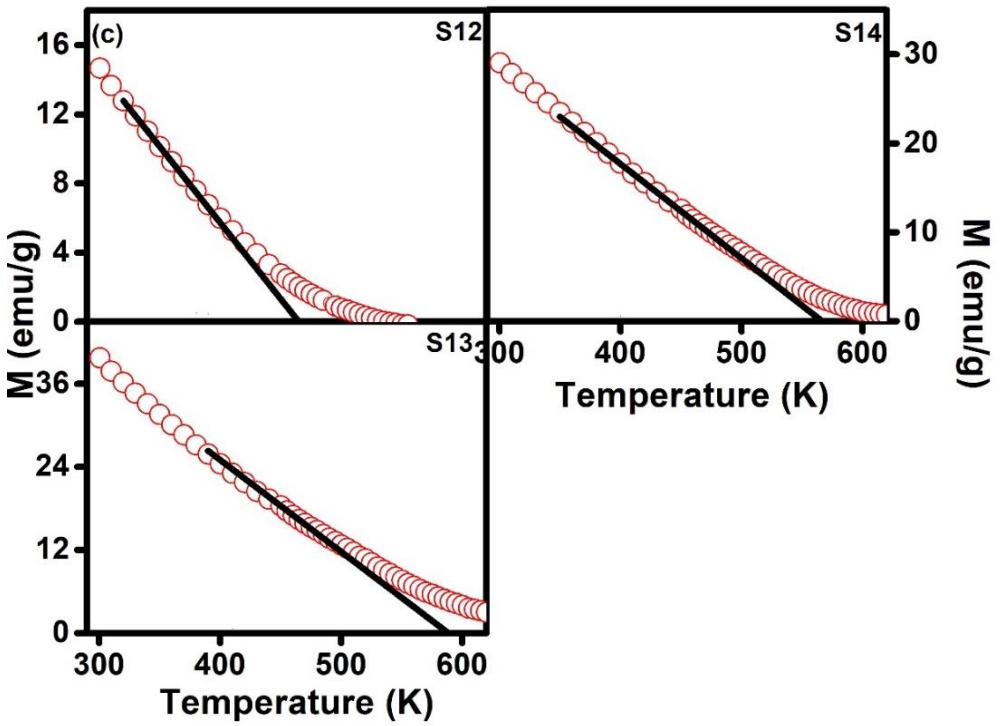

Fig. 3.15. (c) M → T plots of MZ4 nanoparticles synthesized as a function of reaction temperature. Here 1 emu/g = 1 Am^2/Kg.

As-synthesized MZ4 nanoparticles having mixed spinel structure ($Zn^{2+}_{0.4}\ Mn^{2+}_{0.4}\ Fe^{3+}_{0.2}\ [Mn^{2+}_{0.2}\ Fe^{3+}_{0.8}\ Fe^{3+}]\ O^{2-}_{4}$), have Curie temperatures that ranges from 392 K to 665 K. As the A–A interactions are 10 times weaker than the A–B and B–B interactions in these ferrites, T_c depends on the occupancy of Mn^{2+} ions in the spinel matrix. In MZ4 nanoparticles it is assumed that Mn^{2+} occupies the tetrahedral A–sites. Partial presence of Mn^{2+} at the octahedral B–sites may change the T_c from its original value. The highest value of T_c for sample S3 (prepared at pH 11) can be explained in terms of the site occupancy of Mn^{2+} ions. For higher pH (pH >11), Curie temperature decreases with increase in the particle size due to the decrease in the occupancy of Mn^{2+} ions at the B–sites **(Fig 3.16).** For lower pH (pH <11), Curie temperature increases with increase in the magnetic particle size.

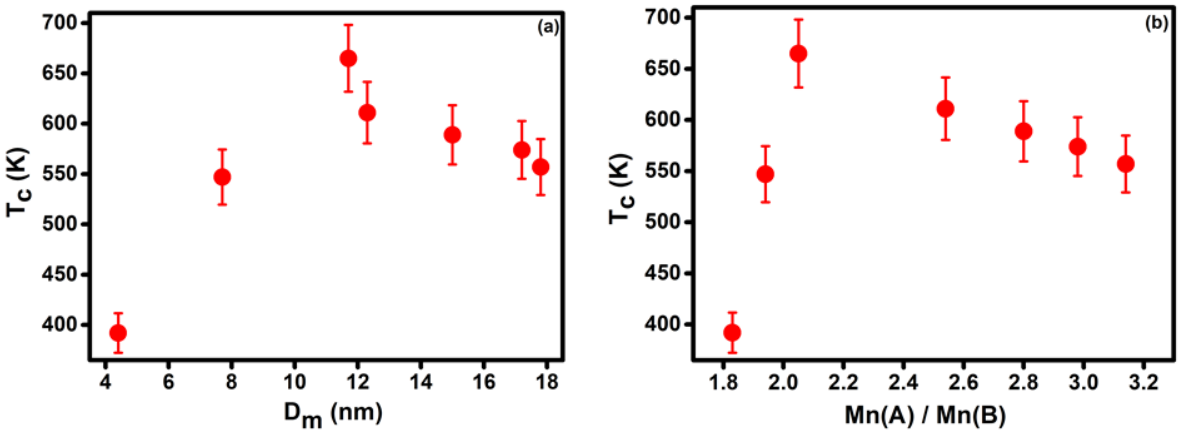

Fig. 3.16. Curie temperature (T_c) of MZ4 nanoparticles (prepared at different reaction pH) as function of (a) magnetic diameter of nanoparticles and (b) ratio of occupancy of Mn^{2+} at A–sites and B–sites in the spinel structure.

Effect of reaction time on the Curie temperature of MZ4 nanoparticles is shown in **Fig. 3.17.** It has been observed that the Curie temperature of MZ4 nanoparticles increases with increase in the reaction time from 1h to 3h. This is because of the increase in the magnetic particle size of MZ4 nanoparticles. A sharp decrease in T_C was observed for MZ4 nanoparticles prepared at 4h. This variation in T_c of MZ4 nanoparticles has similar dependency on magnetic particle size and ratio of occupancy of Mn^{2+} ions at tetrahedral A–sites and octahedral B–sites in the spinel structure **(Fig. 3.17).**

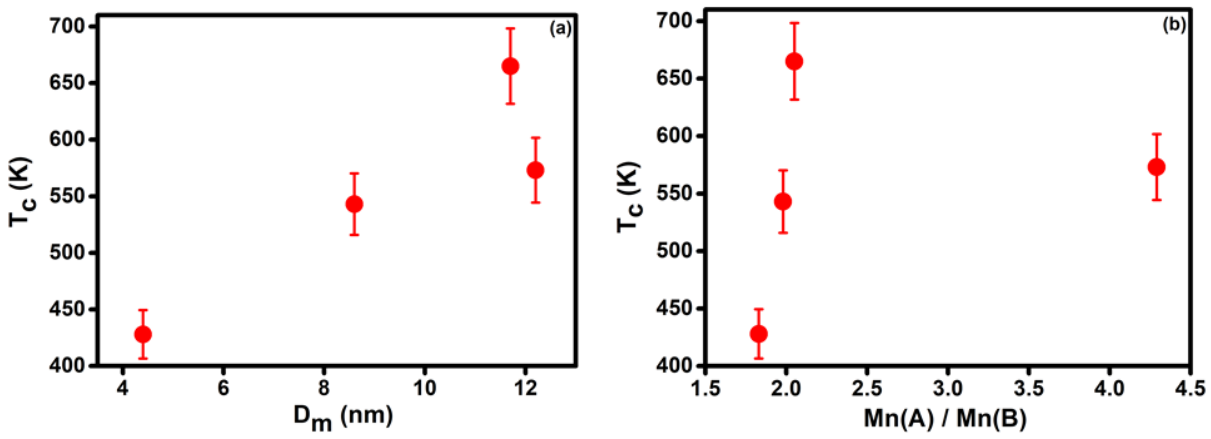

Fig. 3.17. Curie temperature (T_c) of MZ4 nanoparticles (prepared at different reaction time) as function of (a) magnetic diameter of nanoparticles and (b) ratio of occupancy of Mn^{2+} ions at A–sites and B–sites in the spinel structure.

Effect of reaction temperature on the Curie temperature of MZ4 nanoparticles are shown in **Fig 3.18.** It has been observed that Curie temperature of MZ4 nanoparticles increases with increase in the reaction temperature from 80 ºC to 90 ºC and with further increase in temperature T_c decreases **(Fig. 3.18).** This decrease in T_c at higher reaction temperature was caused by the corresponding changes in the occupancy of Mn^{2+} cations at A–sites and at B–sites.

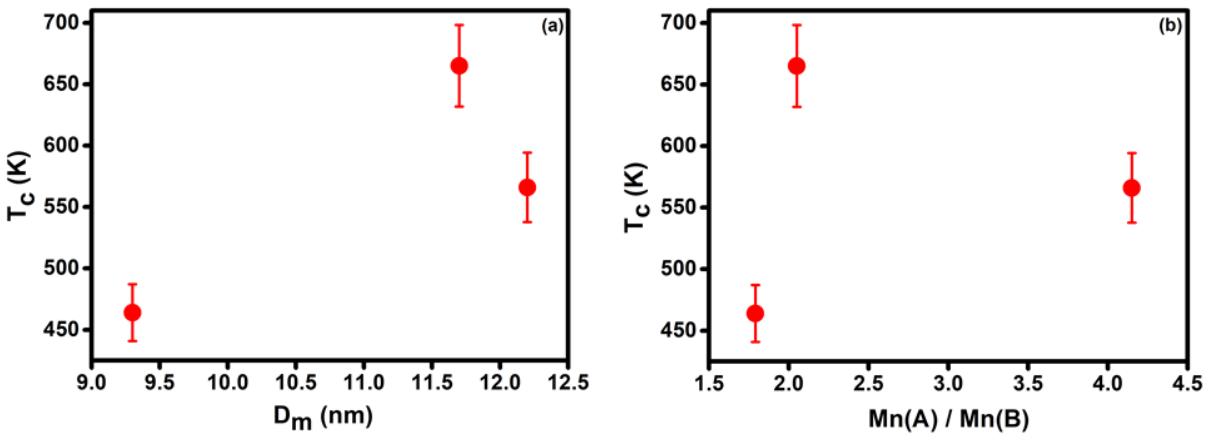

Fig. 3.18. Curie temperature (T_c) of MZ4 nanoparticles (prepared at different reaction temperature) as a function of (a) magnetic diameter of nanoparticles and (b) ratio of occupancy of Mn^{2+} ions at A–sites and B–sites in the spinel structure.

Structural and hence magnetic properties of MZ nanoparticles can be tuned by optimizing either the degree of Zn-ion substitution in spinel matrix or by controlling the reaction conditions (pH, temperature, time) of co-precipitation reaction. Amongst MZ nanoparticles, MZ4 nanoparticles are best suited for intended applications due to their small size and higher magnetization. The co-precipitation conditions of reaction pH = 11, reaction temperature = 90 ºC and reaction time = 3h yield MZ4 nanoparticles with optimum magnetic properties.

References

1. R. V. Mangalaraja, S. Ananthakmar, P. Manohar, F. D. Gnanam, M. Awano, *Mater. Sci. Eng. A.* **367** (2004) 301.
2. W. H. Lin, S. K. J. Jean, C. S. Hwang, *J. Mater. Res.* **14** (1999) 204.
3. R. Arulmurugan, B. Jeyadevan, G. Vaidyanathan, S. Sendhilnatha, *J. Magn. Magn. Mater*. **288** (2005) 470.
4. A. Thakur, P. Mathur, M. Singh, *J. Phys. Chem. Solids.* **68** (2007) 378.
5. S. K. Pradhan, S. Bid, M. Gateshki, V. Petkov, *Mater. Chem. Phys.* **93** (2005) 224.
6. K. Mazz, A. Mumtaz, S. K. Hasanin, A. Ceylan, *J. Magn. Magn. Mater* **308** (2007) 289.
7. N. T. Lan, T. D. Hien, N. P. Duong, D. V. Truong, *J. Korean Phys. Soc*. **52** (2008) 1522.
8. R. Arulmurugan, G. Vaidyanathan, S. Sendhilnathan, B. Jeyadevan, *J. Magn. Magn. Mater.* **298** (2006) 83.
9. E. V. Gopalan, I. A. Al-Omari, K. A. Malini, P. A. Joy, D. S. Kumar, Y. Yoshida, M. R. Anantharaman, *J. Magn. Magn. Mater.* **321** (2009) 1092
10. M. Chand, A. Kumar, Annveer, S. Kumar, A. Shankar, R. P. Pant, *Indian J. Eng. Mater. Sci.* **18** (2011) 385.
11. L. B. McCusker, R. B. Von Dreele, D. E. Cox, D. Loue, P. Scardi, *J. Appl. Cryst.* **32** (1999) 36.
12. D. S. Mathew, R. S. Juang, *Chem. Eng. J.* **129** (2007) 51.
13. C. Rath, S. Anand, R. P. Das, K. K. Sahu, S. D. Kulkarni, S. D. Date, N. C. Mishra, *J. Appl. Phys.* **91** (2002) 2211.
14. N. Kaur, B. Chudasama, *Micro Nano Lett.* **12** (2017) 151.
15. J. Smit, H. P. J. Wijn, *Ferrites-physical properties of ferromagnetic oxides in relation to their technical applications*, New York: Wiley (1959).
16. C. Suryanarayana, M. G. Norton, *X-ray Diffraction a Practical Approach*, Plenum Press, New York and London, (1998) 213.
17. M. Daniil, Y. Zhang, H. Okumura, G. C. Hadjipanayis, *IEEE T Magn.* **38** (2002) 2973.
18. K. Parekh, R. V. Upadhyay, R. V. Mehta, *Bull. Mater. Sci.,* **23** (2000) 91.
19. N. Andhariya, B. Chudasama, R. V. Mehta, R. V. Upadhyay, *J Nanopart Res* **13** (2011) 3619.
20. M. Knobel, W. C. Nunes, A. L. Brandl, J. M. Vargas, L. M. Socolovsky, D. Zanchet, *Physica B* **354** (2004) 80.
21. B. D Cullity, *Introduction to magnetic materials* (Addison Wesley, Reading) (1972).
22. M. D. Mukadam, S. M. Yusuf, P. Sharma, S. K. Kulshreshtha, *J. Magn. Magn. Mater.* **269** (2004) 317
23. N. Kaur, B. Chudasama, *J. Magn. Magn. Mater.* **441** (2018) 647.
24. M. Atif, S. K. Hasanian, M. Nadeem, *Solid State Commun.* **138** (2006) 416.
25. S. Ammar, N. Jouini, F. Fievet, Z. Beji, L. Smiri, P. Moline, M. Danot, J. M. Greneche, *J. Phys.: Condens. Matter*. **18** (2006) 9055
26. S. M. Daliya, R. S. Juang, *Chem. Eng. J.* **129** (2007) 51
27. L. Jianjun, Y. Hongming, L. Guodong, Liu, Yanju, J. Leng, *J. Magn. Magn. Mater.* **322** (2010) 3396
28. V. A. M. Brabers, *Handbook of Magnetic Materials*, New York, **8** (1995).

29. Y. Xuan, Q. Li, G. Yang, *J. Magn. Magn. Mater*. **312** (2007) 464.
30. J. Nogues, J. Sort, V. Langlias, V. Skumryev, S. Surinach, J. S. Munoz, M. D. Baro, *Physics Reports* **422** (2005) 65
31. C. Guillaud, H. Creveaux, *C. R. Acad. Sci. (Paris)* **230** (1950) 1458.
32. M. R. Anantharaman, S. Jagadeeshan, K. A. Malini, S. Sindhu, A. Narayanasswamy, C.N. Chinnasamy, J. P. Jacobs, S. Rejine, K. Sheshan, R. H. H. Smits, H. H. Brongersma, *J. Magn. Magn. Mater*. **189** (1998) 83.
33. F. K. Lotgering, *J. Phys. Chem. Solids* **27** (1966) 139.
34. L. Rabkin, S. Soskin, B. Epsstein, *Ferrites: Structure, properties and technology Leningrad* (1968) 263.
35. R. Desai, V. Davariya1, K. Parekh, R. V. Upadhyay, *Pramana-J Phys* **73** (2009) 765.
36. M. Yokoyarna, E. Ohta, T. Sato, T. Komaba, T. Sato, *J. Phys IV France* **7** (1997) C1.
37. Z. X. Tang, C. M. Sorensen, K. J. Klabunde, *Phys Rev Lett.* **67** (1991) 3602.
38. P. J Van der Zaag, A. Noordermeer, M. T. Johnson, P.F. Bongers, *Phys Rev Lett*. **68** (1992) 3112.

CHAPTER 4

SYNTHESIS AND CHARACTERIZATION OF MAGNETIC FLUID

4.1 INTRODUCTION

Magnetic fluids for heat exchange devices should possess large thermomagnetic coefficient and suitable Curie temperature, which should be matching with the operating temperature of the device. As discussed in **Chapter 3**, MZ nanoparticles are well suited for temperature sensitive magnetic fluids as they possess moderate saturation magnetization and tunable Curie temperature. Magnetic nanoparticles when dispersed in transformer oil should be able to withstand the device's operating temperature without any loss in their dispersity [1]. Stability of magnetic fluids largely depends on the characteristics of the nanoparticles and quality of their dispersion in transformer oil. It has been observed that various fluids have different degree of dispersion stability, which is a function of particle concentration in fluids and degree of zinc substitution in MZ nanoparticles [2, 3]. Another important parameter that effects the stability of the magnetic fluids is the size of nanoparticles and its distribution. Small size of nanoparticles and narrow size distribution is essential to prepare stable magnetic fluids [4]. Moreover, variation in composition, synthesis route and conditions of synthesis like reaction pH, reaction time and reaction temperature play an important role in controlling the particle size and its distribution in magnetic fluids. Therefore, it is desirable to synthesize MZ fluids in transformer oils that possess good dispersion qualities.

In this Chapter, detailed discussion on the development of synthesis protocols for MZ fluids is described. Effect of degree of Zn-ion substitution under optimized condition of MZ nanoparticles, on the dispersion quality and magnetic properties of MZ fluids are investigated in this chapter.

4.2 SYNTHESIS OF MZ FLUIDS

4.2.1 Materials

AR grade oleic acid was obtained from S.D. fine-chem Ltd., ammonia solution was purchased from LOBA chemicals, acetone and ethanol was purchased from Merck. Transformer oil was gifted by M/S Savita Oil Technologies Limited, India. All chemicals were used as-received without any purification. Aqueous solutions were prepared in Milli-Q ultrapure water (ρ = 18.2 MΩ)

4.2.2 Synthesis process

To prepare magnetic fluids, MZ nanoparticles are synthesized by the co-precipitation method by following the protocols described in **Chapter 3**. These as-synthesized MZ nanoparticles were coated with monolayer of oleic acid to disperse them in transformer oil. The schematic diagram of synthesis protocols followed for the preparation of MZ nanoparticles based magnetic fluids are summarized in **Fig. 4.1** and described in detail in **Annexure–I (A3).**

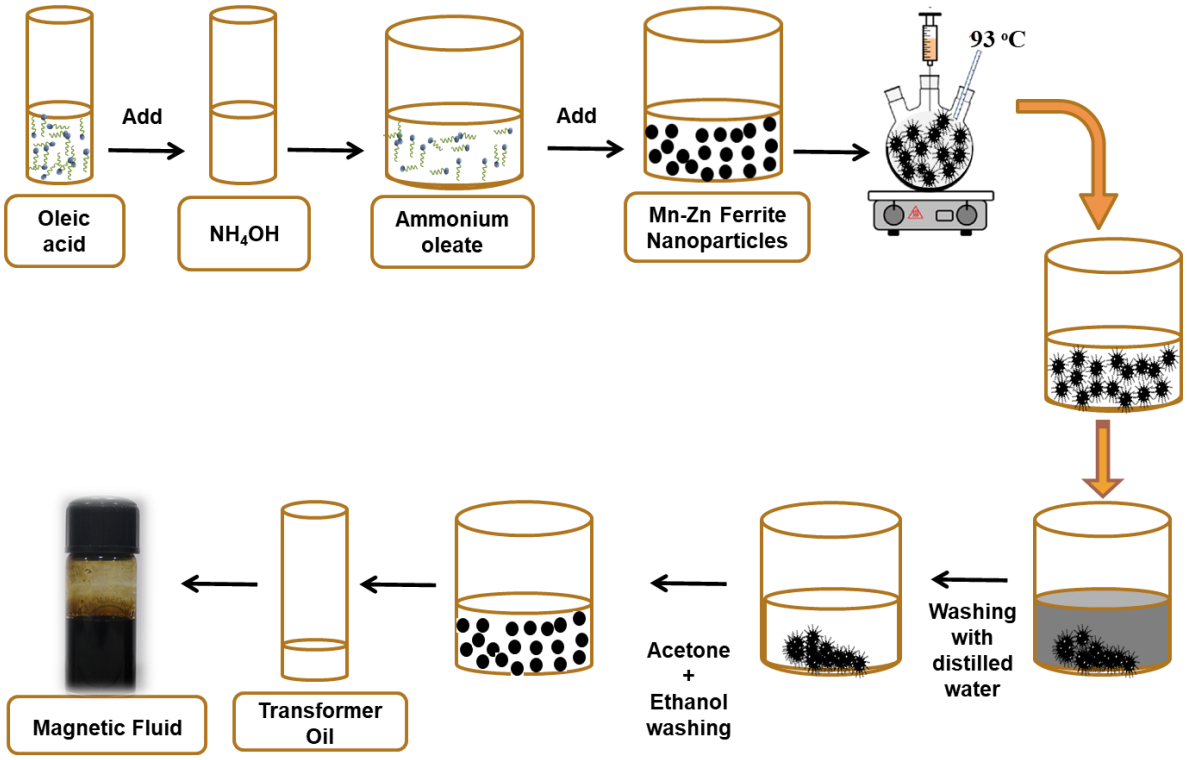

Fig. 4.1. Schematic diagram representing synthesis of MZ magnetic fluids.

Ammonium oleate was prepared by adding oleic acid (2.3 mL) drop by drop into diluted ammonia solution (40 mL water + 10 Ml (25 %) ammonia solution) under continuous stirring. It was heated at 60 °C till a clear transparent solution is prepared. This ammonium oleate was allowed to cool at room temperature and it was then added into the equal volume of aqueous dispersion of MZ nanoparticles. It was homogenized by continuous stirring for 1 h at room temperature. Oleic acid to nanoparticle w/w ratio was 1:1. It was then heated to 93 °C. At this temperature, ammonium oleate decompose and oleic acid chemi-adsorbed on the surface of magnetic nanoparticles through metal-hydroxyl bonds. After cooling to room temperature, the oleic acid coated magnetic nanoparticles were focculated with dilute HCl. For focculation dilute

HCl was added into dispersion of nanoparticles till its pH drops below 5. Nanoparticles were magnetically decanted and washed several times with warm distilled water to remove excess surfactants. Finally they were washed with a solution of acetone-ethanol (v/v = 1:1). Nanoparticles are then redispersed in commercial grade 20 mL transformer oil. By following these protocols, five sets of magnetic fluids are prepared. Volume fraction (φ) of MZ nanoparticles was kept at 2.2% in each fluids. Sample codes along with composition of magnetic nanoparticles of each fluids are mentioned in **Table 4.1**

Table 4.1. Sample codes and composition of temperature sensitive magnetic fluids.

Sample code	Composition of magnetic fluids
MZ0-F	$Mn_{1.0}Zn_{0.0}Fe_2O_4$
MZ2-F	$Mn_{0.8}Zn_{0.2}Fe_2O_4$
MZ4-F	$Mn_{0.6}Zn_{0.4}Fe_2O_4$
MZ6-F	$Mn_{0.4}Zn_{0.6}Fe_2O_4$
MZ8-F	$Mn_{0.2}Zn_{0.8}Fe_2O_4$

4.3 CHARACTERIZATION OF MZ FLUIDS

Fig. 4.2 shows the magnetization curves of as-synthesized MZ fluids. With increase in the external magnetic field, the magnetization of MZ fluids increases because of progressive alignment of ensemble of magnetic particles dispersed in transformer oil along the external field direction. All samples except MZ0-F exhibit superparamagnetism i.e. zero remanence and zero coercivity **(Fig. 4.2).** A very narrow hysteresis loop is observed in MZ0-F (Inset of **Fig. 4.2**). It may because of the small ferrimagnetic contribution from MZ0 nanoparticles having their size greater than the superparamagnetic limit. Saturation magnetization of MZ fluids have same dependence on degree of Zn-substitution as observed for MZ nanoparticles in **Chapter 3**. The only difference between the alignment of magnetic moments in this and previous case of nanoparticles is the type of rotation. In case of MZ nanoparticles, the only possible rotation is the Neel rotation; while in fluids, in addition to the Neel rotation, Brownian rotation is also possible [5]. The schematic diagram of these two types of rotation are shown in **Fig. 4.3.**

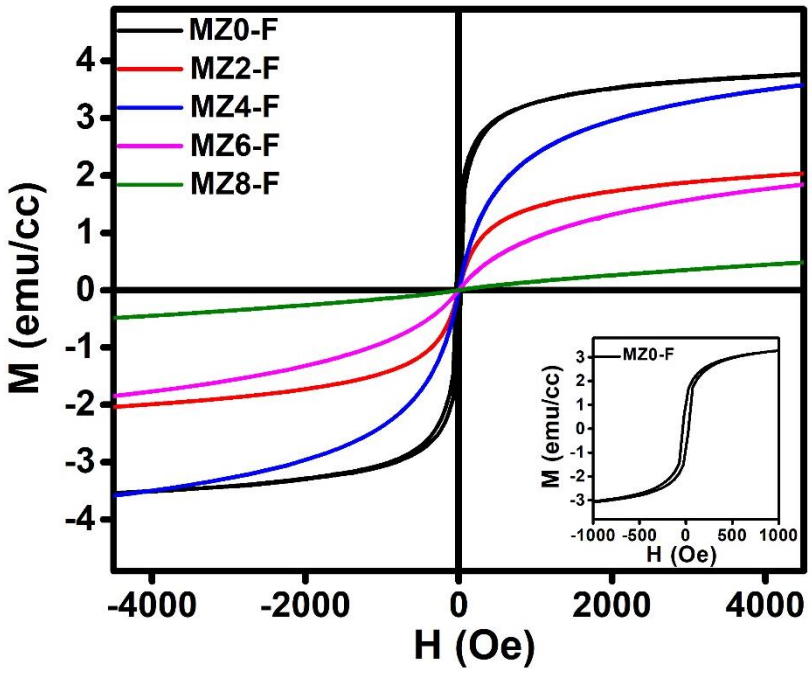

Fig. 4.2. Magnetization as-synthesized MZ fluids measured at room temperature. Here 1 emu/cc = 1000 A/m and 1 Oe = 79.61 A/m.

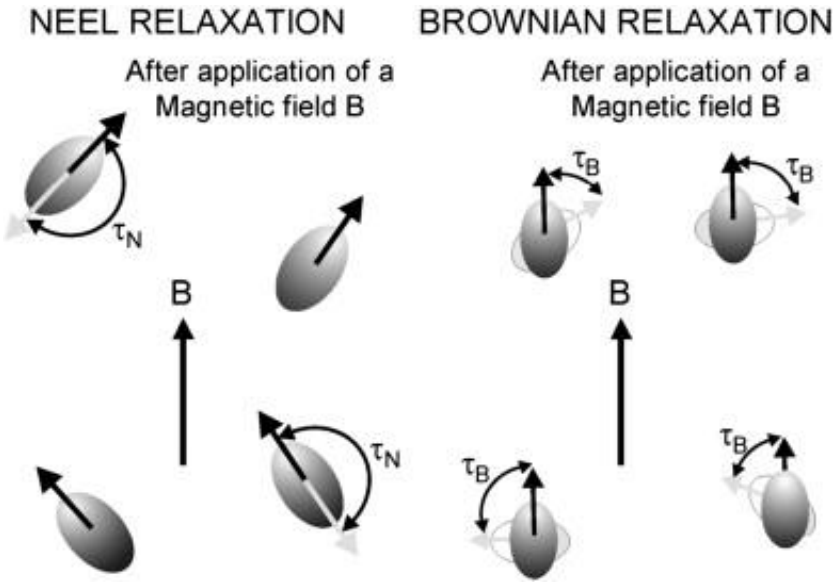

Fig. 4.3. Schematic diagram representing Neel and Brownian rotation in MZ fluids [5].

Magnetization of an assembly of isolated superparamagnetic nanoparticle can be described by the modied Langevin's theory [6].

$$M = M_s \int_0^\infty f(D)\, L\left(\frac{\mu(H+H_{int})}{k_B T}\right) dD + \chi H \qquad (4.1)$$

where M_s is the saturation magnetization of nanoparticles and $L(\alpha) = \coth\alpha - 1/\alpha$ is the Langevin function. The Langevin parameter $\alpha = \mu(H + H_{int})/k_BT$. μ is the magnetic moment of individual spin cluster, H is the applied external magnetic field, $H_{int} = \lambda M_1$; λ is the mean field constant (dimensionless) and M_1 is the internal field acting on each particle/cluster, f(D)dD is the log-normal cluster diameter distribution function with mean cluster diameter D_m and width σ and χ is the susceptibility of nanoparticles having size above superparamagnetic limit.

Magnetization of as-synthesized MZ fluids fitted modified Langevin theory is shown in **Fig. 4.4.** From the fit, magnetic particle diameter (D_m), saturation magnetization (M_s), polydispersity (σ), mean field constant (λ) and ferrimagnetic susceptibility (χ) have been determined, which are also reported in **Table 4.2.** Effect of degree of Zn-substitution on the saturation magnetization (M_s) is plotted as a function of Zn content for as-synthesized MZ fluids in **Fig. 4.4 (b).** Saturation magnetization of MZ fluids varies from 0.1 emu/cc to 3.5 emu/cc **(Table 4.2).** Both the mean field constant and mean internal field as obtained from the fits increases with the increase in the Zn content (x = 0.2 - 0.8), indicating inter-particle interaction between magnetic nanoparticle increases with increase in the Zn content. This interaction depends not only on the distance between magnetic particles but also on the mutual orientation of their magnetic moments, which are now strongly correlated due to the Brownian rotation of nanoparticles in the fluid [7]. Magnetic particle size (D_m) as obtained from the fits of magnetization data with the Langevin theory decreases with the increase in the Zn content **(Fig. 4.4).**

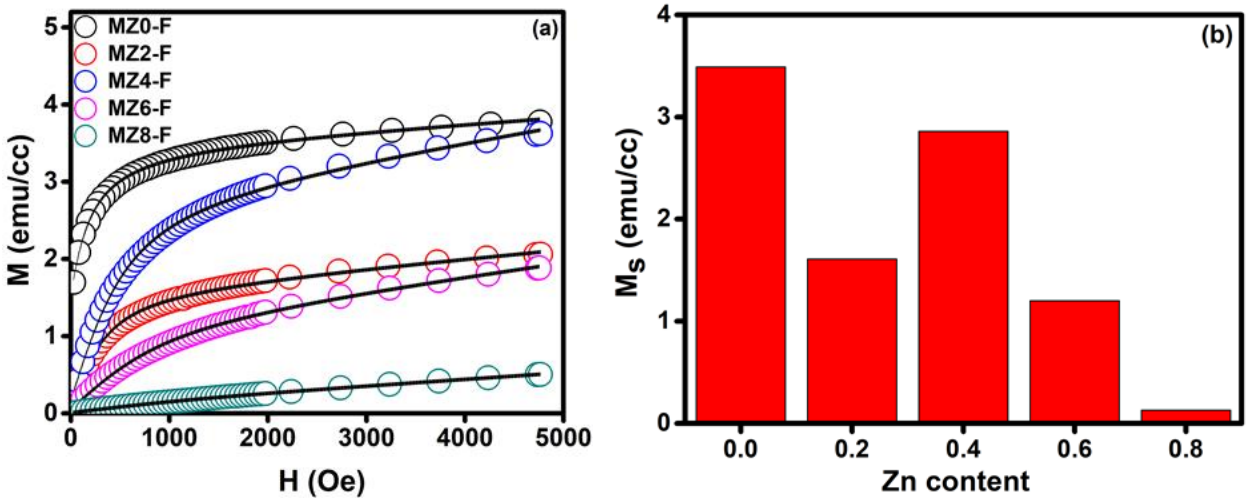

Fig. 4.4. (a) Magnetization of MZ fluids fitted with modified Langevin theory and (b) Saturation magnetization of as-synthesized MZ fluids as a function of degree of Zn substitution. Here 1 emu/cc = 1000 A/m and 1 Oe = 79.61 A/m.

Table 4.2. Magnetic parameters of MZ fluids derived from the fits of magnetization data with modified Langevin theory. Here 1 emu/cc = 1000 A/m and 1 O_e = 79.61 A/m.

Parameters	MZ0-F	MZ2-F	MZ4-F	MZ6-F	MZ8-F
M_s (emu/cc)	3.49	1.61	2.86	1.20	0.13
σ	0.22	0.24	0.23	0.23	0.23
D_m (nm)	14.80	13.9	11.6	9.30	9.00
λ	49.32	23.84	26.31	27.89	38.26
H_{int} (O_e)	146.90	34.32	41.80	47.13	88.38
χ ($\times 10^{-5}$)	7.92	11.10	19.70	16.60	8.23

D_m of MZ fluids decreases with increase in the Zn-content **(Fig. 4.5).** Polydispersity of MZ fluids obtained from the fits of magnetization data is also shown in **Fig. 4.6.** It varies from 0.22 to 0.24 and is nearly constant irrespective of degree of Zn-substitution. This relatively small and constant value of polydispersity indicates good dispersion stability of all MZ fluids **(Fig. 4.7).** Hydrodynamic size (D_H) of MZ fluids varies between 16 and 26.5 nm **(Fig. 4.5).** No systematic trend is observed in the hydrodynamic size of MZ fluids with degree of Zn-substitution. However, the broader trend is identical to the changes in the magnetic particle size of the fluids.

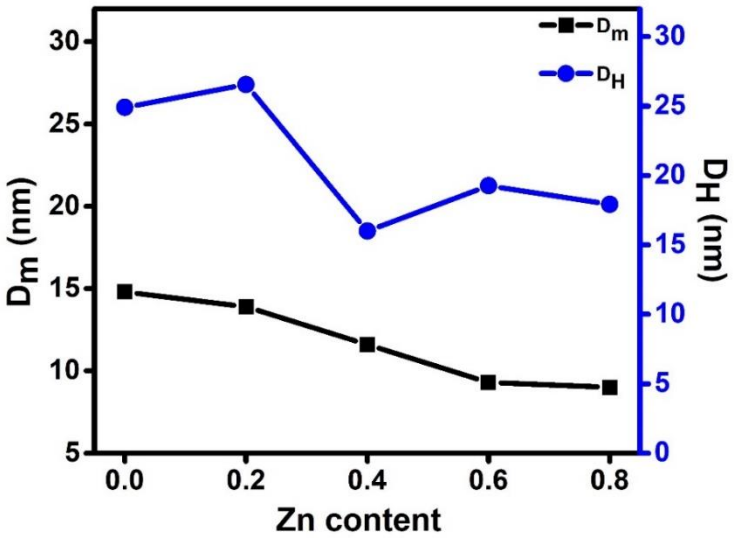

Fig. 4.5. Effect of Zn-substitution on magnetic diameter (D_m) and hydrodynamic diameter (D_H) of MZ fluids.

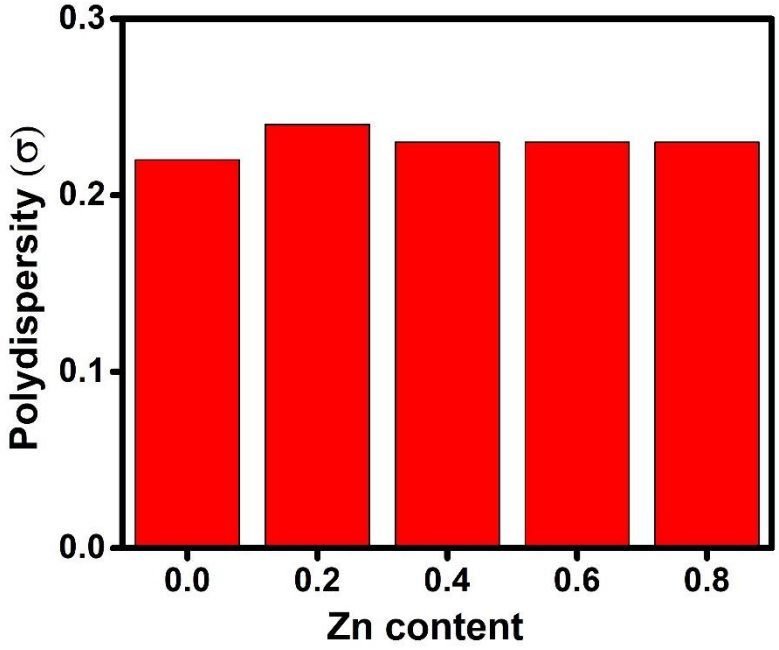

Fig. 4.6. Polydispersity of as-synthesized MZ fluids as a function of Zn content.

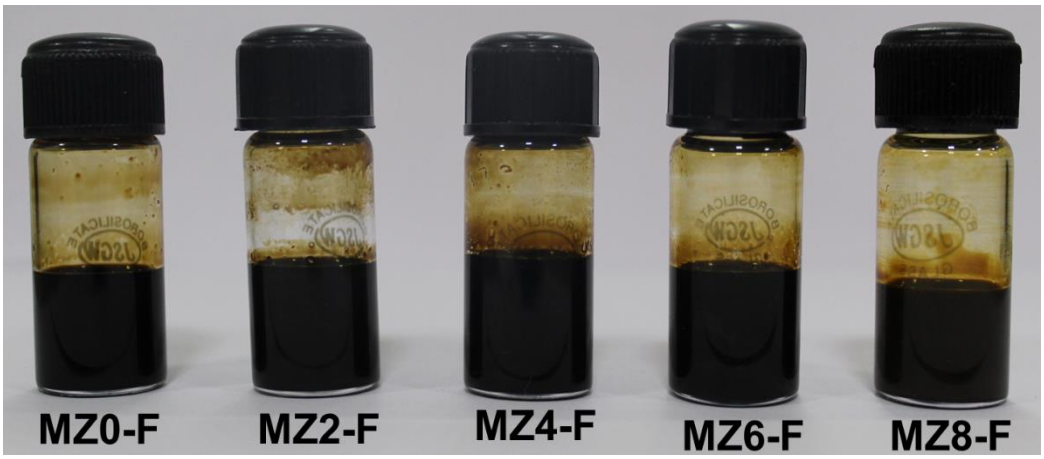

Fig. 4.7. Photographic view of as-synthesized MZ fluids showing good dispersion stability at room temperature.

Dispersion quality of MZ fluids also depends on oleic acid coating. Nanoparticles deficient with oleic acid monomers on their surface tend to agglomerate and lose their dispersion stability over time. A monolayer of oleic acid is desired for the good dispersion stability of nanoparticles [8]. To investigate the oleic acid coating on MZ fluids, thermogravimetric analysis was performed on MZ nanoparticles which are obtained by washing MZ fluids with acetone followed by vacuum dry at 25 °C. TGA thermograms of nanoparticles are shown in **Fig. 4.8.**

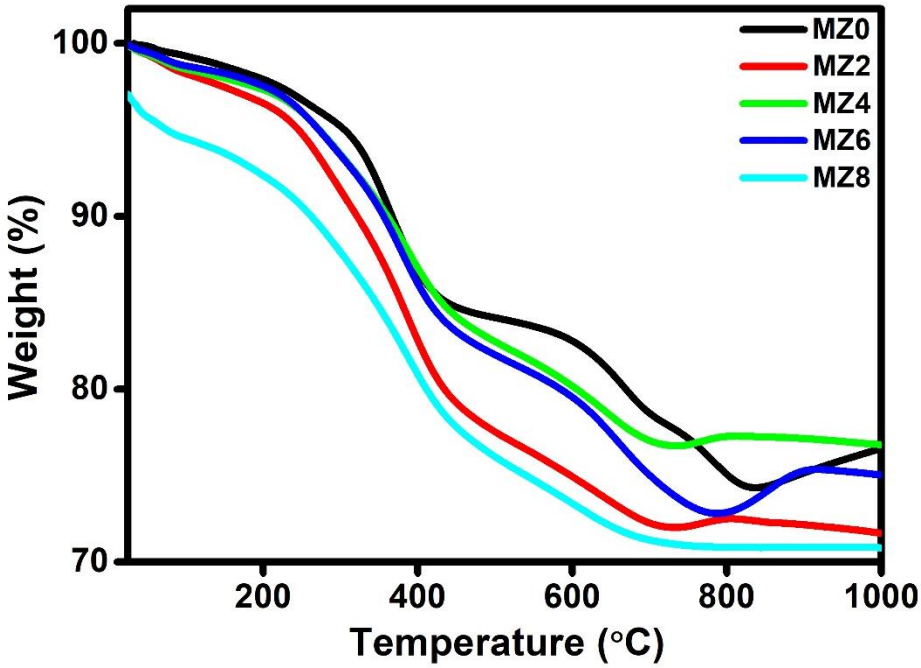

Fig. 4.8. TGA thermograms of oleic acid coated MZ nanoparticles.

Single-step weight loss of 0 – 30 % is observed in each thermogram. This is because of the decomposition of oleic acid. This weight loss corresponds to monolayer coating of oleic acid coating on the surface of the MZ nanoparticles [8]. This further confirms good dispersion stability of nanoparticles in transformer oil. A magnetic nanoparticle having its diameter 10 – 20 nm will show 20 – 30 % weight loss in their TG thermograms, if they are coated with a monolayer of oleic acid [8]. Instead, if multilayers of oleic acid is coated on the nanoparticle surface than the weight loss will be > 30%.

As-synthesized MZ fluids in transformer oil show good dispersion stability owing to their small size (<25 nm), moderate polydispersity (<0.25) and monolayer coating of nanoparticles. Their magnetic properties are strongly correlated with the degree of Zn-ion substitution in the dispersed MZ nanoparticles. The saturation magnetization (M_s) and magnetic particle size (D_m) decreases with increase in the Zn-ion substitution. Colloidal stability of these as-synthesized MZ fluids under aging are further investigated in next chapters.

References

1. K. Parekh, R. V. Upadhyay, *Indian J. Eng. Mater. Sci.* **11** (2004) 262.
2. K. Shah, R. V. Upadhyay, V. K. Aswal, *Smart Mater. Struct.* **21** (2012) 075005.
3. A. Jozefczak, T. Hornowski, A. Skumiel, *Int J Thermophys* **32** (2011) 795.
4. R. E. Rosensweig, *Ferrohydrodynamic*s, Dover Publications, inc. Mineola, New York (1997).
5. S. Laurent, S. Dutz, U. O. Hafeli, M. Mahmoudi, *Adv. Colloid Interface Sci*. **166** (2011) 8.
6. N. Kaur, B. Chudasama, *J. Magn. Magn. Mater*. **451** (2018) 647.
7. A. O. Ivanov, S. S. Kantorovich, *Phys. Rev. E.* **70** (2004) 021401
8. N. Andhariya, B. Chudasama, R. Patel, R. V. Upadhyay, R V. Mehta , *J. Colloid Interface Sci*. **323** (2008) 153.

CHAPTER 5

COLLOIDAL STABILITY OF MAGNETIC FLUIDS

5.1 INTRODUCTION

Colloidal stability of magnetic fluids plays an important role in cooling applications in power transformers. For stable magnetic fluids, magnetic nanoparticles need to be dispersed in transformer oil with good colloidal stability [1]. Agglomeration of magnetic nanoparticles results in the sedimentation of fluids, which could cause clogging of micro-channels in transformers that could result into permanent reduction in the cooling efficiency of the device. This particle agglomeration can also lead to the decrease in the thermal conductivity of magnetic fluids. Therefore, investigation on the colloidal stability of magnetic fluids is an important aspect and needs detailed investigation.

It is important to study and analyse factors influencing the colloidal stability of magnetic fluids when aged. One of the important parameter that affects the colloidal stability of the magnetic fluids is the size of nanoparticles and their distribution in the dispersing medium. Small size of nanoparticles and narrow size distribution improve the colloidal stability of fluids [2]. It was reported that magnetic particles dispersed in fluids remain in Brownian motion when their size is between 4 nm to 20 nm [3]. When diluted; magnetic nanoparticles in the fluid tend to aggregate and disturb the colloidal stability by formation of aggregates of nanoparticles, whose size ranges between 100 – 200 nm [3, 4]. These aggregates may adhere together and settle under the influence of gravity. Stability denotes that the particles do not aggregate at significant rate. This chapter aims to estimate the lifetime of MZ fluids. Role of dipole-dipole interaction in aggregation and their influence on the colloidal stability of transformer oil based fluids have also been probed in this chapter.

5.2 EFFECT OF AGING ON THE COLLOIDAL STABILITY OF MZ FLUIDS

MZ fluids were synthesized by following the protocols as described in **Chapter 4**. Five samples of MZ fluids were prepared simultaneously under identical conditions. Sample codes and composition of magnetic nanoparticles of each fluids are previously mentioned in **Table 4.1.** To understand the effect of aging on the stability of magnetic fluids, MZ fluids were examined by photon correlation spectroscopy (PCS) and vibration sample magnetometery (VSM) after every

30 days. This study was extended over a period of 210 days. Colloidal stability of MZ fluids were evaluated on the basis of changes in the magnetic and hydrodynamic size and size distribution of MZ fluids **(Annexure–I (A4)).**

Hydrodynamic particle size distributions of magnetic fluids obtained by photon correlation spectroscopy are shown in **Fig. 5.1.** Each histogram is fitted with lognormal particle size distribution function [5].

$$P(D) = \frac{1}{D\sigma(2\pi)^{1/2}} e^{\frac{-\ln\left(\frac{D}{D_o}\right)^2}{2\sigma^2}} \quad (5.1)$$

where, σ is polydispersity, D is particle diameter and ln (D_o) a mean of ln (D) [6].The mean hydrodynamic size and size distribution of magnetic nanoparticles in fluids are determined from these fits. Mean hydrodynamic size determined from the fits of particle size distribution histogram **(Fig. 5.1)** of MZ fluids as a function of aging time is shown in **Fig. 5.2.** Irrespective of the composition of MZ fluids, their hydrodynamic size increases with aging. This might be caused by the aggregation of magnetic nanoparticles, irrespective of the composition of MZ fluids. Polydispersity index obtained from the fits of hydrodynamic particle size distributions also increases with aging **(Fig. 5.3).** This increase in polydispersity is also an indication of the increasing aggregation of magnetic nanoparticles in fluids.

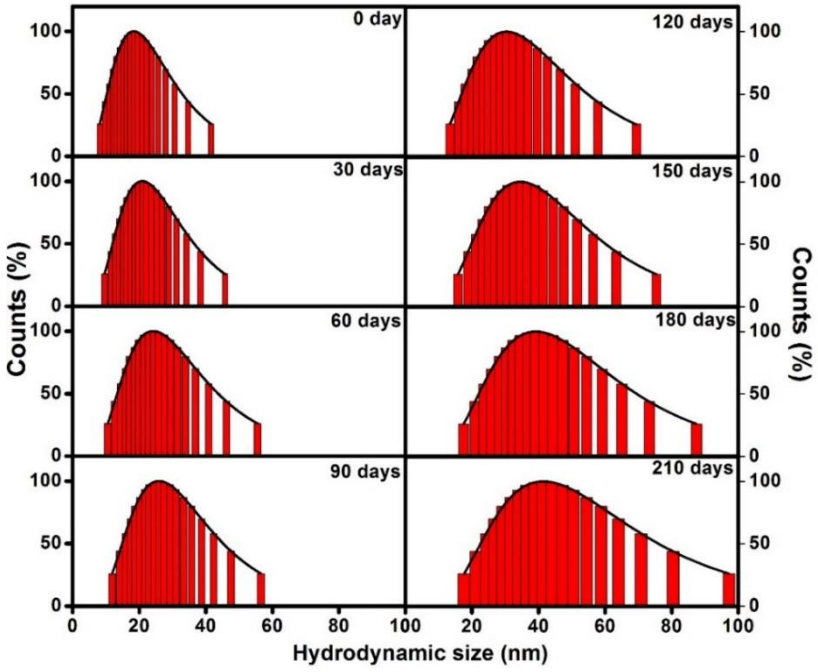

Fig 5.1(a). Effect of aging on the hydrodynamic particle size distribution of MZ0-F fluids.

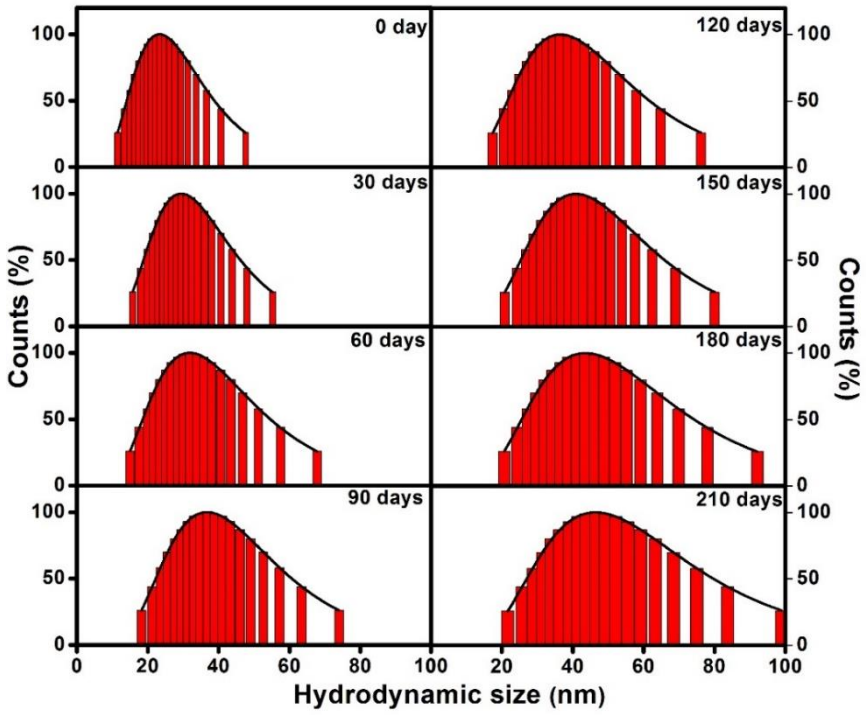

Fig 5.1(b). Effect of aging on the hydrodynamic particle size distribution of MZ2-F fluids.

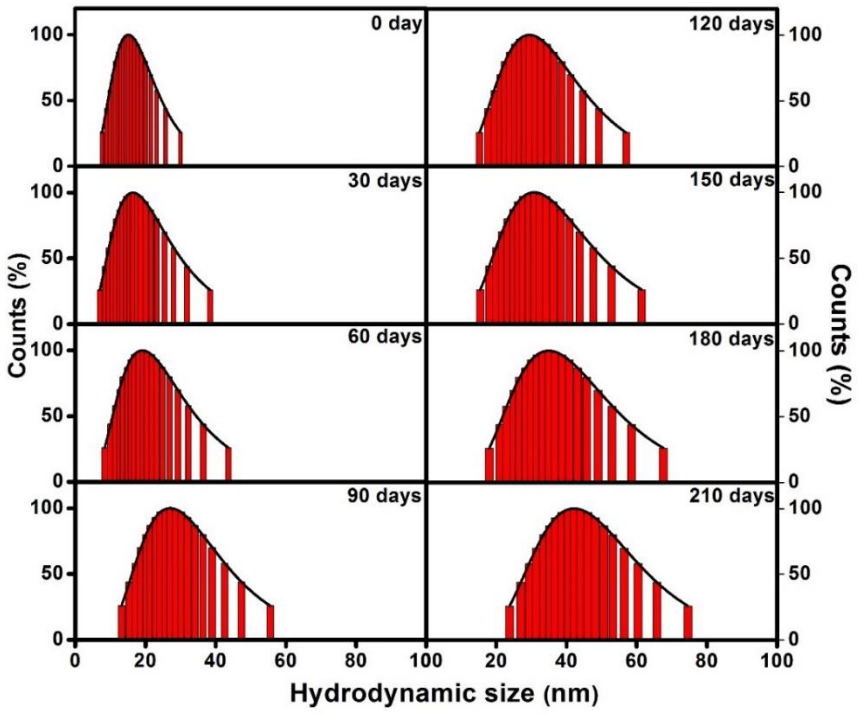

Fig 5.1(c). Effect of aging on the hydrodynamic particle size distribution of MZ4-F fluids.

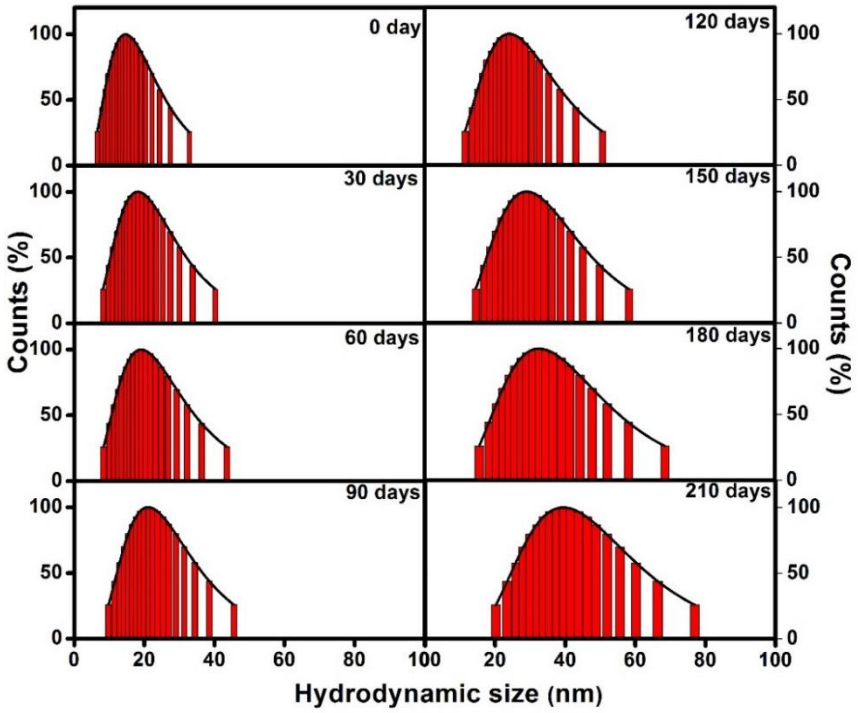

Fig 5.1(d). Effect of aging on the hydrodynamic particle size distribution of MZ6-F fluids.

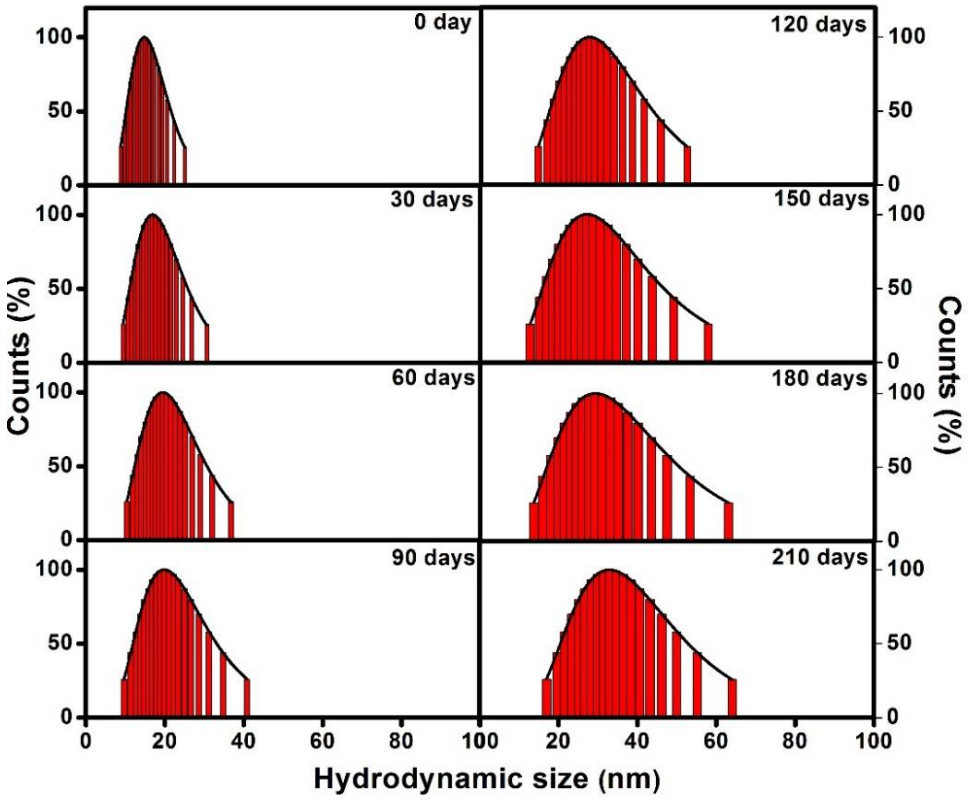

Fig 5.1(e). Effect of aging on the hydrodynamic particle size distribution of MZ8-F fluids.

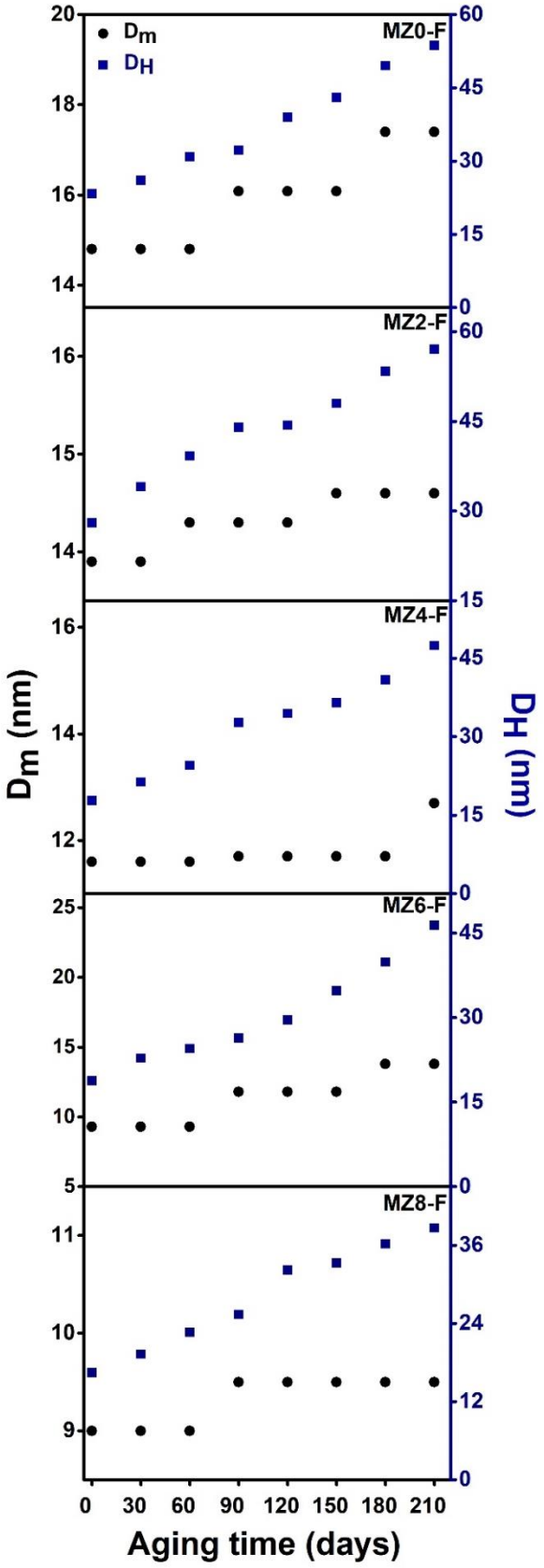

Fig. 5.2. Effect of aging on hydrodynamic particle size (D_H) and magnetic particle size (D_m) of MZ fluids.

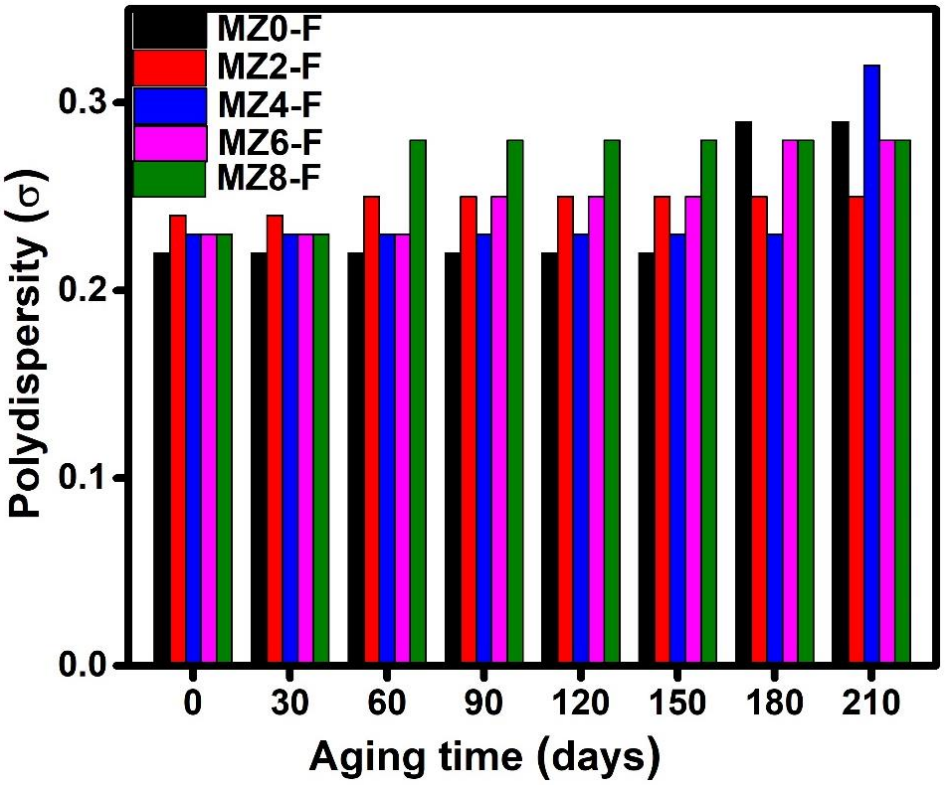

Fig. 5.3. Effect of aging on polydispersity of MZ fluids.

This aging induced aggregation of magnetic nanoparticles in fluids can also be confirmed from their magnetization measurements. Magnetization of MZ fluids was measured after every aging cycle of 30 days for a period of 210 days. Magnetization data of MZ fluids fitted with the modified Langevin equation is shown in **Fig 5.4** [7].

$$M = M_s \int_0^\infty f(D)\, L\left(\frac{\mu(H+H_{int})}{k_B T}\right) dD + \chi H \qquad (5.2)$$

where M_s is the saturation magnetization of nanoparticles and $L(\alpha) = \coth\alpha - 1/\alpha$ is the Langevin function. The Langevin parameter; $\alpha = \mu(H + H_{int})/k_B T$. μ is the magnetic moment of individual particle / spin clusters, H is applied external magnetic field, $H_{int} = \lambda M_1$; λ is mean field constant and M_1 is the internal field acting on each particle / cluster, f(D)d(D) is the log-normal cluster diameter distribution function with mean particle cluster diameter D_m and width σ and χ is the susceptibility of nanoparticles having their size greater than the superparamagnetic limit. From the fit, magnetic particle diameter (D_m), saturation magnetization (M_s), polydispersity (σ), mean field constant (λ) and ferrimagnetic susceptibility (χ) have been determined, which are reported in **Table 5.1**.

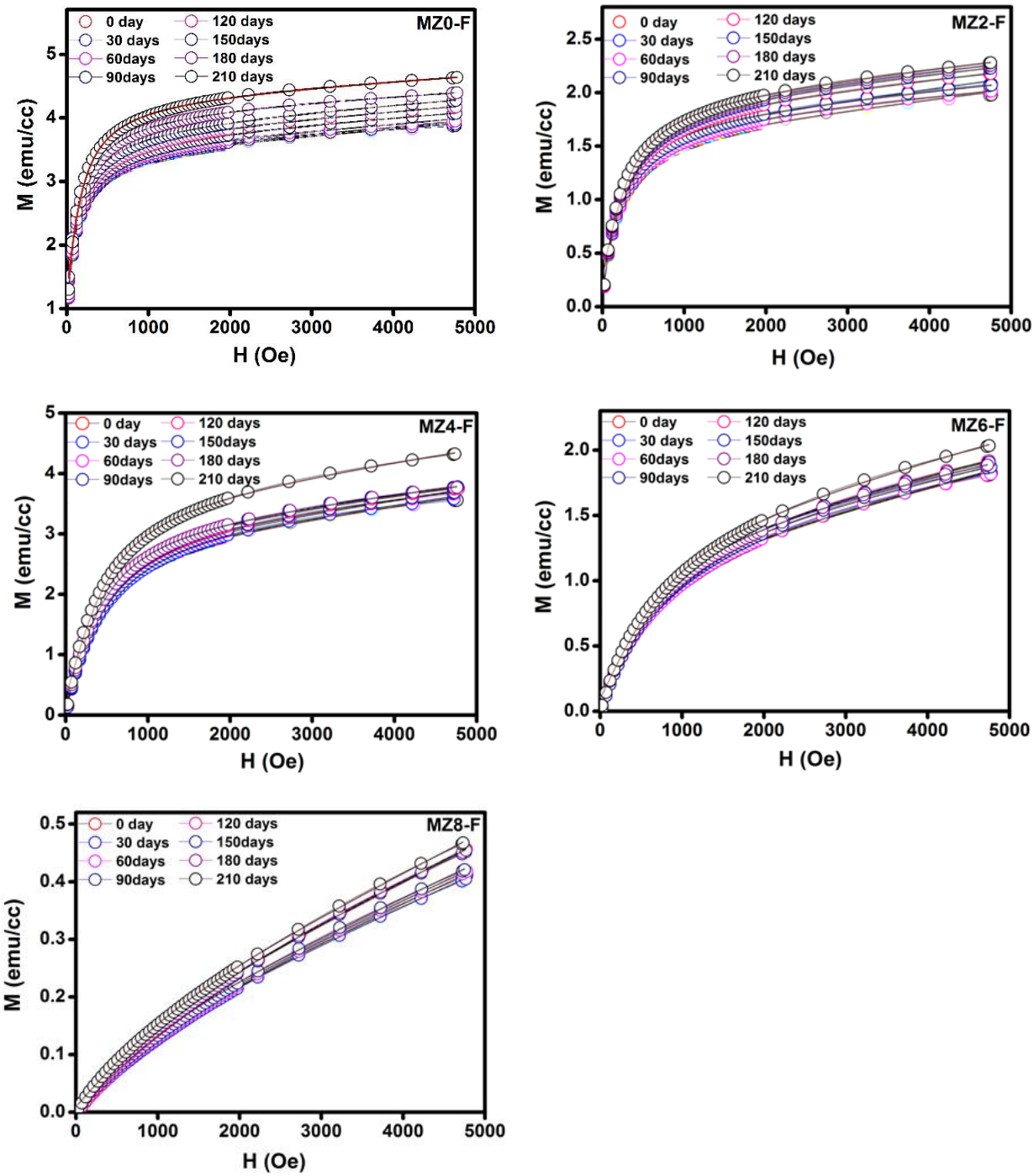

Fig. 5.4. Effect of aging on magnetization of MZ fluids. All curves are fitted with modified Langevin equation 5.2. Here 1 emu/cc = 1000 A/m and 1 Oe = 79.61 A/m.

Table 5.1(a). Effect of aging on magnetic properties of MZ0-F fluid. Here 1 emu/cc = 1000 A/m and 1 O_e = 79.61 A/m.

Magnetic parameters	Aging time (days)							
	0	**30**	**60**	**90**	**120**	**150**	**180**	**210**
M_s (emu/cc)	3.49	3.51	3.55	3.70	3.80	3.89	4.10	4.30
σ	0.22	0.22	0.22	0.22	0.22	0.22	0.29	0.29
D_m (nm)	14.80	14.80	14.80	16.08	16.08	16.08	17.40	17.40
λ	42.02	42.02	42.02	44.2	44.2	44.2	37.5	37.5
H_{int} (O_e)	1.40	1.40	1.40	2.60	2.60	2.60	2.20	2.20
χ ($\times 10^{-5}$)	9.60	9.70	9.80	9.10	9.30	9.50	7.06	7.46

Table 5.1(b). Effect of aging on magnetic properties of MZ2-F fluid. Here 1 emu/cc = 1000 A/m and 1 O_e = 79.61 A/m.

Magnetic parameters	Aging time (days)							
	0	**30**	**60**	**90**	**120**	**150**	**180**	**210**
M_s (emu/cc)	1.61	1.69	1.75	1.80	1.88	1.93	1.95	1.97
σ	0.24	0.24	0.25	0.25	0.25	0.25	0.25	0.25
D_m (nm)	13.90	13.90	14.30	14.30	14.30	14.60	14.60	14.60
λ	24.34	24.34	55.90	55.90	52.54	52.54	52.54	52.54
H_{int} (O_e)	1.47	1.47	1.44	1.44	1.44	1.44	1.44	1.44
χ ($\times 10^{-5}$)	9.00	9.47	6.65	6.83	7.44	7.60	7.70	7.70

Table 5.1(c). Effect of aging on magnetic properties of MZ4-F fluid. Here 1 emu/cc = 1000 A/m and 1 O_e = 79.61 A/m.

Magnetic parameters	Aging time (days)							
	0	**30**	**60**	**90**	**120**	**150**	**180**	**210**
M_s (emu/cc)	2.89	2.92	2.97	3.11	3.2	3.22	3.24	3.62
σ	0.23	0.23	0.23	0.23	0.23	0.23	0.23	0.32
D_m (nm)	11.60	11.60	11.60	11.60	11.70	11.70	11.70	12.70
λ	23.00	21.80	22.90	28.30	36.00	30.50	37.10	33.80
H_{int} (O_e)	1.40	1.32	1.38	1.59	1.59	1.59	1.59	1.59
χ ($\times 10^{-5}$)	1.70	1.70	1.80	1.50	1.40	1.50	1.46	1.80

Table 5.1 (d). Effect of aging on magnetic properties of MZ6-F fluid. Here 1 emu/cc = 1000 A/m and 1 O_e = 79.61 A/m.

Magnetic parameters	Aging time (days)							
	0	**30**	**60**	**90**	**120**	**150**	**180**	**210**
M_s (emu/cc)	0.12	0.12	0.12	0.14	0.14	0.14	0.14	1.42
σ	0.23	0.23	0.23	0.25	0.25	0.25	0.28	0.28
D_m (nm)	9.30	9.30	9.00	11.80	11.80	11.80	11.80	11.80
λ	27.80	27.50	26.51	37.50	33.02	31.36	37.08	35.70
H_{int} (O_e)	1.68	1.66	1.60	2.27	2.00	1.90	2.24	2.16
χ ($\times 10^{-5}$)	1.48	1.49	1.47	1.30	1.34	1.32	1.26	1.53

Table 5.1 (e). Effect of aging on magnetic properties of MZ8-F fluid. Here 1 emu/cc = 1000 A/m and 1 O_e = 79.61 A/m.

Magnetic parameters	Aging time (days)							
	0	**30**	**60**	**90**	**120**	**150**	**180**	**210**
M_s (emu/cc)	0.12	0.12	0.13	0.13	0.14	0.14	0.14	0.15
σ	0.23	0.23	0.28	0.28	0.28	0.28	0.28	0.28
D_m (nm)	9.00	9.00	9.50	9.50	9.50	9.50	9.50	9.50
λ	19.38	23.57	24.57	33.65	27.35	40.48	39.51	40.97
H_{int} (O_e)	1.10	1.42	1.48	2.03	1.65	2.40	2.30	2.40
χ ($\times 10^{-5}$)	6.35	6.19	6.30	6.37	6.90	6.70	6.80	6.97

Saturation magnetization (M_s) of MZ fluids is plotted as a function of aging time **(Fig. 5.5).** It has been observed that saturation magnetization of MZ fluids increases gradually with aging irrespective of degree of Zn-substitution. This increase in M_s may be ascribed to the corresponding increase in their magnetic particle size **(Table 5.1).** Both the mean field constant and mean internal field as obtained from the fits increases with aging **(Table 5.1).** This enhanced inter-particle interaction during aging may be responsible for aggregation of nanoparticles in magnetic fluids. Because of this colloidal stability of MZ fluids decreases with aging. These results are in good agreement with those obtained from photon correlation spectroscopy.

Lifetime of MZ fluids have also been calculated from the increase in the hydrodynamic size of magnetic fluids during aging. Hydrodynamic size of MZ fluids as a function of time can be expressed as

$$D_H(t) = D_H(0)e^{\frac{t}{\tau}} \quad (5.3)$$

Where, $D_H(0)$ is the hydrodynamic size of MZ fluid at t = 0 day, $D_H(t)$ is the hydrodynamic size of MZ fluid after aging time 't' and τ is the lifetime of the fluid whose colloidal stability is under investigation. Time dependent hydrodynamic particle size of MZ fluids are shown in **Fig**

5.6. It is fitted with **Eq. 5.3** and from the fits, life time (τ) of MZ fluids have been estimated. Lifetime of MZ fluids as obtained from the fits are shown in **Table 5.2**. The lifetime of fluids vis-à-vis to its colloidal stability is of the order of 200+ days. Maximum lifetime was observed for MZ2-F fluid (277 days). Although all MZ fluids are prepared with same protocols, they show different life expectancy. No correlation is observed between the lifetime of MZ fluids and degree of Zn substitution in MZ fluids. This might be because of the strong dependence of colloidal stability of magnetic fluids on the surface characteristics of the dispersed nanoparticles.

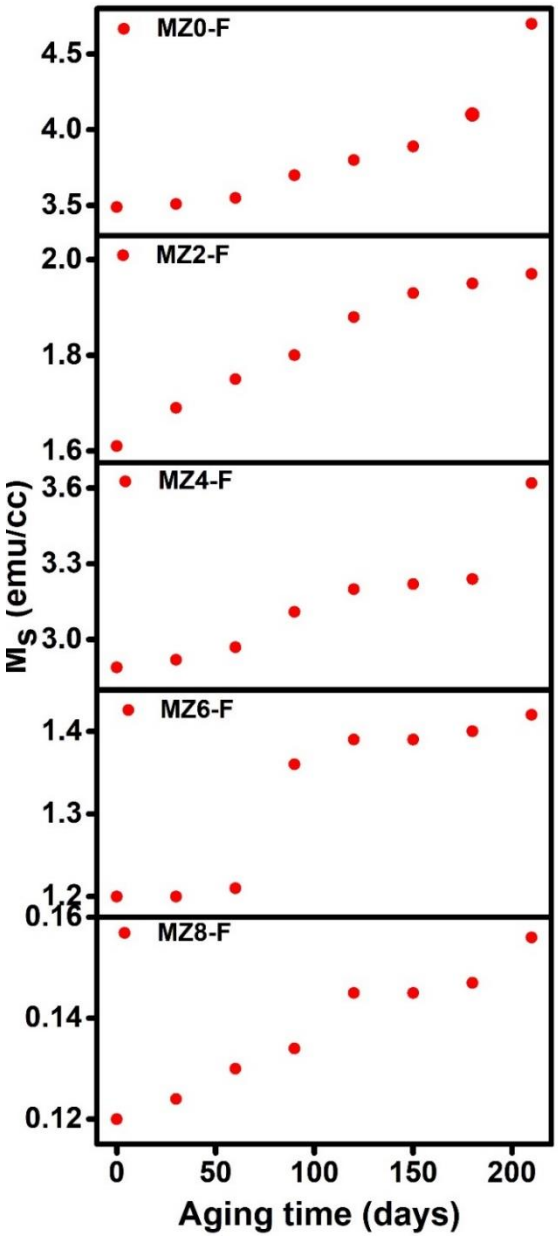

Fig. 5.5. Saturation magnetization of MZ fluids as a function of aging time. Here 1 emu/cc = 1000 A/m.

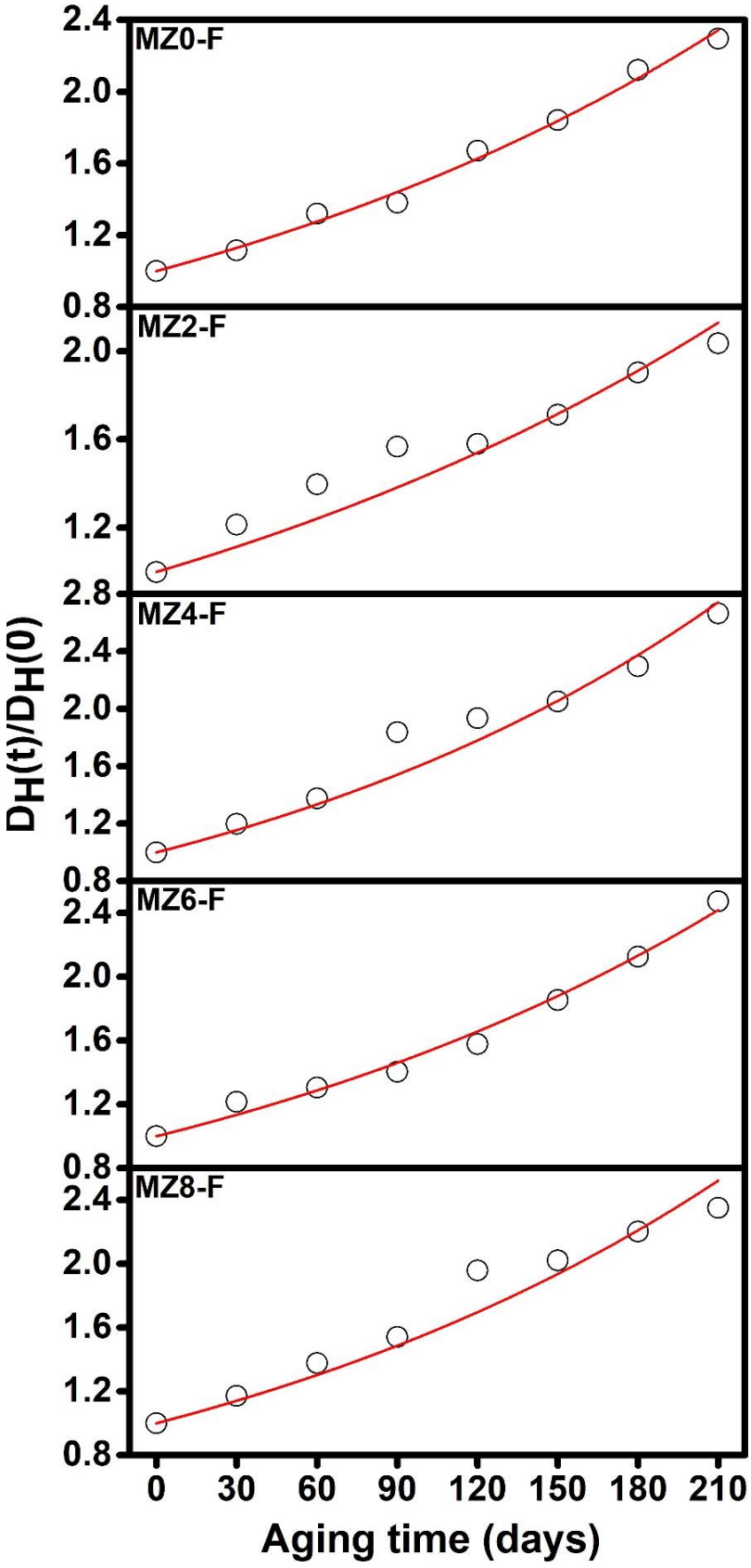

Fig. 5.6. Effect of aging on the hydrodynamic particle size of MZ fluids.

Table 5.2. Lifetime of MZ fluids.

Fluid	Lifetime (τ) (days)
MZ0-F	246
MZ2-F	277
MZ4-F	218
MZ6-F	237
MZ8-F	227

Colloidal stability of MZ fluids depends on the interplay between the colloidal medium and nanoparticles surface [8]. Inter-particle interaction due to the Brownian motion and dipole-dipole interactions between magnetic nanoparticles affect the aggregation kinetics of nanoparticles [9]. Effect of aging on the colloidal stability of MZ fluids can be understood if change in the magnetic particle size and polydispersity of MZ fluids are correlated. The initial (Day – 1) and final (Day – 210) magnetic particle / cluster size and polydispersity of MZ fluids are reported in **Table 5.3.** A strong correlation between the colloidal stability of MZ fluids and corresponding changes in magnetic particle size (D_m) and polydispersity (σ) is observed. When MZ fluids are aged; an increase in the polydispersity (σ) is observed. Corresponding changes in D_m however, is negligible **(Table 5.3).** This shows that when MZ fluids are aged; the domain growth of magnetic particles is negligible while most of the energy goes in the aggregation of particles. This might be because of presence of Zn in the spinel structure, which also acts as grain / domain growth inhibitor [10, 11]. Increase in the aggregation of nanoparticles in MZ fluid under aging can be understood on the basis of dipole-dipole interaction. If the particle / cluster size increases, the dipole-dipole interaction energy also increases by an order of magnitude greater than the thermal energy. This interaction depends not only on the distance between magnetic particles but also on the mutual orientation of their magnetic moments. Due to this dipole-dipole interactions between magnetic particles, particles tend to attract each other and form chain-like structure [12] **(Fig. 5.7).** In these chain like aggregates of magnetic nanoparticles, magnetic moments are in "head-to-tail" position [12]. Schematic representation of mechanism of chain formation of magnetic nanoparticles in fluids is shown in **Fig.5.7.**

Table 5.3 Initial (before aging) and final (after aging for 210 days) polydispersity and magnetic particle (cluster) diameter of MZ fluids.

Fluid	Polydispersity		Magnetic particle (cluster) size	
	σ_i	σ_f	D_{mi} (nm)	D_{mf} (nm)
MZ0-F	0.22	0.29	14.8	17.4
MZ2-F	0.24	0.28	13.9	14.4
MZ4-F	0.23	0.32	11.6	12.7
MZ6-F	0.23	0.28	9.3	11.8
MZ8-F	0.23	0.28	9.0	9.5

σ_i – initial polydispersity, σ_f – final polydispersity,
D_{mi} –initial magnetic particle size, D_{mf} – final magnetic particle size

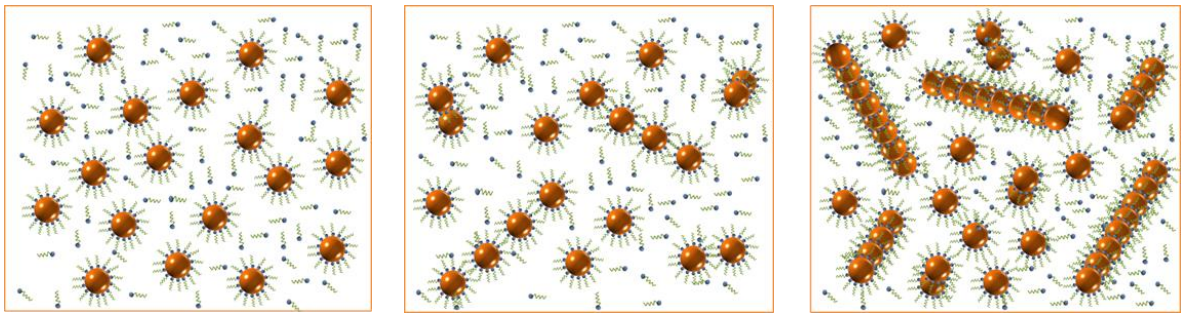

Fig. 5.7. Schematic representation of chain formation of oleic acid coated magnetic nanoparticles in MZ fluid with aging. Here T_1, T_2, T_3 represents time intervals, where $T_1 < T_2 < T_3$.

Strong dipolar interactions between the suspended magnetic nanoparticles lead to the formation of chain like complex nanostructures. This aggregation of nanoparticles was influenced by the size distribution of nanoparticles. An increase in the aggregation index (polydispersity) with aging is an indication of the increase in the clustering of nanoparticles. Irrespective of the composition of MZ fluids all fluids show enhancement in polydispersity (0.22 - 0.29) when aged. A photographic view of MZ fluids before and after the aging is shown

in **Fig. 5.8** for visual comparison. No visible changes in the dispersion quality of MZ fluids can be observed when aged for 210 days, however a significant increase in polydispersity is observed, leading to the stronger dipole interactions between nanoparticles, which eventually affect their colloidal stability.

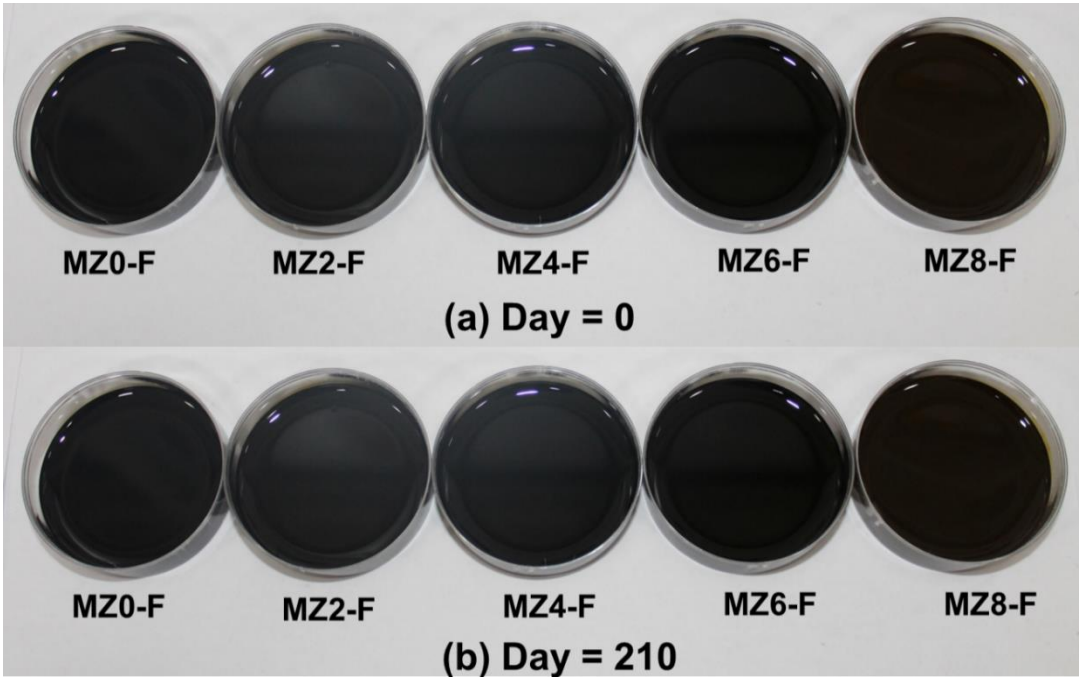

Fig. 5.8. Photographic view of MZ fluids (a) before and (b) after aging for 210 days. No visible changes can be observed in the dispersion quality of the fluids.

As-synthesized MZ fluids possess good dispersion stability. When aged, each fluid exhibits enhanced hydrodynamic and magnetic particle sizes leading to an increase in their polydispersity. These enhanced polydispersity of MZ fluids is responsible for reduction in their colloidal stability when aged. The lifetime of MZ fluids is of the order of 200+ days.

References

1. K. Parekh, R. V. Upadhyay, Indian *J. Eng. Mater. Sci.* **11** (2004) 262.
2. R. E. Rosensweig, *Ferrohydrodynamics*, Dover Publications, inc., Mineola, New York (1997).
3. T. Hornowski, A. Jozefczak, B. Kolodziejczyk, M. Timko, A. Skumiel, M. Rajnak, *J. Phys. D: Appl. Phys.* **48** (2015) 175303.
4. V. Y. Constantine, *J. Magn. Magn. Mater.* **431** (2017) 27.
5. J. C. Thomas, *J. Colloid Interface Sci.* **117** (1987) 187.
6. K. Parekh, R. V. Upadhyay, R. V. Mehta, *Bull. Mater. Sci.* **23** (2000) 91.
7. N. Kaur, B. Chudasama, *J. Magn. Magn. Mater.* **451** (2018) 647.
8. L. Vekas, D. Bica, O. Marinica, *Rom Rep Phys* **58** (2006) 257.
9. V. S. Mendelev, A. O. Ivanov, *Phys Rev E* **70** (2004) 051502.
10. N. Kaur, B. Chudasama, *Micro Nano Lett.* **12** (2017) 151.
11. M. Daniil, Y. Zhang, H. Okumura, G. C. Hadjipanayis, *IEEE T Magn.* **38** (2002) 2973.
12. A. O. Ivanov, S. S. Kantorovich, *Phys Rev E* **70** (2004) 021401.

CHAPTER 6

THERMAL AGING OF MAGNETIC FLUIDS

6.1 INTRODUCTION

Temperature sensitive magnetic fluids with tunable magnetic properties hold immense potential to be used as coolant in high power transformers [1]. The major challenge in their commercial use is poor colloidal stability under thermal aging. Properties of temperature sensitive magnetic fluids are strongly influenced by thermal aging [2-6]. Magnetic nanoparticles dispersed in transformer oil should be able to withstand the device's operating temperature without any loss in their dispersion stability [7, 8]. One of the important parameter that effects the colloidal stability of the magnetic fluids under thermal aging is the hydrodynamic size of nanoparticles and its distribution at elevated temperature. Effect of thermal aging on the hydrodynamic size of the nanoparticles in industrial grade transformer oils and its influence on the magnetic properties and colloidal stability of magnetic fluids are not well understood.

In this chapter, effect of thermal aging on the colloidal stability and magnetic properties of MZ fluids prepared in industrial grade transformer oil have been investigated. Effect of accelerated thermal aging on the dispersion stability and magnetic properties have been evaluated by photon correlation spectroscopy and vibration sample magnetometry, respectively. Effect of accelerated thermal aging on the dispersion stability and magnetic properties has been evaluated in the vicinity of the operating temperature of transformer. So far there is no such study reported in literature in which colloidal stability of transformer oil based magnetic fluids against thermal aging have been investigated in detail.

6.2 EFFECT OF ACCELERATED THARMAL AGING ON COLLOIDAL STABILITY OF MAGNETIC FLUIDS

To understand the effect of thermal aging; each magnetic fluids are subject to thermal aging at 50°C , 75 °C, 100 °C, 125 °C and 150 °C for 24 h, 48 h and 72 h. To monitor the effect of thermal aging on the dispersion stability and magnetic properties of nanoparticles in transformer oil, after each aging cycle; magnetic fluids are characterized by photon correlation spectroscopy and vibrating sample magnetometery, respectively **(Annexure–I (A5)).** Magnetization of as-synthesized MZ fluids measured after aging at 25 – 150 °C for 24 h, 48 h and 72 h are shown **Fig. 6.1.** This magnetization data is fitted modified Langevin theory [9]

$$M = M_s \int_0^\infty f(D)\, L\left(\frac{\mu(H+H_{int})}{k_B T}\right) dD + \chi H \qquad (6.1)$$

where M_s is the saturation magnetization of nanoparticles and $L(\alpha) = \coth\alpha - 1/\alpha$ is the Langevin function. The Langevin parameter $\alpha = \mu(H + H_{int})/k_B T$. μ is the magnetic moment of individual spin cluster, H is the applied external magnetic field, $H_{int} = \lambda M_1$; λ is mean field constant and M_1 is the internal field acting on each particle/cluster, f(D)dD is log-normal cluster diameter distribution function with mean cluster diameter D_m and width σ and χ is the susceptibility of nanoparticles having size above superparamagnetic limit. From the fit, magnetic particle diameter (D_m), saturation magnetization (M_s), polydispersity (σ), mean field constant (λ) and ferrimagnetic susceptibility (χ) have been determined, which are also reported in **Table 6.1.**

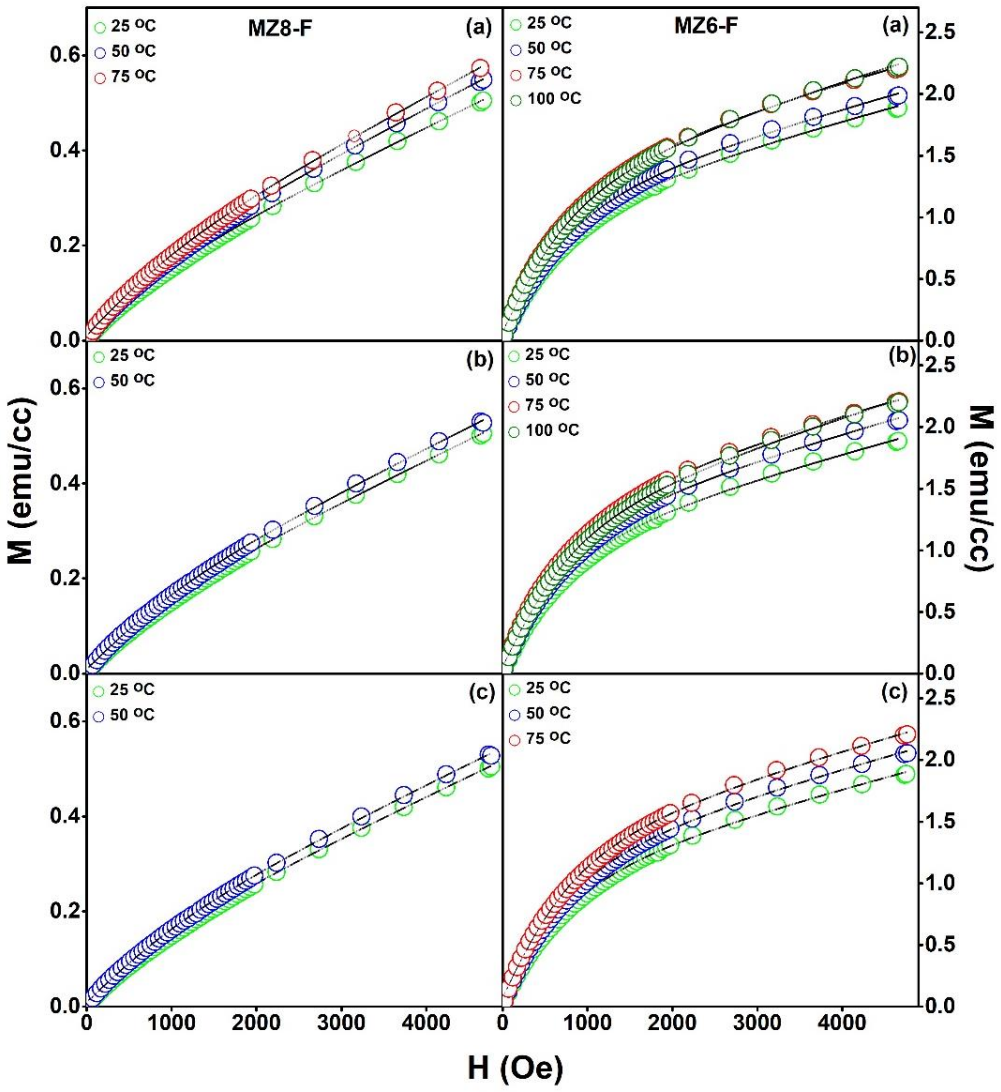

Fig. 6.1(a). Magnetization of MZ8-F and MZ6-F fluids fitted with modified Langevin theory **(eq. (6.1))**, after aging for (a) 24 h, (b) 48 h, and (c) 72 h. Here 1 emu/cc = 1000 A/m and 1 Oe = 79.61 A/m.

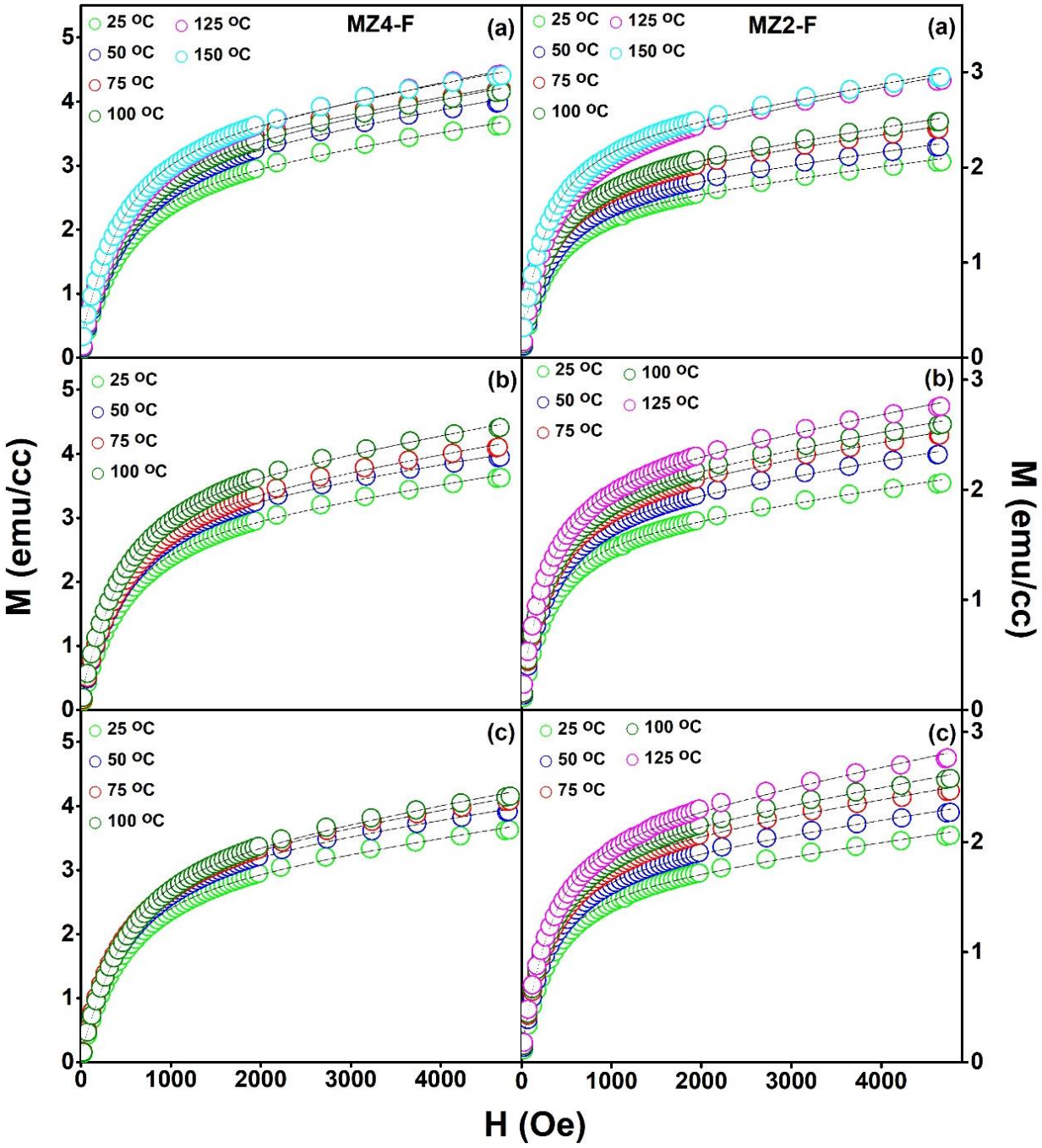

Fig. 6.1 (b). Magnetization of MZ4-F and MZ2-F fluids fitted with modified Langevin theory **(eq. (6.1))**, after aging for (a) 24 h, (b) 48 h, and (c) 72 h. Here 1 emu/cc = 1000 A/m and 1 Oe = 79.61 A/m.

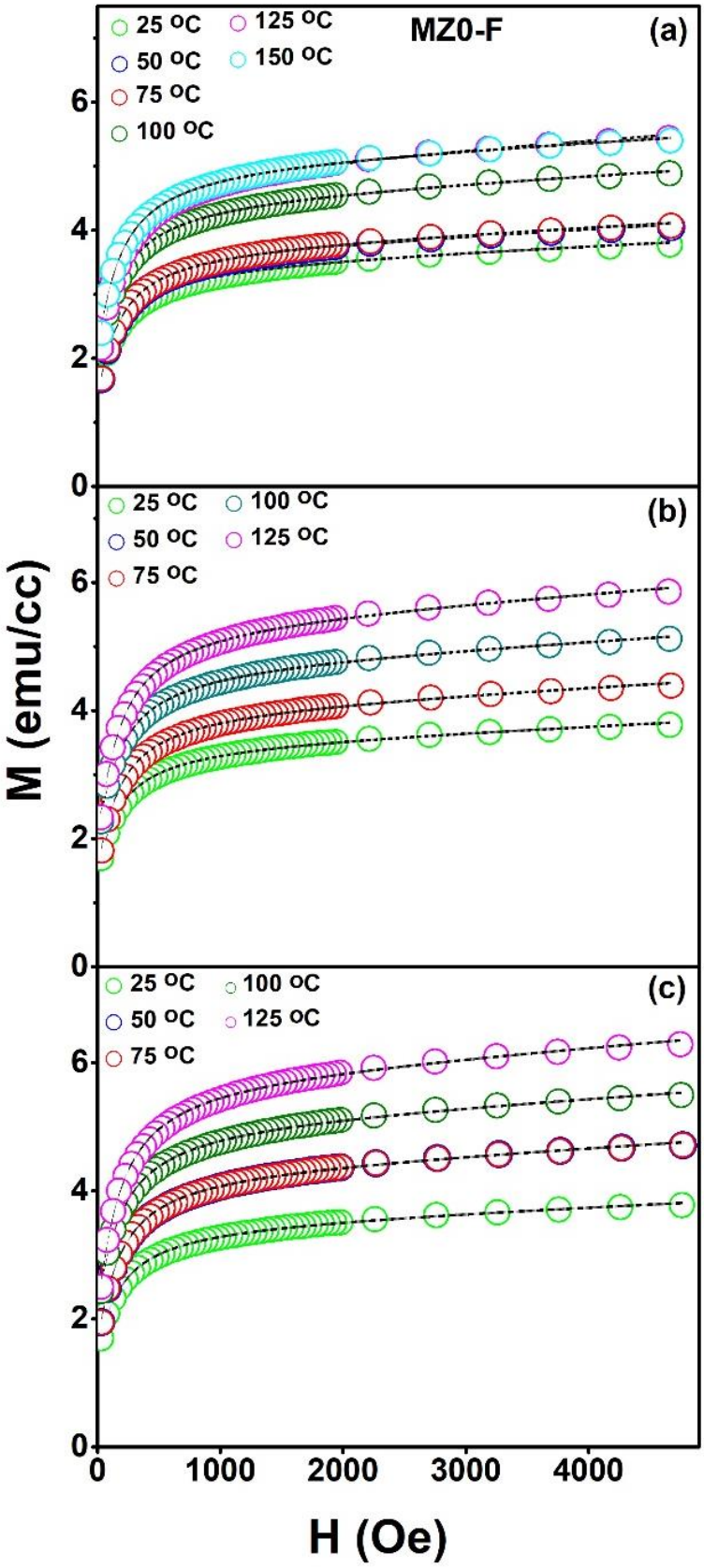

Fig. 6.1(c). Magnetization of MZ0-F fluid fitted with modified Langevin theory **(eq. (6.1)),** after aging for (a) 24 h, (b) 48 h, and (c) 72 h. Here 1 emu/cc = 1000 A/m and 1 Oe = 79.61 A/m.

Table 6.1 (a). Magnetic properties of MZ8-F fluids derived from the fit of magnetization data with modified Langevin theory. Here 1 emu/cc = 1000 A/m and 1 O_e = 79.61 A/m.

Aging Temp. (°C)	Aging Time (h)	M_s (emu/cc)	σ	D_m (nm)	λ	H_{int} (O_e)	χ ($\times 10^{-5}$)
25	24	0.13	0.23	9.00	38.26	88.38	8.23
	48	0.13	0.23	9.00	38.26	88.38	8.23
	72	0.13	0.23	9.00	38.26	88.38	8.23
50	24	0.15	0.28	9.50	41.80	105.70	8.42
	48	0.15	0.28	9.50	41.80	105.70	8.42
	72	0.15	0.28	9.50	43.63	115.18	8.71
75	24	0.16	0.28	10.00	43.79	116.04	9.12
	48	-	-	-	-	-	-
	72	-	-	-	-	-	-

Table 6.1(b). Magnetic properties of MZ6-F fluids derived from the fits of magnetization data with modified Langevin theory. Here 1 emu/cc = 1000 A/m and 1 O_e = 79.61 A/m.

Aging Temp. (°C)	Aging Time (h)	M_s (emu/cc)	σ	D_m (nm)	λ	H_{int} (O_e)	χ ($\times 10^{-5}$)
25	24	1.20	0.23	9.30	27.89	47.13	16.60
	48	1.20	0.23	9.30	27.89	47.13	16.60
	72	1.20	0.23	9.30	27.89	47.13	16.60
50	24	1.28	0.25	11.80	27.50	46.47	17.20
	48	1.35	0.25	11.80	28.60	49.47	17.30
	72	1.35	0.25	11.80	28.60	49.47	17.30
75	24	1.50	0.28	13.80	31.48	59.81	17.50
	48	1.50	0.28	13.80	31.48	59.81	17.50
	72	1.50	0.28	13.80	31.48	59.81	17.50
100	24	1.44	0.31	14.90	31.09	58.44	19.00
	48	1.40	0.31	14.90	28.40	48.50	19.40
	72	-	-	-	-	-	-

Table 6.1(c). Magnetic properties of MZ4-F fluids derived from the fits of magnetization data with modified Langevin theory. Here 1 emu/cc = 1000 A/m and 1 O_e = 79.61 A/m.

Aging Temp. (°C)	**Aging Time (h)**	**M_s (emu/cc)**	**σ**	**D_m (nm)**	**λ**	**H_{int} (O_e)**	**χ ($\times 10^{-5}$)**
25	24	2.86	0.23	11.60	26.31	41.80	19.70
	48	2.86	0.23	11.60	26.31	41.80	19.70
	72	2.86	0.23	11.60	26.31	41.80	19.70
50	24	3.17	0.23	11.70	27.10	44.40	21.30
	48	3.17	0.23	11.70	28.13	47.82	19.50
	72	3.22	0.25	11.70	28.76	50.04	19.10
75	24	3.24	0.32	12.70	28.10	47.70	21.70
	48	3.29	0.32	12.70	27.90	47.15	21.30
	72	3.44	0.32	12.70	30.12	54.81	19.80
100	24	3.30	0.32	15.50	27.60	46.09	22.20
	48	3.58	0.32	15.50	27.60	46.09	21.80
	72	3.58	0.32	15.50	27.60	46.09	21.80
125	24	3.53	0.32	17.20	26.88	43.54	23.30
	48	-	-	-	-	-	-
	72	-	-	-	-	-	-
150	24	3.57	0.31	17.30	34.37	71.64	22.00
	48	-	-	-	-	-	-
	72	-	-	-	-	-	-

Table 6.1(d). Magnetic properties of MZ2-F fluids derived from the fits of magnetization data with modified Langevin theory. Here 1 emu/cc = 1000 A/m and 1 O_e = 79.61 A/m.

Aging Temp. (°C)	**Aging Time (h)**	**M_s (emu/cc)**	**σ**	**D_m (nm)**	**λ**	**H_{int} (O_e)**	**χ ($\times 10^{-5}$)**
25	24	1.61	0.24	13.90	23.84	34.32	11.10
	48	1.61	0.24	13.90	23.84	34.32	11.10
	72	1.61	0.24	13.90	23.84	34.32	11.10
50	24	1.74	0.25	14.30	24.29	35.70	11.70
	48	1.80	0.25	14.30	25.60	39.68	11.60
	72	1.84	0.25	14.30	25.76	40.18	11.90
75	24	1.91	0.25	14.60	26.29	41.80	12.80
	48	1.92	0.25	14.60	27.05	44.09	11.90
	72	1.98	0.25	14.60	27.03	44.05	12.60
100	24	1.95	0.27	16.50	25.70	39.83	13.00
	48	2.02	0.27	16.50	25.58	39.39	13.00
	72	2.02	0.27	16.50	25.58	39.39	13.00
125	24	2.26	0.28	17.70	24.70	37.05	16.00
	48	2.26	0.28	17.70	24.70	37.05	16.00
	72	2.26	0.28	17.70	24.70	37.05	16.00
150	24	2.36	0.30	18.50	33.13	66.26	14.60
	48	-	-	-	-	-	-
	72	-	-	-	-	-	-

Table 6.1(e). Magnetic properties of MZ0-F fluids derived from the fits of magnetization data with modified Langevin theory. Here 1 emu/cc = 1000 A/m and 1 O_e = 79.61 A/m.

Aging Temp. (°C)	Aging Time (h)	M_s (emu/cc)	σ	D_m (nm)	λ	H_{int} (O_e)	χ ($\times 10^{-5}$)
25	24	3.49	0.22	14.80	49.32	146.90	7.92
	48	3.49	0.22	14.80	49.32	146.90	7.92
	72	3.49	0.22	14.80	49.32	146.90	7.92
50	24	3.72	0.22	16.08	45.80	126.80	8.94
	48	4.03	0.22	16.08	45.80	126.80	9.69
	72	4.33	0.22	16.08	45.80	126.80	10.40
75	24	3.74	0.29	17.40	45.80	126.80	8.99
	48	4.03	0.29	17.40	45.80	126.80	9.69
	72	4.33	0.29	17.90	45.80	126.80	10.40
100	24	4.58	0.29	17.90	45.60	124.90	7.91
	48	4.79	0.29	17.90	45.60	124.90	8.28
	72	5.15	0.29	17.90	45.60	124.90	8.89
125	24	5.01	0.31	19.30	45.20	123.30	18.00
	48	5.40	0.31	19.30	45.20	123.30	12.70
	72	5.80	0.31	19.30	45.20	123.30	13.60
150	24	5.07	0.31	21.60	48.40	141.80	9.43
	48	-	-	-	-	-	-
	72	-	-	-	-	-	-

Saturation magnetization (M_s) of MZ fluids are plotted as a function of aging temperature for various aging times in **Fig. 6.2 (a).** It has been observed that the M_s of MZ fluids increases with aging irrespective of degree of Zn-substitution **(Fig. 6.2 (b)).** This increase in magnetization of MZ fluids with aging might be caused by the temperature induced aggregation of nanoparticles resulting into clustering. The changes in the magnetic particle diameter (D_m) as a function of aging temperature as obtained from the fits of M–H data with Langevin **eq. (6.1)** is shown in **Fig. 6.3.** Corresponding changes in the hydrodynamic size of the MZ fluids after each aging cycle are also plotted in **Fig. 6.3**. Both the D_m and D_H increases with

the aging temperature irrespective of the degree of Zn-substitution. Polydispersity of aged MZ fluids obtained from the fits of magnetization data is also shown in Fig**. 6.4(a).** Irrespective of degree of Zn-ion substitution, polydispersity increases with aging temperature **(Fig 6.4(b)).**

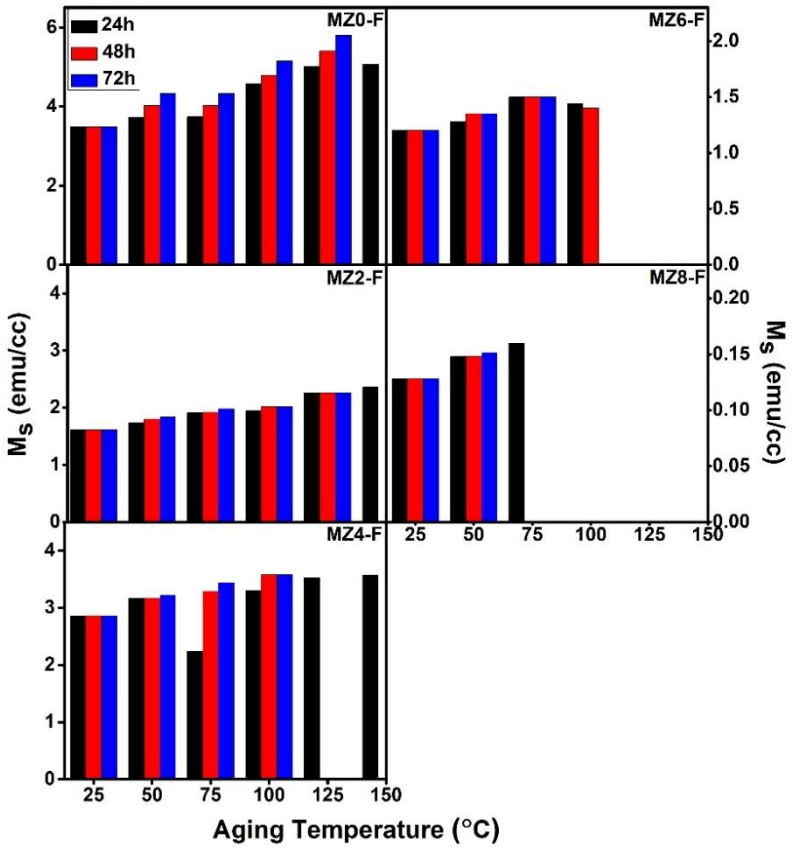

Fig. 6.2 (a). Saturation magnetization of MZ fluids after aging for 24h, 48h and 72h at 25 °C – 150 °C. Here 1 emu/cc = 1000 A/m.

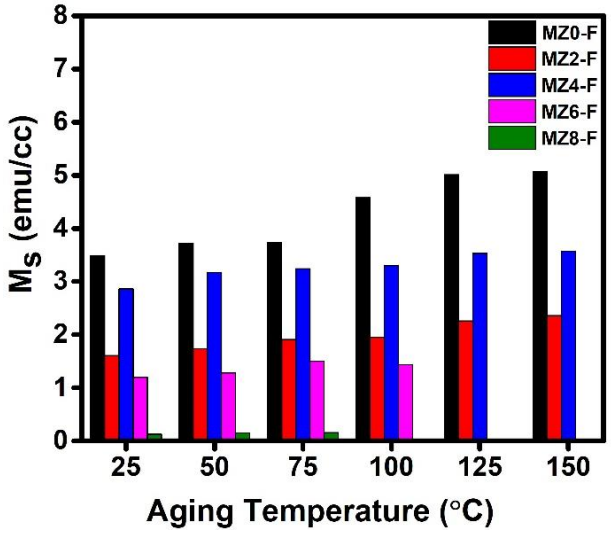

Fig. 6.2 (b). Saturation magnetization of MZ fluids measured after thermal aging for 24h at 25°C – 150 °C. Here 1 emu/cc = 1000 A/m.

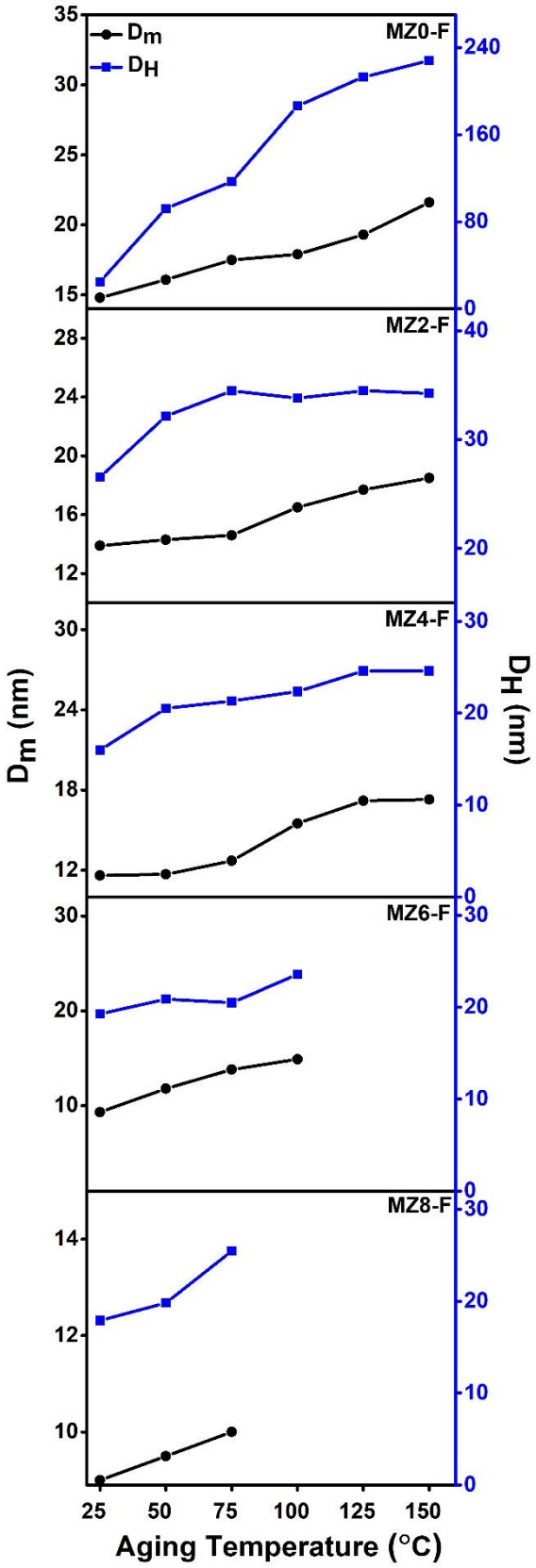

Fig. 6.3. Effect of thermal aging on magnetic diameter (D_m) and hydrodynamic diameter (D_H) of MZ fluids.

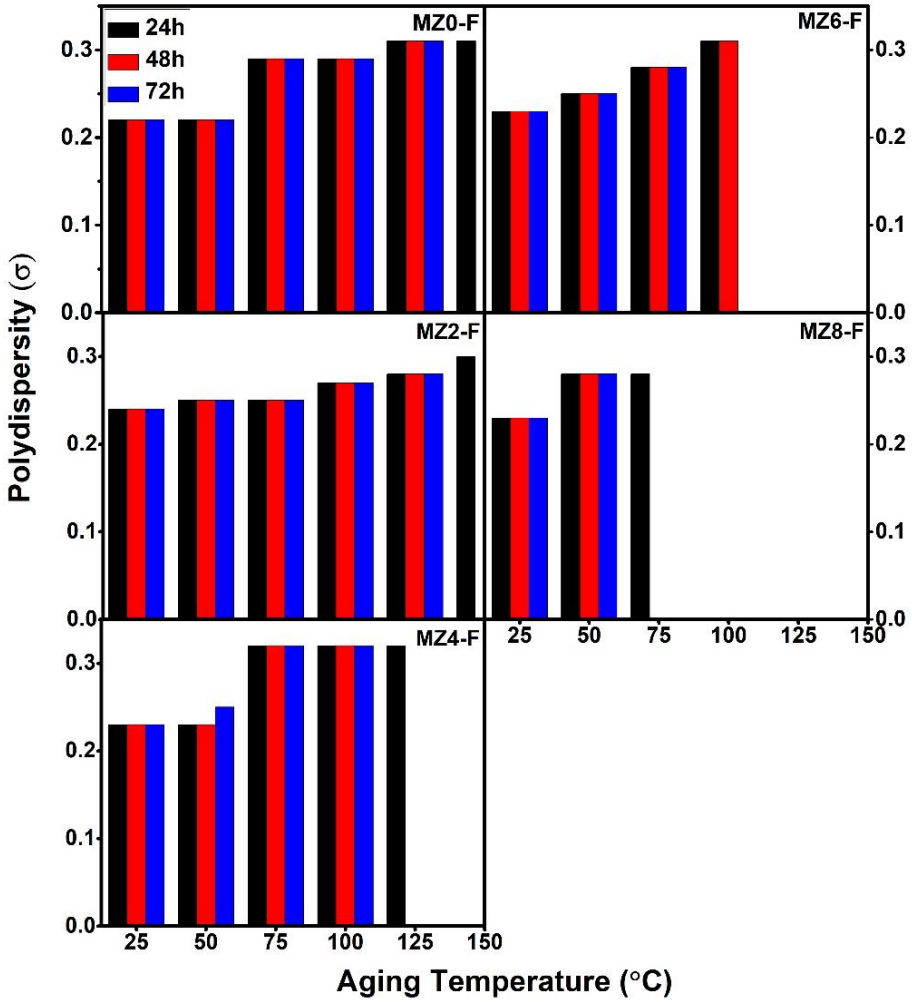

Fig. 6.4 (a). Effect of thermal aging on polydispersity (σ) of MZ fluids.

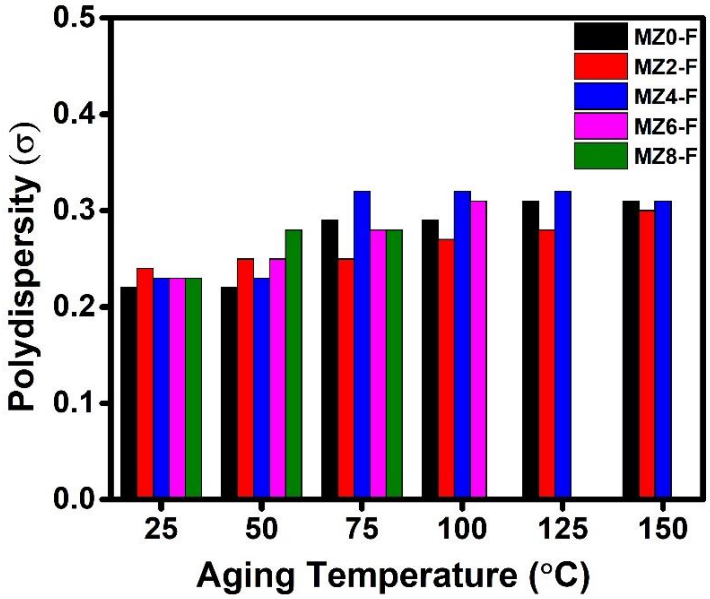

Fig. 6.4 (b). Average polydispersity (σ) of MZ fluids measured at 25 – 150 °C aging temperature.

Magnetization of MZ8-F fluids after aging for 24–72 h at 25–100 °C is shown in **Fig. 6.1 (a).** Magnetization of MZ8-F increases gradually with aging temperature. This might be due to the domain growth under accelerated thermal aging. Magnetic diameter and polydispersity also increases with the corresponding increase in thermal aging **(Table 6.1).** Hydrodynamic size increases with aging temperature as well **(Fig. 6.3),** indicating thermally triggered aggregation of nanoparticles. Both the mean field constant and mean internal field as obtained from the fits increases with aging at elevated temperatures. This enhanced inter-particle interaction at elevated temperatures is responsible for aggregation, which eventually leads to sedimentation of fluid. MZ8-F fluid is stable only upto 50 °C. When subjected to thermal aging at 75 °C; it loses its fluidity due to strong aggregation of nanoparticles. MZ6-F fluid under accelerated thermal aging show identical behavior to MZ8-F. However, its stability under accelerated thermal aging is better than MZ8-F. It is stable upto 75 °C when aged. At 100 °C, MZ6-F loses its colloidal stability and sediments due to strong aggregation of nanoparticles (polydispersity, σ = 0.31) **(Table 6.2).**

Magnetization of MZ4-F fluids after aging for 24–72 h at 25−150 °C is shown in **(Fig 6.1(b)).** The saturation magnetization (M_s) of MZ4-F fluid increases with increase in the aging temperature (**Fig 6.1(b)).** Both D_m and D_H **(Fig. 6.3)** increase gradually with increase in the aging temperature along with the polydispersity **(Fig. 6.4(b)).** In MZ4-F fluid, a sharp increase in magnetic particle size is observed when fluid is aged at 100 °C, however no hysteresis has been observed in the magnetization data for MZ4-F fluid aged at 100 °C, indicating that most of the thermal energy goes into the aggregation of nanoparticles. This fluid is stable upto 100 °C. At 125 °C, it loses its fluidity, due to heavy aggregation of nanoparticles (σ = 0.32). MZ2-F fluid show identical behavior as shown by MZ4-F when aged. It is stable upto 125 °C. At 150 °C, it loses its fluidity due to same reasons as explained previously. MZ0-F fluid under accelerated thermal aging is stable upto 125 °C. A photographic view of MZ0-F fluid before and after the aging at 125 °C is shown in **Fig. 6.5**. No change in the physical state of fluid is observed when aged at 125 °C. However, when aged at 150 °C, the fluid loses its colloidal stability and undergoes complete sedimentation.

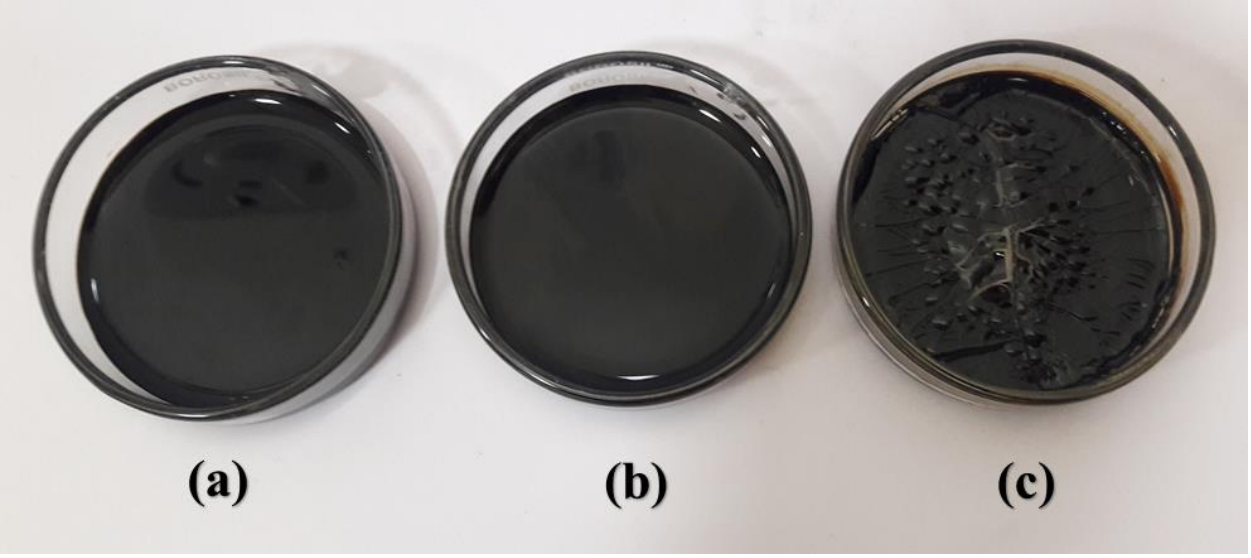

Fig. 6.5. Photographic view of MZ0-F fluid, (a) before and (b) after accelerated aging at 125 °C for 72 h. No change in the dispersion quality has been observed due to aging at high temperature, (c) after accelerated aging at 150 °C, fluid loses its colloidal stability.

Table 6.2 shows the comparison of colloidal stability of MZ fluids under investigation at different temperatures (25 °C to 150 °C) after aging for 72 h. Although all MZ fluids are prepared with same protocols and aged under identical conditions, they show different colloidal stability against thermal aging. As shown in **Table 6.2,** the colloidal stability under thermal aging increases with decrease in the Zn-content in the MZ fluid. Such unusual dependence of thermal stability of MZ fluids on zinc-content is not expected. Colloidal stability of fluids is governed by the interplay between the colloidal medium and nanoparticle surface [10]. Inter-particle interaction due to the Brownian and magnetic interactions also affects the aggregation of nanoparticles [11].

Table 6.2: Colloidal stability of magnetic fluids after thermal aging for 72 h (green arrow: stable; red arrow: unstable)

Fluid	Temperature (°C)					
	25	50	75	100	125	150
MZ8-F						
MZ6-F						
MZ4-F						
MZ2-F						
MZ0-F						

The role of Zn-content in the observed thermal stability of MZ fluids under accelerated thermal aging can be understood if the influence of aging on the magnetic particle size and polydispersity of MZ fluids are correlated. The magnetic particle size and polydispersity of MZ fluids are shown in **Table 6.3.** Here D_{mi} and σ_i are the magnetic particle size and polydispersity of MZ fluids before the aging and D_{mf} and σ_f represents the magnetic particle size and polydispersity recorded at highest temperature for the largest time of thermal aging. A strong correlation between the colloidal stability of MZ fluids under thermal aging and corresponding changes in D_m and is observed. When the fluid contains higher degree of Zn (MZ8-F); polydispersity (σ) increases from 0.23 to 0.28 when aged **(Table 6.3).**

Table 6.3: Initial (before aging) and final (after aging for longest period at highest temperature) polydispersity and magnetic particle size of MZ fluids.

Sample	Polydispersity		Magnetic particle size (nm)	
	σ_i	σ_f	D_{mi}	D_{mf}
MZ8-F	0.23	0.28	9.0	9.5
MZ6-F	0.23	0.28	9.3	13.8
MZ4-F	0.23	0.32	11.6	15.5
MZ2-F	0.24	0.28	13.9	17.7
MZ0-F	0.22	0.31	14.8	19.3

σ_i – initial polydispersity, σ_f – final polydispersity,
D_{mi} –initial magnetic particle size, D_{mf} – final magnetic particle size

The corresponding change in D_m is from 9 nm to 9.5 nm. This means that when MZ8-F fluid is aged, the domain growth is negligible while most of the thermal energy goes into the aggregation of nanoparticles. This might be because of the presence of high Zn, which also acts as domain growth inhibitor [12, 13]. When MZ fluids with lower Zn contents are aged; they have higher domain growth **(Table 6.3).** Thus, when Zn content is lowered; it favours the domain growth of magnetic nanoparticles (14.8 nm to 19.3 nm in MZ0-F). Hence part of the thermal energy now goes into the domain growth of magnetic nanoparticles and minimizes the rate of aggregation of nanoparticles. Thus decreasing Zn content in MZ fluids favours domain growth

under thermal aging, which minimizes thermally triggered aggregation of nanoparticles leading to enhance colloidal stability of MZ fluids at elevated temperature.

This study indicates that dispersion stability of these magnetic fluids against thermal aging decreases with increase in the degree of Zn-substitution in MZ nanoparticles. Decreasing Zn-content in MZ fluids favours domain growth under thermal aging, which minimizes thermally triggered aggregation of nanoparticles leading to enhance colloidal stability. Under optimized conditions, MZ0-F and MZ2-F fluids are stable upto 125 °C for 72h of thermal aging.

References

1. E. Blums, *J. Magn. Magn. Mater.* **252** (2002) 189.
2. K. Parekh, R.V. Upadhyay, R. V. Mehta, *Bull. Mater. Sci.* **23** (2000) 91.
3. V. Segal, D. Nattrass, K. Raj, D. Leonard, *J. Magn. Magn. Mater.* **201** (1999) 70.
4. V. Segal, A. Rabinovich, D. Nattrass, K. Raj, A. Nunes, J. *Magn. Magn. Mater.* **215-216** (2000) 513.
5. J. Patel, K. Parekh, R.V. Upadhyay, *Int J Therm Sci.* **103** (2016) 35.
6. J. Patel, K. Parekh, R.V. Upadhyay, *Int J Therm Sci*. **114** (2017) 64.
7. K. Parekh, R. V. Upadhyay, *Indian J. Eng. Mater. Sci.* **11** (2004) 262.
8. R. E. Rosensweig, *Ferrohydrodynamics*, Dover Publications, inc., Mineola, New York (1997).
9. M. Knobel, W. C. Nunes, A. L.Brandl, J. M. Vargas, L. M. Socolovsky, D. Zanchet, *Physica B* **354** (2004) 80.
10. L. Vekas, D. Bica, O. Marinica, *Rom Rep Phys* **58** (2006) 257.
11. V. S. Mendelev, A. O. Ivanov, *Phys Rev E.* **70** (2004) 051502.
12. N. Kaur, B. Chudasama, *Micro Nano Lett.* **12** (2017) 151.
13. M. Daniil, Y. Zhang, H. Okumura, G. C. Hadjipanayis, *IEEE T Magn.* **38** (2002) 2973.

CHAPTER 7

CONCLUSIONS AND SCOPE FOR FUTURE WORK

7.1 CONCLUSIONS

7.1.1 Structural and magnetic properties of MZ nanoparticles / fluids

A series of $Mn_{1-x}Zn_xFe_2O_4$ (x = 0–1) (MZ) nanoparticles have been synthesized by chemical co-precipitation method by controlling the degree of Zn-substitution, reaction pH, reaction temperature and reaction time. All synthesized nanoparticles are superparamagnetic. They possess mixed spinel structure. No specific trend has been observed on the degree of substitution of bivalent metal ions (Mn^{2+}) at the tetrahedral A-sites. However, a strong correlation has been observed between the crystallite, physical and magnetic particle sizes with the magnetic properties (magnetization and Curie temperature) of MZ nanoparticles. All the three types of particle sizes decrease with increase in the degree of Zn-substitution in the spinel matrix. This confirms that Zn acts as grain / domain growth inhibitor in the spinel matrix.

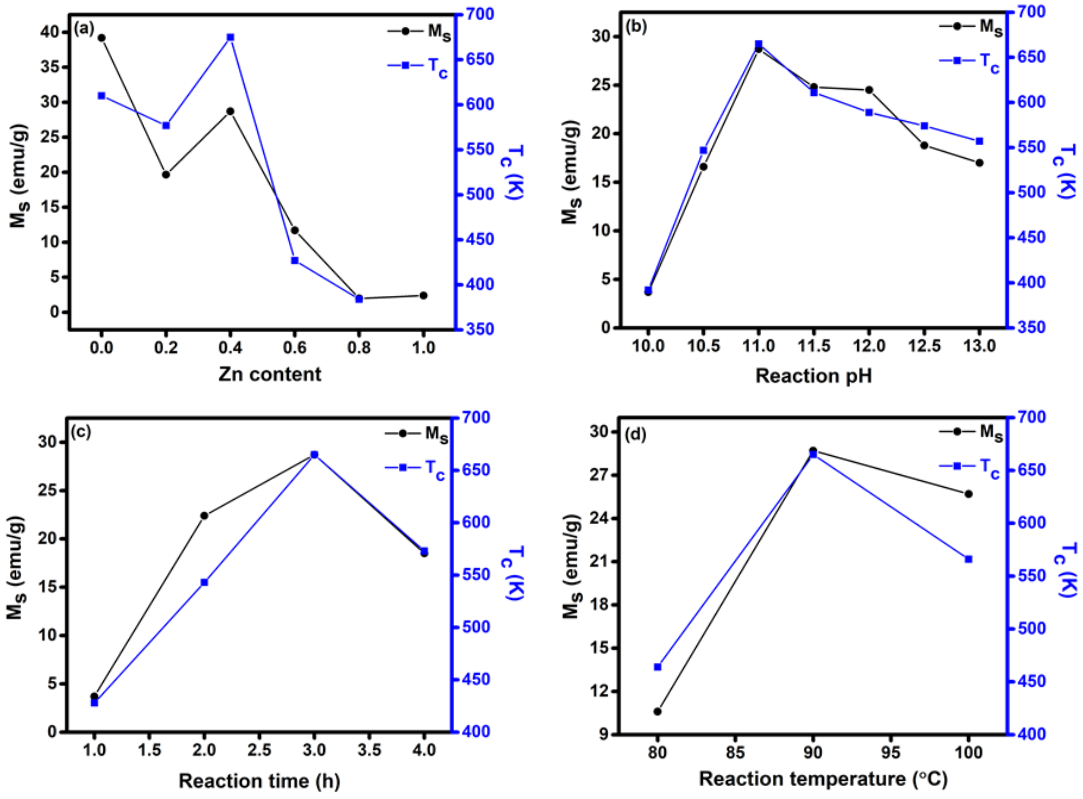

Fig. 7.1. Saturation magnetization (M_s) and Curie temperature (T_c) of MZ nanoparticles as a function of (a) Zn content, (b) reaction pH, (c) reaction time and (d) reaction temperature. Here 1 emu/g = $1Am^2/Kg$.

For smaller values of x (i.e. x = 0.2 – 0.4), the M_s of the MZ nanoparticles increases and for x > 0.4 it decreases with increase in the degree of Zn-substitution. An analogous trend of Curie temperature of MZ nanoparticles has also been observed. Synthesis conditions (pH, reaction time, reaction temperature) affect the degree of Zn-substitution in the spinel matrix and hence can be used to tune the magnetic properties of MZ nanoparticles. Curie temperature of MZ nanoparticles have been tuned from 384 K to 665 K, which covers the entire operating temperature range of high power transformers **(Fig 7.1)**.

An analogous trend has been observed in the magnetic properties of MZ fluids. Both magnetic and hydrodynamic particle sizes of MZ fluids decrease with the increase in the degree of Zn-substitution. Polydispersity of MZ fluids is independent of degree of Zn-substitution (constant at 0.22-0.24) which suggest negligible agglomeration of nanoparticles leading to high colloidal stability of MZ fluids at room temperature **(Fig 7.2)**

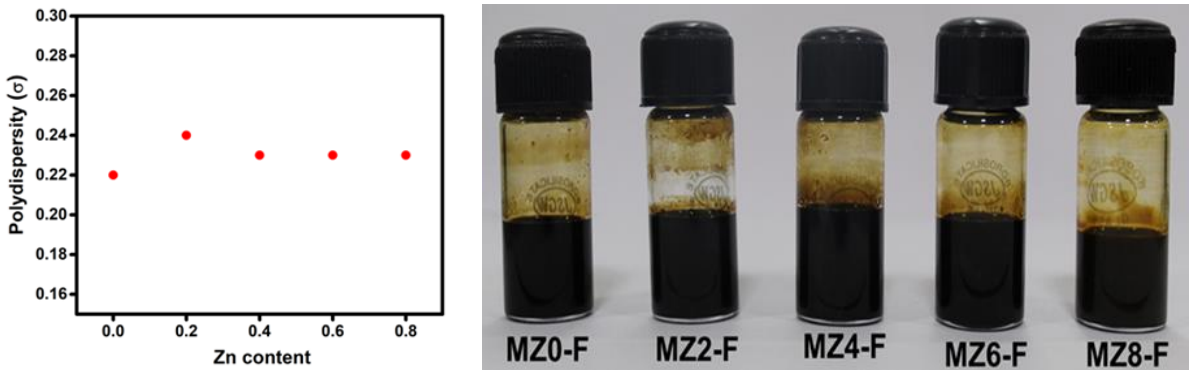

Fig. 7.2. Polydispersity of as-synthesized MZ fluids as a function of Zn content and photographic view of as-synthesized MZ fluids showing good dispersion stability at room temperature.

7.1.2 Effect of aging on the colloidal stability of MZ fluids

As-synthesized MZ fluids possess good dispersion stability. When aged, each fluid exhibits enhanced hydrodynamic and magnetic particle sizes leading to an increase in their polydispersity. These enhanced polydispersity of MZ fluids is responsible for the reduction in the colloidal stability of MZ fluids. Although all MZ fluids are prepared with same protocols, they show different life expectancy. No correlation is observed between the lifetime of the fluids and the degree of Zn-substitution in MZ fluids. The lifetime of MZ fluids is of the order of 200+ days.

Table 7.1. Initial (before aging) and final (after aging for 210 days) polydispersity and magnetic particle (cluster) diameter of MZ fluids.

Fluid	Polydispersity		Magnetic particle (cluster) size	
	σ_i	σ_f	D_{mi} (nm)	D_{mf} (nm)
MZ0-F	0.22	0.29	14.8	17.4
MZ2-F	0.24	0.28	13.9	14.4
MZ4-F	0.23	0.32	11.6	12.7
MZ6-F	0.23	0.28	9.3	11.8
MZ8-F	0.23	0.28	9.0	9.5

σ_i – initial polydispersity, σ_f – final polydispersity,
D_{mi} –initial magnetic particle size, D_{mf} – final magnetic particle size

Effect of accelerated thermal aging on the dispersion stability and magnetic properties has also been studied. Magnetic fluids are stable under accelerated thermal aging at elevated temperatures (from 50 °C to 125 °C), which is critical for their efficient performance in high power transformers. Dispersion stability of these magnetic fluids under thermal aging decreases with increase in the degree of Zn substitution in MZ fluids. Decrease in Zn-content in MZ fluids favours the grain / domain growth. This minimizes thermally triggered aggregation of nanoparticles leading to better colloidal stability of MZ fluids. Under optimized conditions, MZ0-F and MZ2-F fluids are stable upto 125 °C, while other fluids are stable only below 100 °C **(Table 7.1).**

Table 7.2. Colloidal stability of magnetic fluids after thermal aging for 72 h (green arrow: stable; red arrow: unstable).

Sample	Temperature (°C)					
	25	50	75	100	125	150
MZ8-F						
MZ6-F						
MZ4-F						
MZ2-F						
MZ0-F						

7.2 SCOPE FOR FUTURE WORK

Magnetic fluids intended for Transformer cooling are required in larger quantities, typically of the order of few liters. Their Curie temperature should be in the close vicinity of the operating temperature of the power transformers and they should not lose their colloidal stability when aged under magnetic fields and temperature gradients. In this study, a series of stable magnetic fluids have been synthesized having Curie temperatures which cover the entire range of the operating temperature of the transformers. However, the volume of the fluid produced in a typical laboratory batch is limited to only few milliliters, which needs to be scaled-up. Batch to batch variation in the structural and magnetic properties and enhancement in the polydispersity while scaling up throws major challenges. To overcome these difficulties, scale-up protocols needs to be devised by involving digital automation of the entire process and an on-line, in-situ measurement of hydrodynamic particle size and size distribution.

For transformer cooling applications, magnetic particles need to be dispersed in carrier fluids with high colloidal stability for long periods without significant degradation. However, stability of the suspension, especially the long term stability is a crucial factor for practical applications in power transformers. In this thesis, effect of size and size distribution of magnetic nanoparticles on the colloidal stability and magnetic properties of MZ fluids have been evaluated. This study was conducted over a period of 210 days. However, for the better understanding of the colloidal stability of magnetic fluids especially under magnetic field and temperature gradients, this needs to be done for an extended period, as the coolant life in a power transformer is of the order of years.

Magnetic fluid flows under magneto convective and gravitational forces in transformers. This flow is even more complex in the presence of gradient magnetic field and dynamic temperature gradients that exist inside the transformers. Therefore, it is very important to study magnetohydrodynamic properties of magnetic fluids under identical conditions that exist inside the transformers, i.e. gradient magnetic fields and dynamic temperatures. An in-depth study on cooling efficiency and dielectric properties of transformer oil based magnetic fluids designed in this thesis needs to be conducted as well.

ANNEXURE-I

EXPERIMENTAL

Materials

AR grade $FeCl_3$ and oleic acid were obtained from S.D. fine-chem Ltd., $MnCl_2.4H_2O$ and ammonia solution was purchased from LOBA chemicals. $ZnSO_4.7H_2O$, NaOH, ethanol and acetone were purchased from Merck. Transformer oil was gifted by M/S Savita Oil Technologies Limited, India. All chemicals were used as-received without any purification. Aqueous solutions were prepared in Milli-Q ultrapure water (ρ = 18.2 MΩ). The chemical structures of the reagents used for the synthesis of magnetic fluid are shown below:

$FeCl_3$

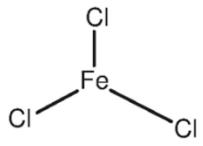

$MnCl_2.4H_2O$

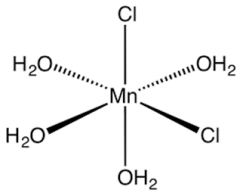

$ZnSO_4.7H_2O$

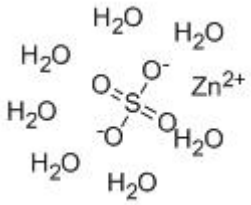

NaOH

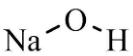

Acetone

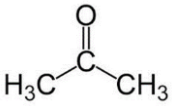

Ethanol

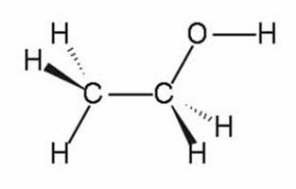

Oleic acid

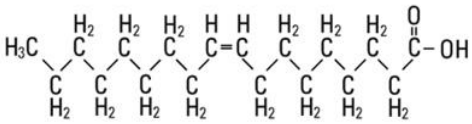

Transformer Oil

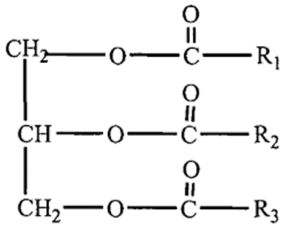

A1. Synthesis of MZ magnetic nanoparticles

A series of $Mn_{1-x}Zn_xFe_2O_4$ (x = 0 – 1) nanoparticles were synthesized by chemical co-precipitation of Fe^{3+}, Mn^{2+} and Zn^{2+} from their aqueous salt solutions. Aqueous solutions of $MnCl_2.4H_2O$, $ZnSO_4.7H_2O$ and $FeCl_3$ were prepared by dissolving stoichiometric quantities of each of these salts in 100 mL distilled water. pH of the solution was adjusted to < 2 with dilute HCl. It was then added under constant stirring into 100 mL aqueous solution of NaOH. The molar ratio of ($MnCl_2.4H_2O$ + $ZnSO_4.7H_2O$) : $FeCl_3$: NaOH was maintained as 1 : 2 : 8. The solution pH was then adjusted to 11 with 1 M NaOH. It was stirred for 20 min. During this, metal salts get converted into their hydroxides

$$(1\text{-}x)\ Mn^{2+} + x\ Zn^{2+} + 2Fe^{3+} + 8OH^- \xrightarrow{90\ ^oC} (1\text{-}x)\ Mn(OH)_2\ x\ Zn(OH)_2\ 2Fe(OH)_3 \qquad (1)$$

These metal hydroxides were then subjected to constant heating at 90 ºC for 3h. During this time hydroxides transform to nanoparticles of metal oxides.

$$(1\text{-}x)\ Mn(OH)_2\ \ x\ Zn(OH)_2\ \ 2Fe(OH)_3 \xrightarrow{90\ ^oC\ /\ 3h} Mn_{(1-x)}Zn_xFe_2O_4 + nH_2O \qquad (2)$$

Magnetic nanoparticles were cooled to room temperature, magnetically decanted and washed multiple times with warm distilled water. The resulting black precipitates were washed with acetone and dried overnight at 100 °C.

A2. Synthesis of MZ4 nanoparticles

A series of $Mn_{0.6}Zn_{0.4}Fe_2O_4$ (MZ4) nanoparticles were prepared by co-precipitation method at varying conditions of pH (10 – 13), reaction temperature (80 – 100 °C) and reaction time (1 – 4 h). $MnCl_2.4H_2O$, $ZnSO_4.7H_2O$ and $FeCl_3$ were used as precursors and sodium hydroxide was used as precipitating agent. Aqueous solutions of $MnCl_2.4H_2O$, $ZnSO_4.H_2O$ and $FeCl_3$ were prepared by dissolving appropriate quantities of each of these reactants in 100 mL distilled water. The pH of the solution was adjusted to < 2 with dilute HCl. It was added to 100 mL NaOH solution under continuous stirring. The molar ratio of ($MnCl_2.4H_2O$ + $ZnSO_4.7H_2O$) : $FeCl_3$: NaOH was kept at 1 : 2 : 8. The solution pH was adjusted between 10 to13 by adding desired quantity of 1 M NaOH solution. Within 20 min of stirring, metal salts were converted into their hydroxides. Metal hydroxides were then subjected to heating at 80 − 100 °C for 1 − 4 h. During this heating cycle, metal hydroxides transform themselves to metal oxide nanoparticles. Magnetic nanoparticles were then cooled to room temperature and decanted with permanent magnet. They were washed multiple times with copious amount of warm distilled water followed by an acetone wash and dried overnight at 100 °C.

A3. Synthesis of MZ fluids

As-synthesized magnetic nanoparticles $Mn_{1-x}Zn_xFe_2O_4$ (x = 0 – 1) were coated with monolayer of oleic acid. For this purpose, ammonium oleate was prepared by reacting oleic acid with ammonium hydroxide under constant magnetic stirring. Ammonium oleate was added into the pre-synthesized nanoparticles. It was heated to 93 °C. At this temperature, ammonium oleate decompose and oleic acid chemi-adsorbed on the surface of magnetic nanoparticles through metal-hydroxyl bonds. After cooling it to the room temperature, the oleic acid coated magnetic nanoparticles were foculated with dilute HCl. Nanoparticles were magnetically decanted and washed several times with warm distilled water to remove excess surfactant. Finally they were washed with acetone-ethanol (v/v = 1:1) solution and redispersed in commercial grade transformer oil by mild heating under continuous stirring.

A4. Colloidal stability of Magnetic Fluids

To understand the effect of aging on the colloidal stability of magnetic fluids; an aging study was performed for 210 days. Effect of aging on the dispersion stability of magnetic fluids were

determined by photon correlation spectroscopy. Changes in the hydrodynamic size of nanoparticles in magnetic fluids also affect their magnetic properties. These aging induced changes in magnetic properties of fluids, were also determined by vibrating sample magnetometry.

A5. Colloidal stability under accelerated thermal aging

To understand the effect of thermal aging; each magnetic fluid was subjected to thermal aging at 50 °C, 75 °C, 100 °C, 125 °C and 150 °C for 24 h, 48 h and 72 h. To monitor the effect of thermal aging on dispersion stability of magnetic nanoparticles in transformer oil, after each aging cycle; magnetic fluids were characterized by photon correlation spectroscopy and vibrating sample magnetometry. The hydrodynamic particle size and polydispersity index of magnetic nanoparticles were determine by Brookhaven "90 plus" particle size analyzer. Magnetization measurements were performed on LakeShore 7404 vibrating sample magnetometer at room temperature.

A6. Characterizations of MZ particles / fluids

Magnetic nanoparticles were characterized by X-ray diffraction. Structural investigation of nanoparticles was carried out on PAN analytical X'pert PRO powder X-ray diffractometer. X-ray diffraction patterns were recorded at room temperature by using monochromatic CuKα radiation ($\lambda = 1.5405$ nm) in the 2θ range of 28° to 70°. X-ray diffraction patterns were refined by Rietveld refinement technique using "Fullprof suite" program. Transmission electron microscopy (TEM) image of magnetic nanoparticles was recorded on JEOL JEM 200 transmission electron microscope, which was operated at 200 kV. Magnetization and Curie temperature measurements of MZ4 nanoparticles were carried out on Lake Shore 7404 vibrating sample magnetometer (VSM). M–H loops were measured at 25 °C for magnetic field strength (H) of 0 to 5 KOe. High temperature M–T measurements were also carried on Lake Shore 7404 VSM with 74035 single stage cryostat oven assembly from 300 K to 700 K.

As synthesized MZ fluids were characterized by vibrating sample magnetometer (VSM) for their magnetic properties, photon correlation spectroscopy (PCS) for their hydrodynamic size and size distribution measurement. Magnetization measurements were performed on LakeShore 7404 vibrating sample magnetometer at room temperature. The hydrodynamic particle size and polydispersity index of MZ fluids were determine by Brookhaven "90 plus" particle size analyzer.